January 2007

Research Report: UCPRC-RR-2005-10

Laboratory Evaluation of Corrosion Resistance of Steel Dowels in Concrete Pavement

Authors:
Mauricio Mancio, Cruz Carlos Jr., Jieying Zhang,

John T. Harvey, and Paulo J. M. Monteiro

Work Conducted as part of Partnered Pavement Research Center Strategic Plan Element No. 4.8: Dowel Bar Retrofit Rehabilitation of Rigid Pavements

PREPARED FOR:

California Department of Transportation

(Caltrans), Division of Research and

Innovation

PREPARED BY:

University of California

Pavement Research Center

UC Davis and Berkeley

DOCUMENT RETRIEVAL PAGE		RR No: UCPRC-RR-2005-10
Title: Laboratory Evaluation of Corrosion Resistance of Steel Dowels in Concrete Pavement		
Authors: Mauricio Mancio, Cruz Carlos Jr., Jieying Zhang, John T. Harvey, and Paulo J. M. Monteiro		
Prepared for: Caltrans Division of Research and Innovation.	**FHWA No.** S/CA/RI-2006/27 **Client Reference No:** Strategic Plan Element Number 4.8	**Date**: January 2007
Strategic Plan Element No: 4.8	**Status:** Final	**Version No:** Stage 5

Abstract: An extensive investigation was carried out on the corrosion performance of several types of steel dowels embedded in concrete beams, to develop recommendations for their use in different environmental conditions.

Specimens were exposed to concentrated chloride solutions to accelerate corrosion. The types of dowel bars evaluated in the study were: bare carbon steel, stainless steel clad, grout-filled hollow stainless steel, microcomposite steel, carbon steel coated with flexible epoxy (green color code), and carbon steel coated with non-flexible epoxies (two types: purple and gray color codes). Half-cell potential measurements (indicative of the probability of corrosion activity),and Linear Polarization Resistance, LPR (for determining corrosion rate) were used. Every epoxy-coated bar examined had one or more defects on the coating, especially along the edges at the ends.

The study was conducted in three phases. Phase I: Dowels were cast in concrete beams with joints and then subjected to a corrosive environment. Half-cell potential was monitored for six months. Phase II: similar to phase I, but using a more permeable concrete and accelerated corrosion for a period of 18 months. Half-cell potential tests, LPR curves, visual inspections, chloride content analyses, and scanning electron microscopic investigations were carried out to evaluate the corrosion performance. Phase III: consisted in testing concrete slabs with transverse joints from a DBR project in Washington State. The slabs and dowels were subjected to half-cell potential tests, LPR curves, chloride content tests, and visual inspections. Measurement of chloride contents of these and other concrete cores we used for comparison of the laboratory and field conditions. The following main recommendations are drawn. 1. Uncoated carbon steel dowels should not be used. 2. Epoxy dowels present some risk of corrosion. It is recommended that: a) Quality control checks to control holidays should be implemented, b) Bar ends should be coated with epoxy, and care must be taken during shipping, storage, and installation. 3.It is recommended that the use of stainless steel clad, hollow stainless steel, or microcomposite steel dowels should be considered for locations with high risk of high chloride exposure (such as on mountain passes and marine environments).

Keywords: Dowel Bar Retrofit, corrosion, chloride exposure, steel dowel bars, stainless steel clad, hollow stainless steel, microcomposite, epoxy coated steel dowel, half-cell potential measurements, linear polarization resistance

Proposals for implementation: Uncoated carbon steel dowels should not be used. Epoxy dowels present some risk of corrosion. It is recommended that: a) Quality control checks to control holidays be implemented, b) Bar ends should be coated with epoxy, and care must be taken during shipping, storage, and installation. Stainless steel clad, hollow stainless steel, or microcomposite steel dowels should be considered for locations with high risk of high chloride exposure.

Related documents: Test Plan for project 4.8 "Dowel Bar Retrofit Rehabilitation of Rigid Pavements". Ukiah and Palmdale HVS Tests Reports.

Signatures:

Mauricio Mancio **1st Author**	Erwin Kohler **Technical Review**	D. Spinner **Editor**	John Harvey **Principal Investigator**	Michael Samadian **Caltrans Contract Manager**

DISCLAIMER

The contents of this report reflect the views of the authors who are responsible for the facts and accuracy of the data presented herein. The contents do not necessarily reflect the official views or policies of the State of California or the Federal Highway Administration. This report does not constitute a standard, specification, or regulation.

PROJECT OBJECTIVES

The work presented in this document is part of UCPRC Strategic Plan Item 4.8: "Dowel Bar Retrofit, Rehabilitation of Rigid Pavements." The goal of this research is to establish whether the dowel bar retrofit (DBR) rehabilitation technique provides adequate performance relative to its cost for the rehabilitation of rigid pavements. In order to obtain the expected outcome, the program addresses the following four areas of research:

1. Accelerated pavement testing with the Heavy Vehicle Simulator (HVS)
2. Live field traffic testing (collection of field data on a long-term basis)
3. Laboratory testing of DBR materials (steel and fiber-reinforced polymer dowel bars)
4. Modeling/analysis (finite element analysis of doweled concrete pavement joint, DBR performance, and life-cycle cost analyses).

This document addresses part of Task No. 3.

The objective of this particular study was to perform a laboratory investigation of the corrosion performance of several types of steel dowels embedded in concrete beams. The concrete beams and dowels were exposed to concentrated chloride solutions intended to accelerate corrosion and simulate environmental conditions. The purpose of the investigation was to develop recommendations for use of different types of dowels for different environmental risk conditions. To provide an indication of the aggressiveness of the laboratory conditions relative to field conditions, a set of field slabs from Washington State was examined, and chloride-content analyses were performed on the concrete beams used in the laboratory studies and on cores taken from nine locations in Washington State.

EXECUTIVE SUMMARY

Dowels are used in jointed concrete pavements to provide load transfer across transverse joints. Their use reduces vertical deflections that cause faulting and stresses that cause corner and longitudinal cracking by transferring part of the load to the unloaded slab. However, if corrosion of the dowels occurs, a number of problems can arise that can compromise the performance of the pavement and lead to premature failure. These problems include (a) the loss of dowel cross-section, which reduces load transfer capability, and (b) the accumulation of corrosion products, which restricts the free expansion and contraction of the slabs.

Dowel bar corrosion has been investigated in the field and laboratory in the past, which has led to the widespread use of epoxy coatings for steel dowels in concrete pavements in place of bare carbon steel. Steel reinforcement in sound concrete is protected from corrosion by a passive film formed due to the high pH (12.5–13.5) of concrete pore solutions. This thin protective film slows the corrosion reaction rate to very low levels. However, if the passive layer is broken or dissolves, then the metal reverts to active behavior and rapid corrosion can occur. The process of steel corrosion in reinforced concrete structures is subdivided into an initiation stage and a propagation stage.

The initiation stage is the time necessary for depassivation of the protective passive layer as a result of the penetration and concentration of aggressive agents such as carbon dioxide and chloride ions. For dowels in concrete pavements, the initiation stage is very short because of easy access to the dowels by aggressive agents through the joints; therefore the corrosion performance of the system depends largely on the properties of the steel dowel being used. Aggressive agents also potentially access the full length of the dowels because the bond between the dowels and concrete is designed to be tight but to have low friction, which probably permits easier diffusion of the agents along the dowel than along other reinforcing materials (rebar). The cyclic horizontal movement of the pavement slabs and the dowels is also likely to increase the risk of damaging protective coatings such as epoxy.

Most state agencies, including the California Department of Transportation (Caltrans), seal the joints of concrete pavements in order to minimize the ingress of water and fine debris into the joint. The effectiveness of this joint-sealing practice in preventing aggressive agents from accessing dowels is unknown. Further, sealing the joint from the surface cannot completely seal the joint from exposure to water and debris because these can still reach the dowel from the sides of the joint or from beneath it. Aggressive agents can also access the dowels by penetrating the concrete.

Dowel Types Evaluated

Seven kinds of steel dowels were evaluated in this study: bare carbon steel, stainless steel-clad, grout-filled hollow stainless steel, microcomposite steel, carbon steel coated with flexible epoxy (green color code, Designation ASTM A775), and carbon steel-coated with non-flexible epoxies (two types: purple and gray color codes, Designation ASTM A934).

The stainless-clad bars have a core of carbon steel covered by an outer layer (approximately 5 mm thick) of stainless steel. The ends of the stainless-clad dowels do not have stainless steel cladding, but they do have a protective paint coat. Epoxy-coated bars were also epoxy-coated at the ends. The stainless hollow dowels consisted of a hollow stainless steel cylinder with a wall thickness of approximately 5 mm, filled with a cementitious grout.

In this study, microcomposite steel refers to microstructurally designed steels with a dislocated lath structure (laths of martensite alternating with thin films of austenite) in which the formation of carbides is avoided. Microcomposite dowels are anticipated to be more resistant to corrosion than carbon steel.

Test Methods

Half-cell potential measurements are indicative of the probability of corrosion activity of the reinforcing steel located beneath the half-cell. The procedure is described by ASTM C876. Half-cell potential measurement has been widely used in the field due to its simplicity and general agreement that this technique is a good indicator of the existence of active corrosion along the steel reinforcement in concrete.

The Linear Polarization Resistance (LPR) technique is a well-established method for determining *corrosion rate* by using electrolytic test cells. The corrosion rate, expressed as the corrosion current density, is inversely related to the polarization resistance. A major concern with the LPR technique is uncertainty about the area of the steel bar that is affected by the current from the counter electrode. In the present study, the counter electrode was placed over a fabricated joint filled with NaCl solution and located above the dowel. Since virtually all the current will flow through the salt solution — which represents a path of very low resistance compared to concrete — it has been assumed that the area polarized corresponds to that part of the dowel exposed to the NaCl solution inside the joint. Epoxy-coated bars, however, could not be evaluated quantitatively using the LPR technique. It was found that the corrosion that occurred in the epoxy-coated dowels was localized and concentrated in small holidays (pinholes, voids, defects, etc.) and defects on the coating, and therefore the assumption about the exposed area does not hold for these bars.

In order to facilitate the identification of corroded areas in the epoxy-coated dowels and the evaluation of the role of defects in the development of localized corrosion, the epoxy-coated dowels were checked for holidays. This was achieved using a low-voltage holiday detector tester before casting the dowels in concrete beams. This mapping of coating defects was used to check against locations of corrosion, identified during the visual inspections of corroded dowels after conditioning. Every epoxy-coated bar examined had one or more defects on the coating, especially along the edges at the ends. These dowels were shipped from the manufacturer directly to the laboratory and were subjected to careful handling in the laboratory.

Chloride analyses were performed on concrete cores extracted from the laboratory beams from around the dowels in pavement slabs obtained from an early dowel bar retrofit project in Washington State, and from slab corners of field slabs at six locations in Washington State. The samples taken from different levels in the cores were tested by the Caltrans chemistry laboratory or Construction Testing Laboratory in Illinois.

Experiment Design

This study was conducted in three phases. Details of the three phases are as follows.

Phase I

Four types of dowels were cast in concrete beams with joints. The four types of dowels investigated were: carbon steel; stainless steel-clad; stainless hollow; and carbon steel coated with flexible epoxy. The dowels (1.5 × 18 in.), were cast in concrete beams measuring (6 × 6 × 22 in.). Electrical connections were made to the steel bars before casting, expansion end caps were installed on the assembly, and the dowels were mounted on plastic chairs. In the middle of the concrete beam, a joint was simulated by using a polystyrene foam spacer that was removed after 30 days.

The specimens were subjected to a corrosive environment (weekly wet and dry cycling with 3% NaCl solution ponded on top of the beams, permitting access of the corrosive solution through the simulated joint) at two temperatures: cold (4.4ºC) and hot (40–43ºC). No mechanical loading was placed on the beams.

Half-cell potential was monitored for six months, and visual inspection of the corroded dowels was made at the end of testing. Three replicates for each dowel type were tested.

Phase II

Seven types of dowels were cast in concrete beams with joints: carbon steel; microcomposite steel; stainless steel-clad; stainless steel hollow; carbon steel coated with flexible epoxy (green color-code); and carbon steel coated (two types) with non-flexible epoxies (purple and gray color codes). The dimensions of the specimens are the same as those in Phase I, however, a more permeable concrete was used, with water-to-cement ratio of 0.65 instead of 0.42, plus a different cement type and larger aggregate size. Corrosion was accelerated by exposing the samples to cycles of a 3.5% NaCl solution at room temperature for a period of 18 months. Half-cell potential tests, Linear Polarization Resistance (LPR) curves, visual inspections, chloride-content analyses, and scanning electron microscopic (SEM) investigations were carried out to evaluate the corrosion performance of the dowels. Four replicates of each type of steel dowel were tested in this phase.

Phase III

Three concrete slabs with two transverse joints were extracted from a dowel bar retrofit project in Washington State. The joints showed loss of load transfer efficiency after 13 years of service. The slabs and dowels were shipped to Richmond, California, and subjected to half-cell potential tests, LPR curves, chloride-content tests, and visual inspections. This phase of the study also included measurement of chloride contents of concrete cores taken from the transverse joints of field slabs in various climate regions in Washington provided by the Washington State Department of Transportation (WSDOT), and of cores taken from the laboratory beam specimens from the Phase II testing, for comparison of the laboratory and field conditions.

Conclusions

The following sections present conclusions from the various phases of the study.

Phase I Testing

- Carbon steel dowels present the shortest corrosion initiation period — when chlorides have direct access to the bar through the joint, the initiation stage can be disregarded and the corrosion propagation phase begins immediately. Epoxy-coated dowels exhibited a considerably lengthened initiation period, while the stainless hollow and stainless clad dowels provided the highest resistance to the onset of corrosion.
- From the visual inspections after six months of cyclic ponding, it was observed that the carbon steel dowels exhibited uniform corrosion along the bar. Epoxy-coated dowels had localized corrosion at defects — mostly at the ends of the bars where the coating is most vulnerable to damage. No visible corrosion was observed on either the stainless steel hollow bars or stainless clad bars.

Phase II Laboratory Testing

- In coated specimens, such as the epoxy-coated specimens included in this study, corrosion is not uniform, but is instead concentrated at localized defective areas (e.g., pinholes, voids, etc.). Given that epoxy is an electrical insulator, polarization only happens at very small locations (defective areas) that cannot be accounted for in the calculation of the polarization resistance (*Rp*) term. Therefore, the epoxy-coated dowels cannot be quantitatively evaluated with the other dowels and must be evaluated qualitatively.

- The carbon steel dowels exhibited the lowest values of *Rp* and therefore have the smallest resistance to charge transfer across the interface. Carbon steel dowels are therefore expected to have the fastest rate of corrosion propagation among the types included in this study.
- Microcomposite steel dowels exhibited polarization resistance approximately 35 times larger than carbon steel dowels, while stainless clad and stainless hollow bars had about 73 times greater polarization resistance. This observation indicates that the microcomposite steel dowels exhibit much greater resistance to corrosion propagation than carbon steel dowels, but not as much as the stainless clad and hollow bars.
- Based on corrosion current density results, it was verified that the carbon steel dowels exhibited very rapid corrosion while microcomposite steel exhibited a moderate level and stainless steel-clad and stainless steel hollow proceeded at low rates of corrosion.
- Visual inspections of the corroded dowels revealed heavy and mostly uniform corrosion along the carbon steel dowels, light corrosion in the microcomposite steel dowels, and no visible corrosion in the stainless steel-clad and stainless steel hollow bars. For the epoxy-coated dowels, the visual inspections generally revealed that visible corrosion was not widespread, but did occur at a few localized defective areas, generally at holidays and at the edges of the bar ends. No significant difference was observed on the performance of non-flexible and flexible epoxy-coated dowels.
- In general, the microscopic investigation by scanning electron microscopic (SEM) matches well the results anticipated by the electrical measurements and visual inspections. However, the analysis has focused mostly on the corroded areas of each sample, and revealed corroded areas that were not visible to the naked eye.
- Statistical analyses of the results show that in all cases, the type of steel dowel has a statistically significant effect on the quantitative parameters studied (i.e., half-cell potential, polarization resistance, and corrosion current density).

Phase III Testing

- In the extracted slabs from which cores were taken at the joints, a considerable amount of corrosion product was verified by means of visual inspection beneath the epoxy coating on the central region of the dowel located below the joint. The corrosion is likely to have contributed to the loss of load transfer efficiency (LTE) of the joint because of the low strength corrosion products at the interface between the concrete and the dowel. Lack of centering of one dowel over the transverse joint is also likely to have contributed to the low LTE.
- Half-cell potential and Linear Polarization Resistance results match the visual observations, indicating the presence of active corrosion.

Chloride Concentration

The following conclusions are drawn from the relationship among the concentrations of chlorides in the laboratory samples, extracted WSDOT field slabs, and cores extracted from slabs at various locations in Washington State.

- Chloride concentrations close to the pavement joints are significantly higher than in other regions of the pavement. At the joint, easier access and accumulation of chlorides leads to higher, localized concentrations.
- When a joint is present, the chloride ions do not diffuse through the concrete (or grout) from the top; instead, they migrate through the open joint to the dowel.

- In the field cores, it was verified that the chloride threshold for carbon steel was exceeded in five out of six projects.
- In the laboratory samples, with open joints located above the dowels, the chloride concentrations are more constant along the depth profile, as compared to the field conditions in which the chlorides have to diffuse through the concrete or migrate through a narrower joint.
- The use of a 3.5% NaCl solution for laboratory experiments may lead to higher chloride concentrations than those found in the field specimens, greatly accelerating the corrosion process compared to the field. As a result of this aggressive environment, corrosion could be observed in nearly all samples in only 18 months of exposure.
- Laboratory results can be used to comparatively evaluate the corrosion resistance of different materials when exposed to the same aggressive environment. However, the chloride concentration analyses indicate that the actual field conditions and local environment should be taken into account when choosing the appropriate material for a given project.

Recommendations

The following recommendations are based on the conclusions presented above.

- The presence of corrosion at the bar ends and along the bar from ponding water on dowels cast in concrete in the laboratory indicates that chlorides can pass all the way to the bar ends from the joint along the horizontal interface between the dowel and the concrete, or through the concrete. For this reason it is recommended that uncoated carbon steel dowels not be used.
- Epoxy dowels present some risk of corrosion, primarily localized at holidays and the ends of the bars. Based on this finding, it is recommended that:

1. Quality control checks to control holidays should be implemented.
2. Bar ends should be coated with epoxy, and care must be taken with epoxy-coated dowels during shipping, storage, and installation. Corrosion will be exacerbated if the bar ends are not coated (observed on various Caltrans construction sites) or if the coated ends are damaged during storage, transport, and installation.

- It is recommended that the use of stainless steel-clad, hollow stainless steel, or microcomposite steel dowels be considered for locations with high risk of high chloride exposure (such as on mountain passes and marine environments), where exposure to corrosive water is anticipated. The selection of a specific corrosion-resistant dowel should be based on further field investigations and cost differences.
- It is recommended that a field study be performed at several mountain pass locations to measure the chloride content of snowmelt after sand/salt application for comparison with the chloride content of the solution used in the laboratory testing in Phases I and II and the core results from Phase III. The results of this study should be used to further refine the risk assessment in these critical locations.

TABLE OF CONTENTS

LIST OF FIGURES

LIST OF TABLES

ABBREVIATIONS AND TERMS USED IN THE TEXT

California Department of Transportation (Caltrans)

Construction Technology Laboratories, Inc. (CTL)

Falling Weight Deflectometer (FWD

Linear Polarization Resistance (LPR)

load transfer efficiency (LTE)

relative humidity (RH)

Scanning Electron Microscope (SEM)

University of California Pavement Research Center (UCPRC)

Washington State Department of Transportation (WSDOT)

Corrosion current density (i_{corr})

Polarization Resistance (R_p)

1 INTRODUCTION

The performance of jointed concrete pavements depends to a large extent on adequate load transfer at the joint. Traffic loads must be effectively transferred across the transverse joints to minimize differential vertical movement between slabs, and the total movement of each slab. Minimization of vertical slab movement through the use of dowels has been found to be the most effective method of slowing the development of faulting, which is a primary cause of roughness on concrete pavements in California. Effective load transfer at transverse joints also reduces stresses in the slabs responsible for corner cracking. (*1*)

Dowels are available in many materials, including stainless steel, epoxy-coated steel, and fiber-reinforced polymer. The most common type is the epoxy-coated steel variety. Dowel bars provide a mechanical connection between slabs to limit differential vertical movement without restricting horizontal joint movement. Dowels are usually placed at mid-depth in the slab and coated with a bond-breaking substance to prevent bonding to the concrete and allow for the aforementioned horizontal movement.

Corrosion of dowels can compromise the performance of the dowels and of the pavement in which they are installed and lead to premature failure. In general, concrete seals the steel dowels from the corrosive effects of weather and environmental exposure, allowing the dowel bars to function effectively as a long-term reinforcement. (*2*) However, if corrosion occurs in a steel-reinforced concrete structure, the expansive steel corrosion products build up tensile stress in the concrete, often large enough to lead to cracking and deterioration of the structure. (*3*)

In the case of doweled pavements, the dowel must not have any "play" in the concrete to achieve maximum load transfer and restriction of vertical movement. The effect of the loss of cross-section of a dowel due to corrosion introduces "play" and reduces the dowel's ability to transfer load and restrain vertical movement. Davids et al. have used finite element analysis to show that a low level of loose fit between the dowel and the concrete can substantially reduce load transfer efficiency (LTE). (4) Finally, the accumulation of the corrosion products may restrict the free expansion and contraction of the slabs, causing pavement lock up and potentially inducing cracks in the pavement.(5)

1.1 Background

The combination of concrete and steel is usually regarded as optimal for both mechanical performance and durability. Theoretically, this combination should be highly durable, as the concrete cover provides a chemical and physical protection barrier to the steel and can potentially eliminate steel corrosion problems.

Steel reinforcement in sound concrete is protected from corrosion by a passive film formed due to the high pH (12.5-13.5) of concrete pore solutions. This thin protective film lowers the corrosion reaction rate to very low levels. However, if the passive layer is broken or dissolves, then the metal reverts to active behavior and rapid corrosion can occur. In reinforced concrete, two major factors cause the passive coating to break down:

1. Carbonation (reaction with CO_2), and
2. The presence of chlorides.

Dowel bar corrosion has been investigated in the field and the laboratory in the past, which has lead to the widespread use of epoxy coatings for steel dowels in concrete pavements in place of bare carbon steel.

1.1.1 Corrosion Vulnerability

In 1982, Tuutti proposed a conceptual model to represent the process of steel corrosion in reinforced concrete structures. In the model, the service life is subdivided into an initiation stage and a propagation stage. (*6*) Figure 1 illustrates this model.

The initiation period is the time necessary for "depassivation" (disruption) of the protective passive layer. The time to corrosion initiation is determined by how rapidly the depassivation process occurs as a result of the penetration and concentration of aggressive agents such as carbon dioxide (CO_2) and chloride ions (Cl^-).

It is important to note that the initiation stage in Tuutti's model assumes that the steel reinforcement or dowels are completely embedded in the concrete, with no direct access by aggressive agents to the steel except through the intact concrete. However, for dowels in concrete pavements there is a drastically reduced initiation stage because the access of the aggressive agents to a dowel bar in a pavement is much easier than to reinforcing steel (rebar) in a structural concrete element. This is due to the unique functions and design requirements of dowels:

1. The joints through which dowels pass typically allow for free penetration of aggressive agents such as oxygen, moisture, and de-icing salts to the bar's surface (Figure 2). It is recognized that it is not possible to construct and maintain a completely water- and airtight joint. Water and air can enter the joint from below, above, and from the sides. Joints are open the widest when temperatures are low, which in California is the time when most rainfall occurs.
2. Unlike steel placed in concrete for structural reinforcement (rebar), the bond between the dowels and concrete is designed to be tight, but to have low friction, which likely permits easier diffusion of the aggressive agents along the dowel than along a rebar.
3. The cyclic horizontal movement between the pavement slabs and the dowel would increase the risk of damaging protective materials like epoxy-coating.

Thus, aggressive agents such as CO_2 and Cl^-, plus water and oxygen, have free access to the steel surface of a dowel, which essentially reduces the time necessary to complete the initiation stage.

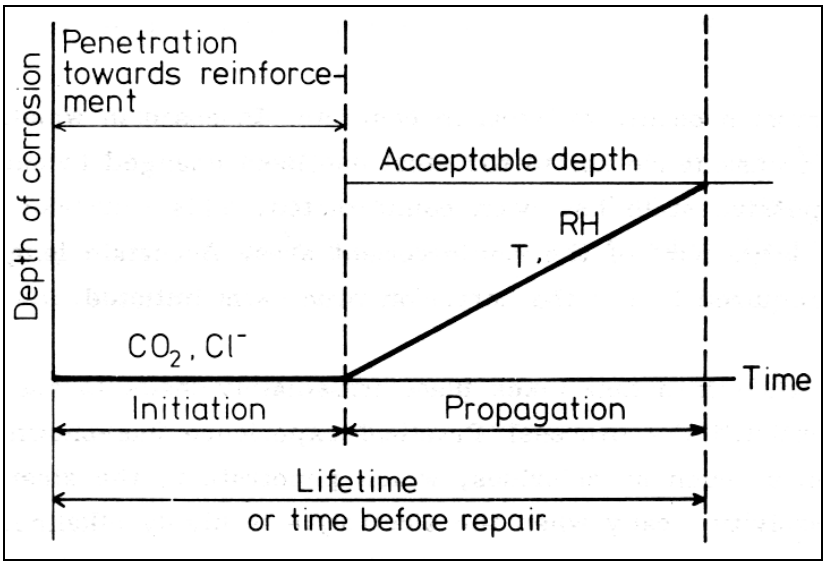

Figure 1. Schematic representation of steel corrosion sequence in concrete. (*6*)

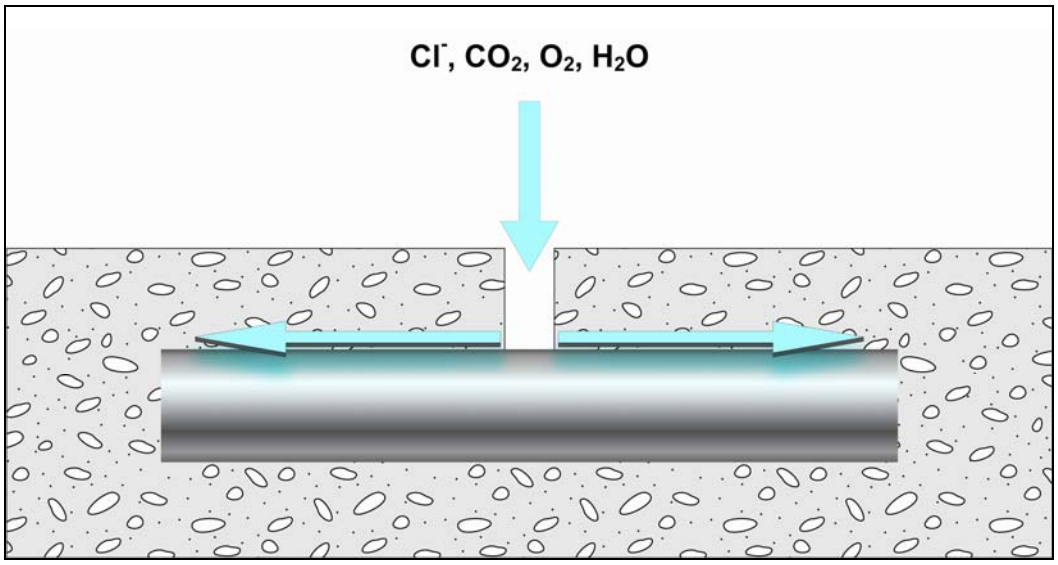

Figure 2. Aggressive agents have free access to dowels and are easily dispersed along the length of the dowel.

The beginning of the corrosion process starts at the propagation stage, and the length of this stage is determined by the rate of corrosion, which is mainly influenced by the moisture content of the concrete, the temperature, the permeability of the concrete, the chemical composition of the pore solution, and the thickness of the concrete cover.(*6*)

1.1.2 Corrosion Prevention

Several methods for reducing the risk of corrosion of steel embedded in concrete exist. Some are based on the properties of the concrete and others on the characteristics of the steel itself.

Over the years, the general approach to improving the durability of reinforced concrete structures has focused primarily on the improvement of concrete performance. Improvement of the cracking resistance of the concrete and reduction of concrete permeability, both of which slow the access of aggressive agents to the passive layer, have produced considerable benefits and will continue to improve the performance of reinforced concrete structures. However, in the case of steel-doweled pavements, as discussed in the previous section, aggressive agents have greater access to the steel than in typical steel-reinforced concrete and therefore the corrosion performance of the system depends largely on the properties of the steel dowel being used.

Most state agencies, including the California Department of Transportation (Caltrans), seal the joints of concrete pavement to minimize the entrance of water and fine debris into the joint. Sealing is often performed at the time of construction, and joints are often resealed at intervals in the pavement life. The cost effectiveness of joint sealing is a subject of discussion in the field of concrete pavements, although most states continue to seal joints. Little research is available in the literature evaluating the effect of joint sealing on dowel corrosion performance. Significant research has also improved the corrosion resistance of concrete reinforcement, for example, the development of coated steel dowel bars and use of steels with higher corrosion resistance, as well as several alternatives to regular carbon steel dowels which are now available.

1.2 Objectives and Scope

The main objective of this study was to investigate in the laboratory the corrosion performance of several types of steel dowels embedded in concrete beams and subjected to environmental conditions intended to accelerate corrosion by exposure to concentrated chloride solutions. In this study, seven types of steel dowels were evaluated for their corrosion performance:

- Bare carbon steel,
- Stainless steel-clad,
- Grout-filled hollow stainless steel,
- Microcomposite steel,
- Carbon steel coated with flexible epoxy (green color code, ASTM Designation A775), and
- Carbon steel coated with non-flexible epoxies (purple and gray color codes, ASTM Designation A934).

Chapter 2 of this report provides an overview of the experimental work and the description of the test procedures. Chapter 3 presents the results and discussions of the different phases of the current study, and Chapter 4 presents the conclusions and recommendations. A review of the detection techniques used, a brief discussion on chloride thresholds, and detailed test data and raw data are presented in the appendices.

2 EXPERIMENT DESIGN AND TEST PROCEDURES

This study included three phases, as follows:

1. Placement of four types of dowels (carbon steel, stainless steel-clad, hollow stainless steel, and epoxy-coated steel dowels) in concrete beams with joints, exposed to a corrosive environment with chlorides, under two temperature extremes (4ºC and 40-43ºC). The evaluation included half-cell potential tests over time for the determination of the corrosion initiation period, and visual inspection at the completion of testing. Three replicates of each type of dowel were tested.
2. Placement of seven types of dowels cast in concrete beams with joints, exposed to an accelerated corrosive environment with chlorides. These specimens were evaluated for corrosion performance using half-cell potential tests, Linear Polarization Resistance (LPR) experiments, visual inspections, chloride analyses, and microscopic investigations by Scanning Electron Microscope (SEM). In this phase, the in-situ corrosion rate was measured in order to determine how fast corrosion occurred in the propagation stage. Four replicates of each type of dowel were tested.
3. Evaluation of three concrete slabs with two transverse joints extracted from a dowel bar retrofit project in Washington State showing loss of load transfer efficiency (LTE) after 13 years of service. This phase of the study also included measurement of chloride contents of concrete cores taken from transverse joints of field slabs in various climate regions in Washington provided by the Washington State Department of Transportation (WSDOT) for comparison of the laboratory and field conditions.

2.1 Phase I: Laboratory Testing

In the first phase, the four types of dowels investigated were:

- **Carbon steel.** Uncoated and untreated, ASTM A615.
- **Stainless steel hollow.** The stainless steel hollow dowels consisted of a hollow type 316 stainless steel cylinder approximately 5 mm thick, filled with a cementitious grout.
- **Stainless steel-clad.** The stainless clad bars consisted of a core of carbon steel covered by an outer layer (approximately 5 mm thick) of stainless steel type 316L. The ends of the dowels did not have stainless steel cladding, but did have a protective paint coat.
- **Carbon steel coated with flexible epoxy.** Epoxy-coated dowels with epoxy patch coating on the ends.

Figure 3 illustrates the dowels used Phase I. All four types of dowels measured 38.1 mm (1.5 in.) in diameter and 460 mm (18 in.) in length. They were cast in concrete beams measuring 150 × 150 × 560 mm (6 × 6 × 22 in.). As shown in Figure 4, before casting, electrical connections were made to one end of the steel bars, expansion end caps were placed, and the dowels were mounted on plastic chairs. In the middle of the concrete beam, a joint was simulated by using a polystyrene foam spacer, which was carefully removed after 30 days of age.

The water-to-cement ratio (w/c) of the concrete was 0.42, and the cement:sand:aggregate ratio was 1:1.84:2.76. Calcium sulfoaluminate cement was used, and the maximum size of the coarse aggregate was 38 mm (1.5 in.). The specimens were demolded 24 hours after casting and cured at 23ºC and 100 percent relative humidity (RH) for 7 days. These specimens were subjected to a corrosive environment (weekly wet and dry cycling with 3 percent NaCl solution ponded on top of the beams, permitting access of the corrosive solution through the simulated joint) at two temperatures: cold (4ºC) and hot (40–43ºC). These temperatures represented average low and high temperatures in different regions in California. No mechanical loading was placed on the beams.

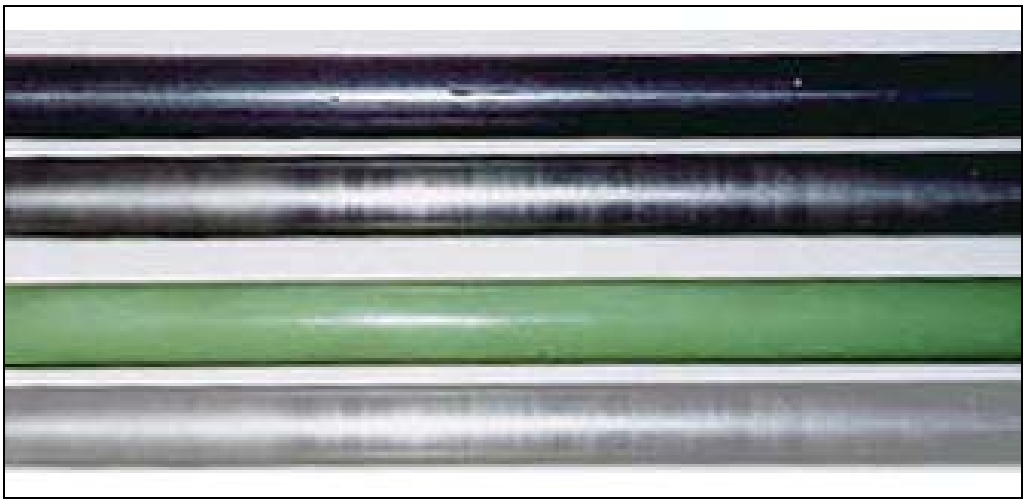

Figure 3. Steel dowel types investigated in Phase I. From top to bottom: carbon steel, stainless steel clad, carbon steel coated with bendable epoxy, and stainless steel hollow.

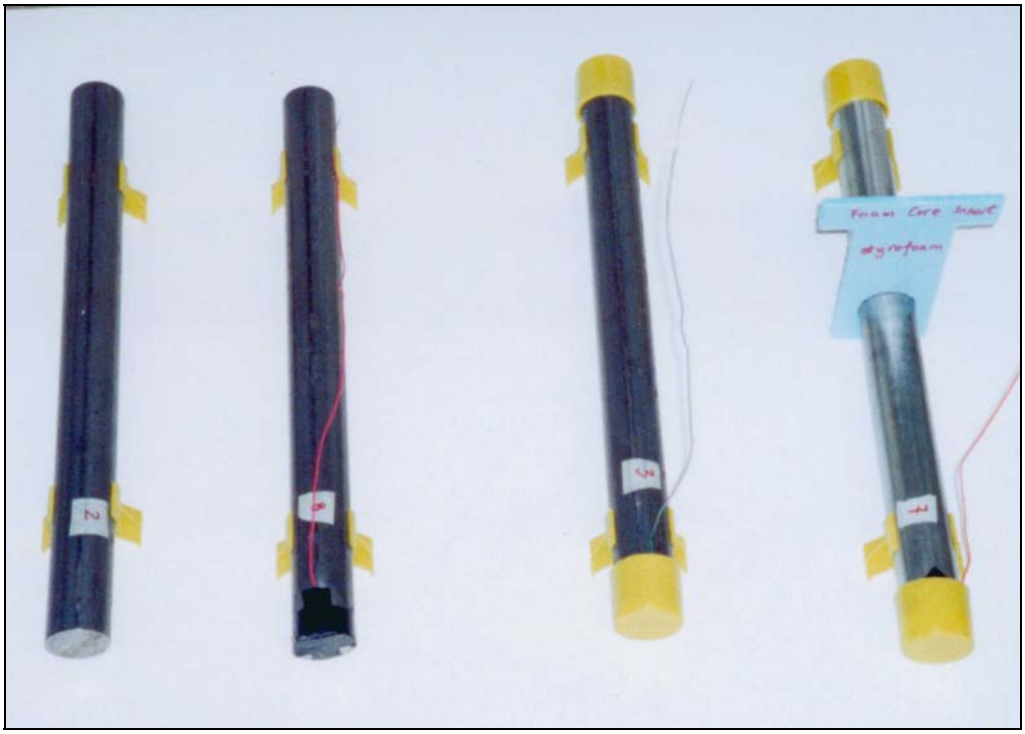

Figure 4. Sequential preparation of dowels before casting in the concrete beams.

Half-cell potential was monitored using a copper/copper sulfate ($Cu/CuSO_4$) electrode placed on the surface of the concrete for six months in order to determine the corrosion initiation period. Visual inspection of the corroded dowels was made after the experiments were completed. The salt solution was removed from the

concrete surface before the electrical measurements were performed. As previously noted, three replicates for each type of steel dowel were tested. Figure 5 illustrates the experimental setup. Details of the half-cell potential test are included in APPENDIX A: Detection Techniques.

Figure 5. Half-cell potential test using a high impedance (10 Meg-Ohm) voltmeter, and a copper/copper sulfate reference cell.

2.2 Phase II: Laboratory Testing

Phase II of the testing considered seven different types of dowels:

- **Carbon steel.** Uncoated and untreated, ASTM A615.
- **Microcomposite steel.** Microcomposite steel refers to microstructurally-designed chromium-containing steels with a dislocated lath structure (laths of martensite alternating with thin films of austenite) that is virtually carbide-free. Conventional steels have ferrite-carbide microstructures and in corrosive environments these carbides become cathodic to ferrite and can develop microgalvanic corrosion cells, which can lead to accelerated corrosion. On the other hand, microcomposite steels are produced in a way that avoids the formation of carbides and thus they are anticipated to be more resistant to corrosion. In this study, the microcomposite steel specimens presented about 9 percent chromium, according to information provided by the manufacturer (Appendix H).
- **Stainless steel hollow.** The stainless steel hollow dowels consisted of a hollow Type 316 stainless steel cylinder approximately 5 mm thick, filled with a cementitious grout.
- **Stainless steel clad.** The stainless clad bars have a core of carbon steel covered by an outer layer (approximately 5 mm thick) of stainless steel Type 316L. The ends of the dowels do not have stainless steel cladding, but do have a protective paint coat.
- Carbon steel coated with flexible epoxy (green color code). Epoxy-coated bars were also epoxy-coated at the ends.

- **Carbon steel coated with non-flexible epoxy (two types).** Two types were studied: purple and gray color code epoxy.

The dimensions of the specimens are the same as those in Phase I, however a more permeable concrete was used with a water-to-cement ratio of 0.65 and mix proportions 1:3.0:3.25 (cement:sand:gravel). Type I/II cement was used, and the maximum aggregate size was 12.8 mm (0.5 in.). The specimens were demolded 24 hours after casting and cured at 23ºC and 100 percent relative humidity (RH) for 28 days.

In the Phase II testing, corrosion was accelerated by exposing the samples to weekly wet-and-dry cycles of a 3.5 percent NaCl solution at room temperature for a period of 18 months. Half-cell potential tests, Linear Polarization Resistance (LPR) curves, visual inspections, chloride analyses, and microscopic investigations were carried out to evaluate the corrosion performance of the dowels. Four replicates of each type of steel dowel were tested in this study. Figure 6 illustrates the different types of dowels used. The in-situ corrosion rate was measured in order to permit estimation of the service life of the dowels under the accelerated conditions. Details of the detection techniques are included in Appendix A. Figures 7 and 8 show the electrical connections. Figures 9 and 10 demonstrate the experiment setup.

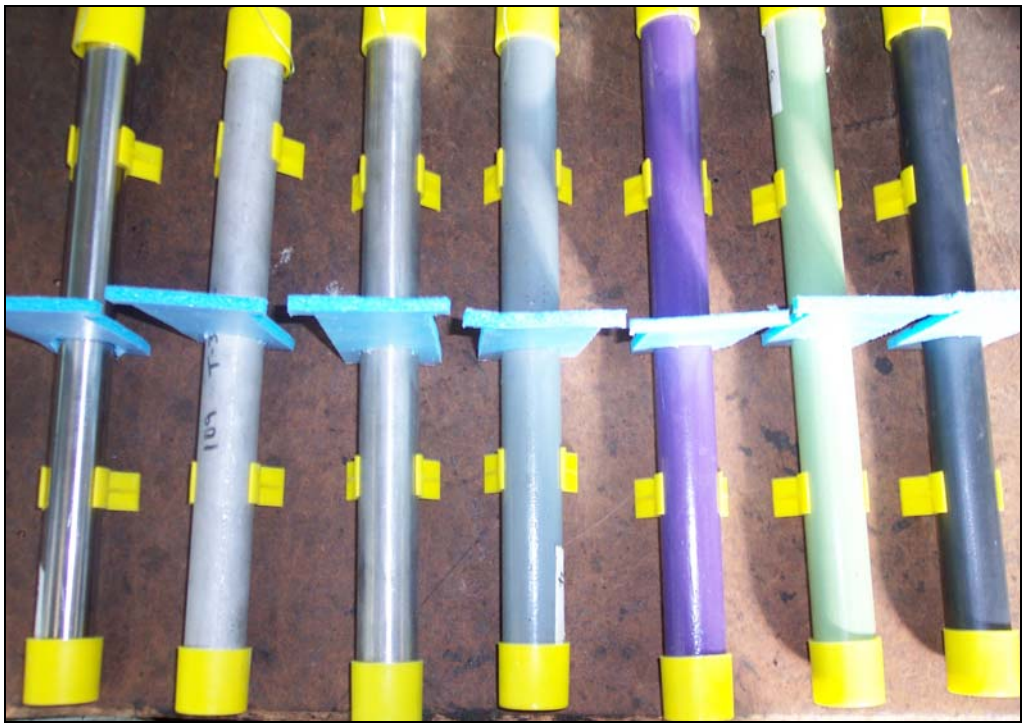

Figure 6. Different types of steel dowels investigated. From left to right: microcomposite steel, stainless steel hollow, stainless steel-clad, non-bendable epoxy-coated dowel (gray coating), non-flexible epoxy-coated dowel (purple coating), flexible epoxy-coated dowel (green coating), carbon steel.

2.3 Phase III: Evaluation of Field Slabs and Chloride Testing of Cores from Field Slabs

In addition to the laboratory experiments described in Section 2.2, further experiments were performed on concrete pavement slabs obtained from a dowel bar retrofit project from the Washington Department of Transportation (WSDOT). These slabs were constructed in 1964; dowel bar retrofit was later performed in 1994. The slabs were extracted from Interstate 90, near the town of Cle Elum in Washington State, and shipped to the University of California Pavement Research Center (UCPRC) at the Richmond Field

Station for testing and evaluation. They were selected because load transfer efficiencies (LTE) measured using the Falling Weight Deflectometer (FWD) indicated that the joints were experiencing a decrease in LTE. This was the first WSDOT dowel bar retrofit project that has shown significant loss of LTE.

According to information provided by WSDOT, until the early 1980s the approximate use of rock salt was 120–150 days per year at a typical rate of 180 pounds per mile using a 5:1 ratio (one scoop of salt to five scoops of sand). Each day typically had at least two applications, and salting typically occurs from mid-November to mid-April. From the early 1980s to 1997 or so, rust inhibitor type de-icers/salts have been used. Since 1997, liquid magnesium chloride has been used at a typical rate of 35 gallons per mile with a range of 15 to 50.

2.3.1 Evaluation of Field Slabs

The slabs used in this study were sawed and sealed during initial construction with a rubberized joint sealer product called "Seal Target 164." In 1994, during the dowel bar retrofit, joints were also sealed with rubberized joint sealant. Figure 11 shows the slabs tested.

The location from which these slabs were removed is at an elevation of 543 m. This location is subject to 568 mm average annual rainfall, 2,070 mm average annual snowfall, and 76 average annual freeze-thaw cycles (air temperatures) (7). The slabs were taken from the outside lane and were subjected to approximately 1 million Equivalent Standard Axle Loads (ESALs) annually during their service life. The dowels are 38 mm (1.5 in.) in diameter and the concrete slabs 228 mm (9 in.) thick. The dowels were carbon steel coated with flexible (green) epoxy. After removing the slabs, half-cell potential tests, Linear Polarization Resistance experiments, chloride analyses, and visual inspection work were performed in order to provide comparison with results obtained in the laboratory under accelerated conditions. All testing was performed at the University of California Pavement Research Center.

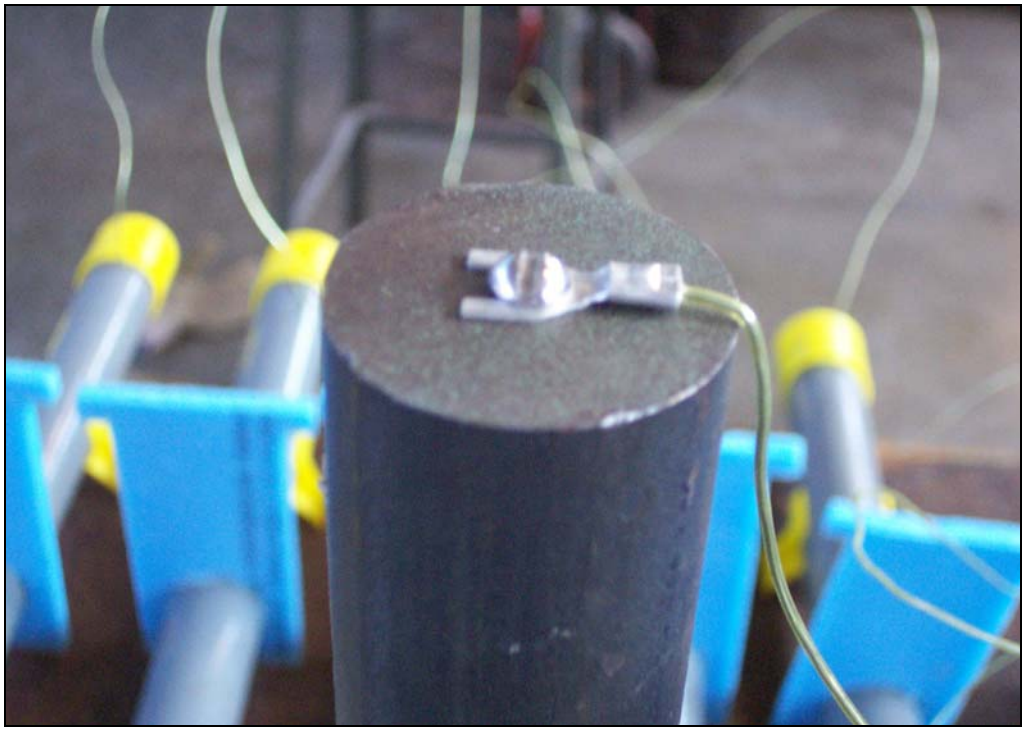

(a)

(b)

Figure 7. Electrical connections made to the dowels (a) before casting them in the concrete in order to perform half-cell potential and Linear Polarization Resistance experiments. Connections were sealed with epoxy (b) before casting.

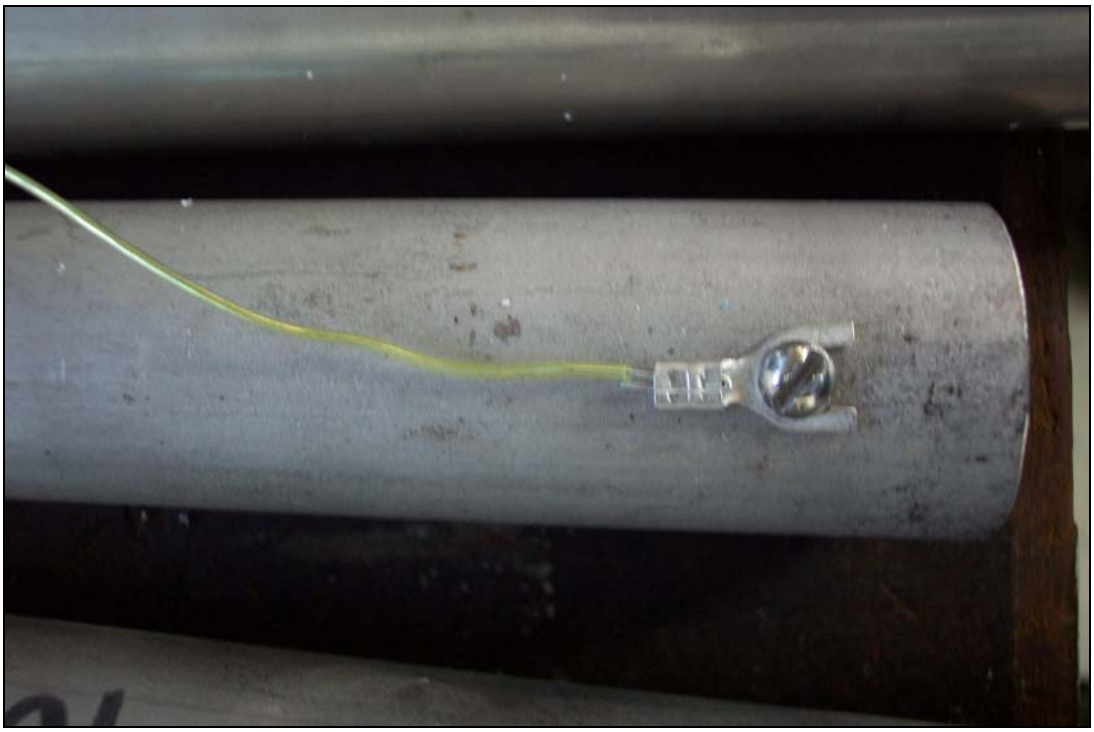

(a)

(b)

Figure 8. Electrical connections made to the stainless steel hollow specimens. Connections were made at the side of the dowel (a) and sealed with epoxy (b) before casting.

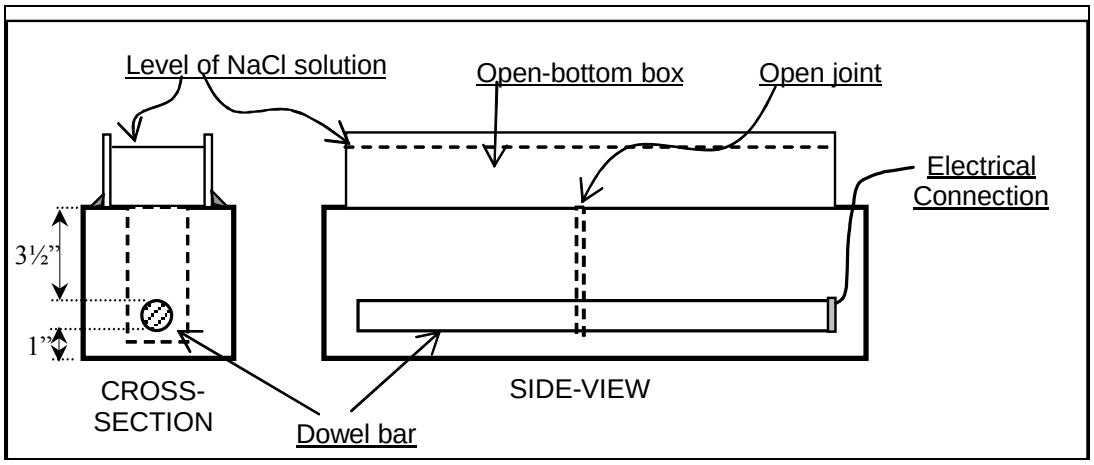

Figure 9. Experiment setup to accelerate corrosion using chloride ponding.

Figure 10. Picture of the experimental setup illustrated in Figure 9.

(a)

(b)

Figure 11. WSDOT slabs at the UC Pavement Research Center lab, located at the University of California, Berkeley Richmond Field Station.

2.3.2 Chloride Testing of Cores from In-Service Pavements

In addition to the testing performed on the WSDOT slab noted in Section 2.3.1, WSDOT extracted two cores from near-joint corners of in-service slabs at various locations in Washington. These cores were tested for chloride content by Construction Technology Laboratories, Inc. (CTL) for comparison with the laboratory results. (Section 3.4.2 describes the locations from which cores were extracted, including years of construction, salt usage, and joint sealing practices.)

2.4 Detection Techniques

Several electrochemical methods have been used to evaluate the corrosion activity of steel reinforcement. The half-cell potential and the LPR methods are among the most commonly used and accepted test methods for in-situ measurements. These tests are easy to perform in the field, and commercial instruments are readily available. As Carino observes, among the many methods that have been investigated for measuring the in-situ corrosion rate of steel embedded in concrete, the Linear Polarization Resistance appears to be gaining most acceptance. (*8*)

The half-cell potential measurements are indicative of the probability of corrosion activity of the reinforcing steel located beneath the half-cell, and the procedure is described in ASTM C876. The setup basically consists of an external electrode (half cell), connecting wires, and a high impedance voltmeter (impedance >10MΩ). A high impedance voltmeter is used so that there is a very little current through the circuit. Copper/copper sulfate ($Cu/CuSO_4$) electrodes were used throughout this research.

The half-cell potential measurement has been widely used in the field due to its simplicity and general agreement among researchers that this technique effectively indicates the existence of active corrosion along the steel reinforcement in concrete. Table 1 illustrates the relationship between measured potential and the likelihood of corrosion activity.

Table 1. Relationship between Half-cell Potential and Corrosion of Steel Embedded in Concrete (ASTM C876)

Half-Cell Potential (mV)*	**Corrosion Interpretation**
> -200	Low probability (10%) of corrosion
-200 to -350	Corrosion activity uncertain
< -350	High probability (90%) of corrosion

* Measurements made with a copper/ copper sulfate electrode.

Thus, the half-cell potential method provides an indication of the likelihood of corrosion activity at the time of the measurement. However, it does not give any indication of the rate of corrosion of the steel.

On the other hand, the LPR technique is a well-established method for determining the rate of corrosion by using electrolytic test cells. The technique basically involves measuring the change in the open-circuit potential of the electrolytic cell when an external current is applied to the cell. For a small perturbation about the open-circuit potential, there is a linear relationship between the change in applied current per unit area of electrode (Δi) and the change in the measured voltage (ΔE). The ratio $\Delta E/\Delta i$ is called the *polarization resistance* (*Rp*). The corrosion rate, expressed as the corrosion current density (i), is inversely related to the polarization resistance, as indicated by the Stern-Geary relationship $i = B/Rp$, where B is a constant (ASTM G59). Some guidelines have been developed to establish a relationship between corrosion current density and corrosion rate, as shown in Table 2. (*9*)

Table 2. Relationship between Corrosion Current Density and Corrosion Rate (*9*)

Corrosion Current Density, I_{corr} (µA/cm^2)	Corrosion Rate
< 0.1	Negligible
0.1 – 0.5	Low
0.5 – 1.0	Moderate
> 1.0	High

A major concern with the LPR method is the uncertainty about the area of the steel bar that is affected by the current from the counter electrode. Usually, it is assumed that the current flows in straight lines perpendicular to the bar and the counter electrode, and the affected bar area is understood to be the bar circumference multiplied by the length of the bar below the counter electrode, which in fact is not the case, as illustrated in Appendix A. However, in the laboratory experiments performed in this study (Phases I and II), this concern is not justified, since virtually all the current will flow through the NaCl solution present in the open joint, which represents a very low-resistivity path compared to concrete. As previously stated, the salt solution was removed from the concrete surface in order to perform the electrical measurements, but the joint remained filled with solution to provide this low-resistivity path for current flow. Note that the counter electrode was placed just above the fabricated joint. Thus, it has been assumed that the area polarized corresponds to that part of the dowel exposed to the NaCl solution inside the fabricated joint.

The Linear Polarization Resistance experiments were performed using a Princeton Applied Research Model 263 Potentiostat-Galvanostat. A detailed description of these detection techniques, along with the explanation of the principles involved, is presented in Appendix A.

2.5 Holiday Check

During Phase II of this research, in order to facilitate the identification of corroded areas in the epoxy-coated dowels and the evaluation of the role of defects on the development of localized corrosion, the epoxy-coated dowels were checked for holidays (pinholes, voids, defects, etc.). This was done before casting the dowels in the concrete beams using a low-voltage holiday detector tester following ASTM G62 and CTM 685 (brand Tinker & Rasor, Model M/1 Holiday Detector). This mapping of coating defects was used to check against locations of corrosion identified during the visual inspections of corroded dowels after conditioning (Section 3.2.2). It is worth mentioning that every single epoxy-coated bar used in Phase II presented one or more defects on the coating, especially along the edges at the dowel ends. These dowels were shipped from the manufacturer directly to the laboratory and were subjected to reasonably careful handling in the laboratory. It would be expected that dowel bars would be subjected to much rougher handling on a construction site. The holidays found in the mapping were not caused by being dropped or banged in the laboratory.

2.6 Chloride Analyses of Laboratory and Field Cores

Several chloride analyses were performed on concrete cores extracted from the laboratory beams and from the pavement slabs obtained from WSDOT in order to evaluate the concentration of chlorides in the region surrounding the steel dowels, particularly in the vicinities of the open joints. It is believed that over time, chloride ions may build up around the joint area and close to the dowels, increasing the chloride concentration to considerable levels, perhaps way above the chloride threshold of the steel being used. The extracted samples were shipped to the Caltrans chemistry laboratory where the chemical analyses were performed. In addition, cores from slab corners were obtained from WSDOT pavement at various locations and were analyzed for chloride content by Construction Technology Laboratories, Inc. Chloride tests are performed according to ASTM C1152.

3 RESULTS AND DISCUSSION

The results of Phase I are presented in Section 3.1 of this report. The results of Phase II are presented in Section 3.2. The Phase III results obtained for the WSDOT slabs from the dowel bar retrofit project on Interstate 90 and the chloride analyses from the WSDOT cores are presented in Section 3.3.

3.1 Phase I Results

In the following text and in Figures 12–19, the specimens are identified as RS ("regular steel," i.e., carbon steel), SS (stainless steel hollow), EX (epoxy-coated [flexible epoxy, green code]), and XX (stainless clad bars), as illustrated in Table 3.

Table 3. Name Code and Environmental Conditions Used During Phase I

Type of Dowel	**Identification of the Specimens**	
	Hot Room (40–43ºC)	**Cold Room (4ºC)**
Carbon Steel	RS-4, RS-5, RS-6	RS-7, RS-8, RS-9
Stainless Hollow	SS-4, SS-5, SS-6	SS-7, SS-8, SS-9
Epoxy-coated	EX-4, EX-5, EX-6	EX-7, EX-8, EX-9
Clad	XX-4, XX-5, XX-6	XX-1, XX-2, XX-3

3.1.1 Half-Cell Potential and Linear Polarization Resistance

Figure 12 through Figure 19 show the measured half-cell potentials with time for the four types of dowels investigated in the first phase of this study. As can be observed in Figure 12, for two of the three replicates of the carbon steels at 40–43ºC, the potentials moved to the active corrosion region lower than -350 mV, indicating a 90 percent probability of corrosion as described in Table 1) after about 75 days. For Specimen RS-5, the potentials were more negative than -350 mV from nearly the beginning of the test.

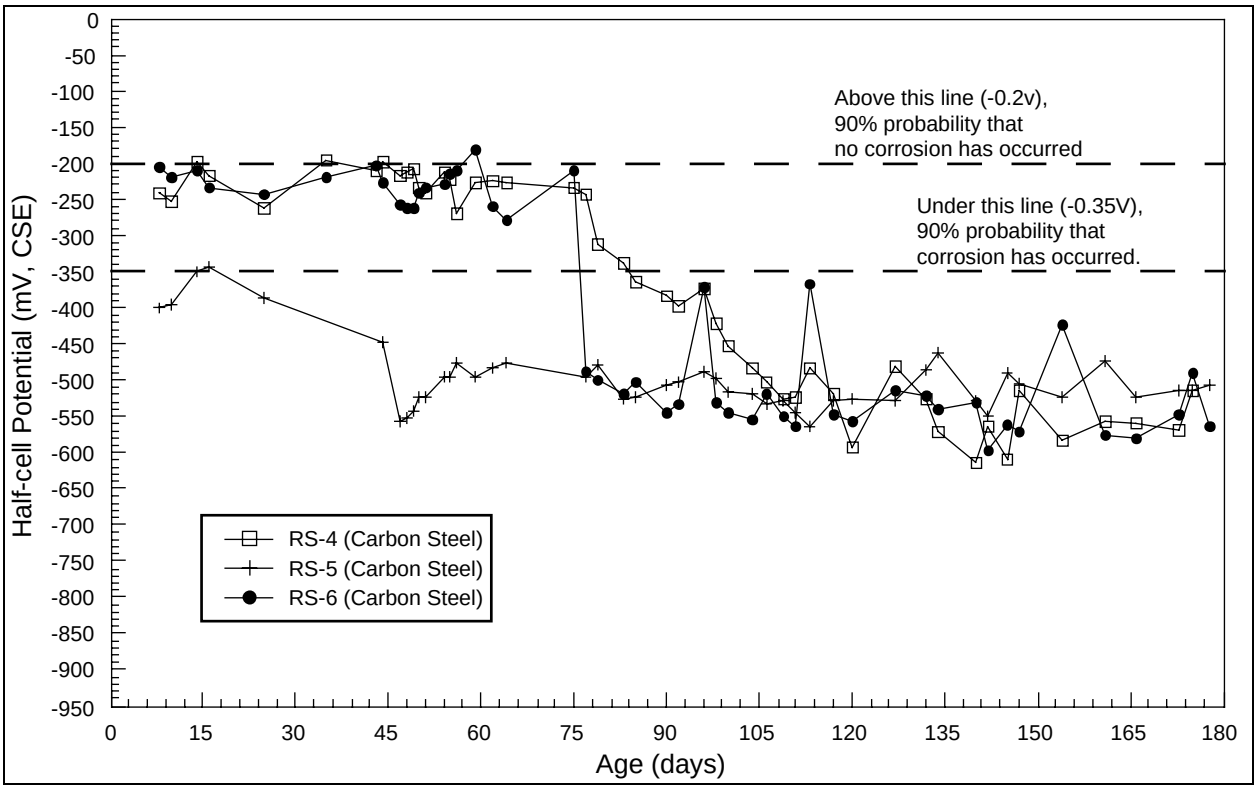

Figure 12. Half-cell potentials of carbon steel bars in chloride ponding at 40–43ºC.

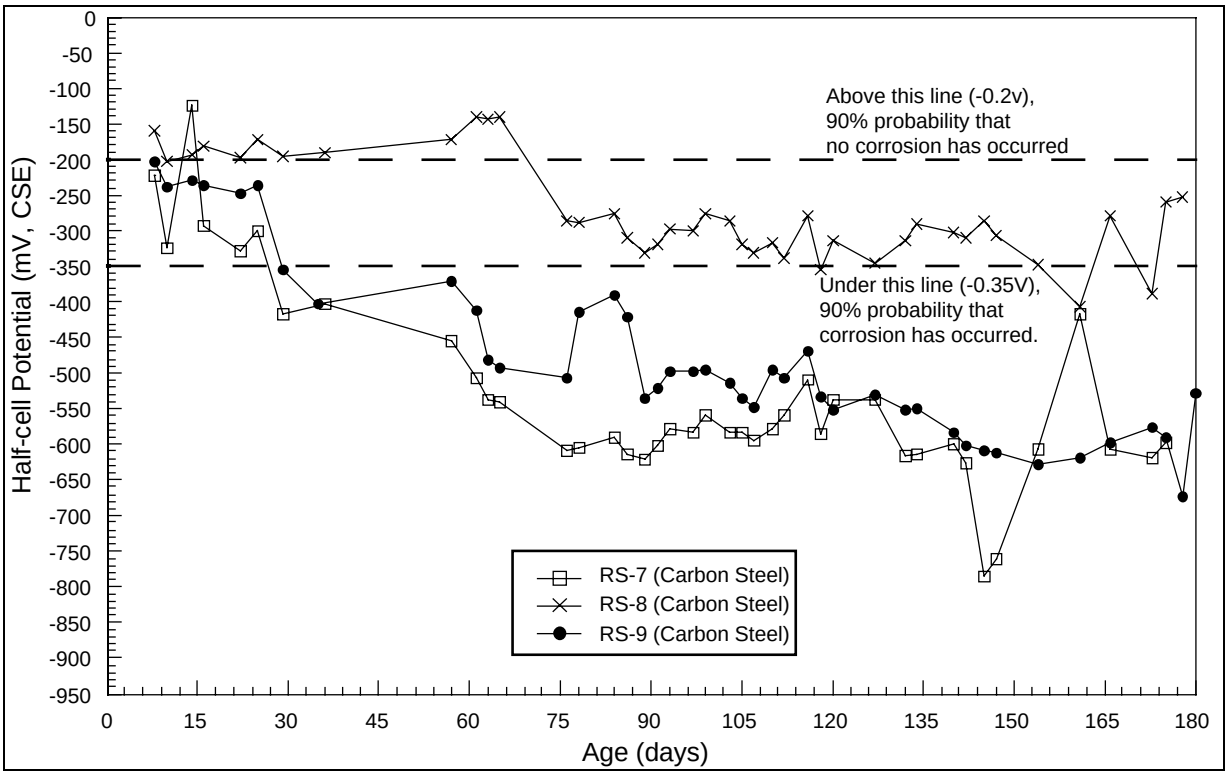

Figure 13. Half-cell potentials of carbon steel bars in chloride ponding at 4.4ºC.

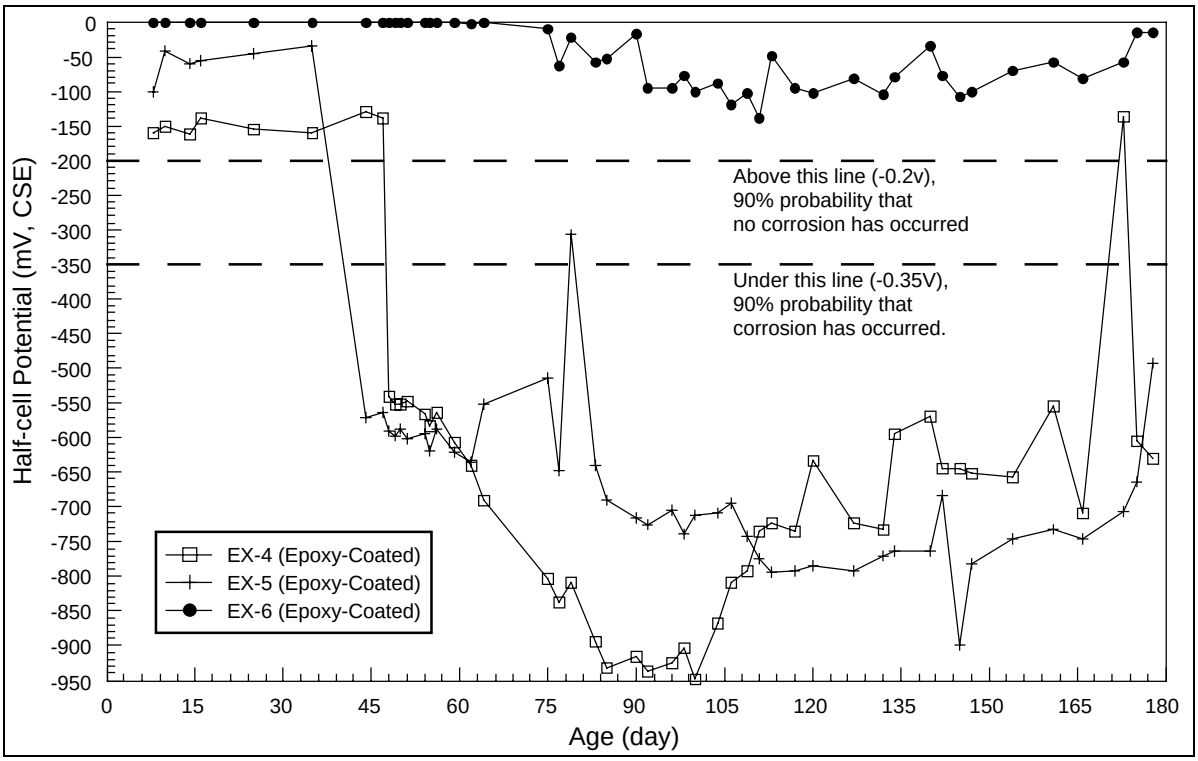

Figure 14. Half-cell potentials of epoxy-coated bars in chloride ponding at 40–43ºC.

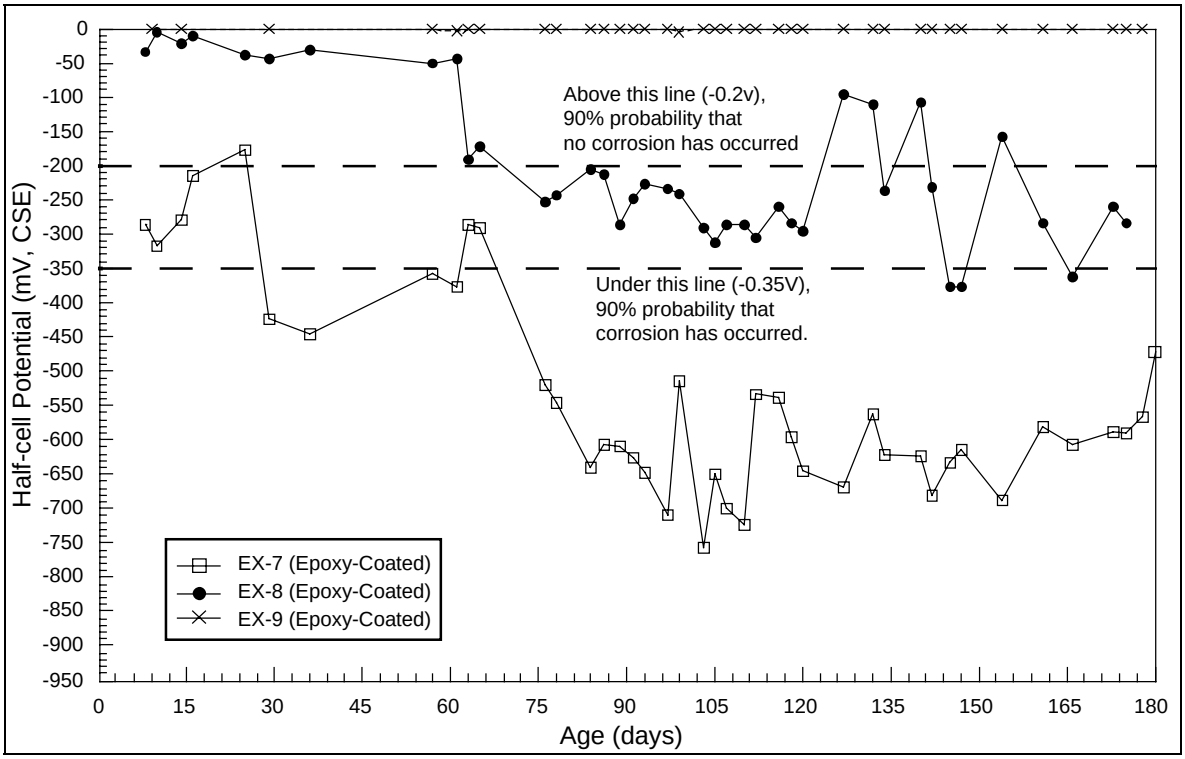

Figure 15. Measured potentials of epoxy-coated bars in chloride ponding at 4.4ºC.

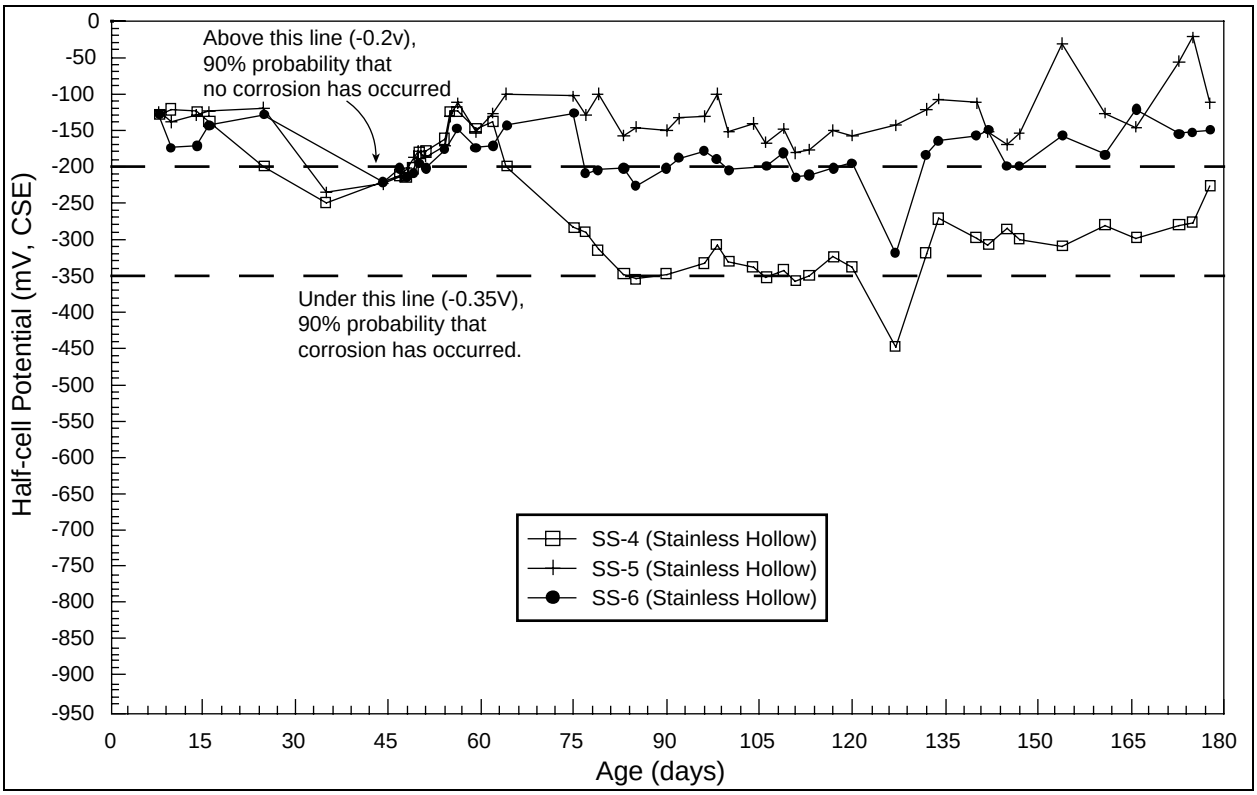

Figure 16. Half-cell potentials of stainless hollow steel bars in chloride ponding at 40–43ºC.

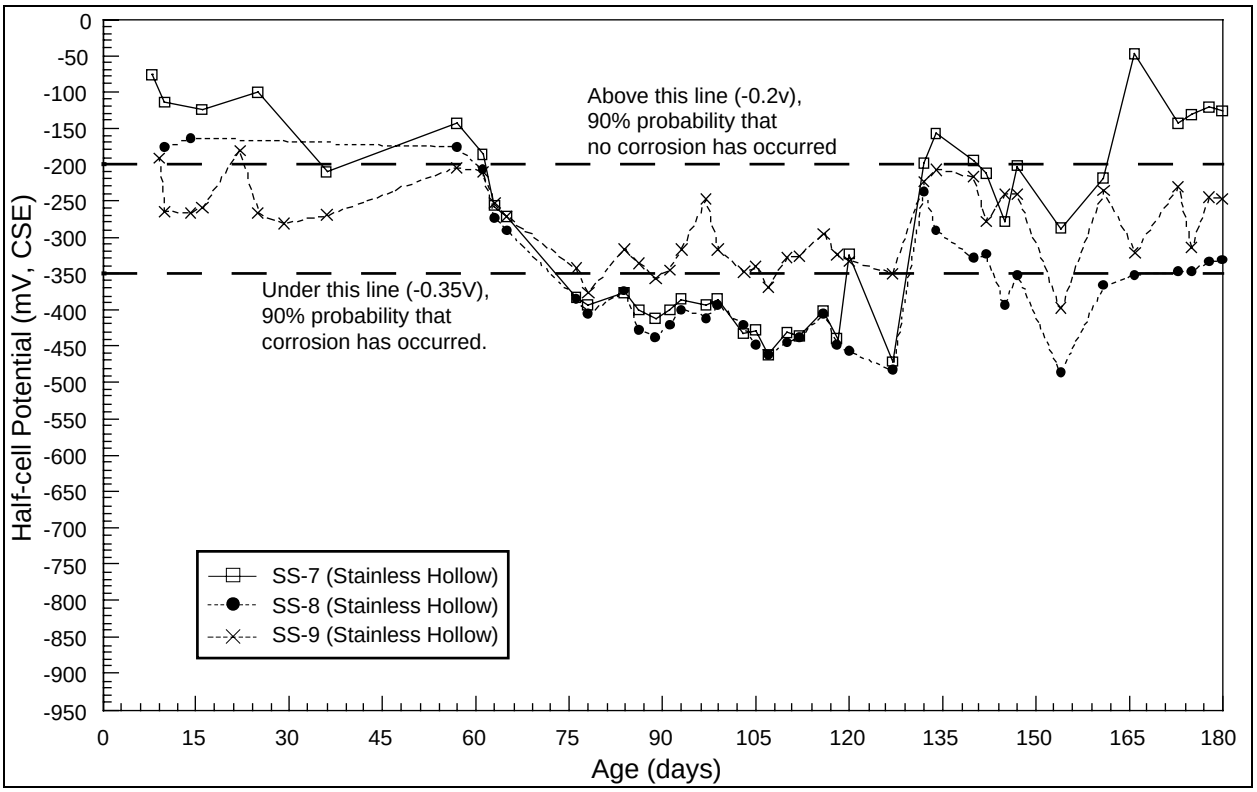

Figure 17. Half-cell potentials of stainless hollow steel bars in chloride ponding at 4.4ºC.

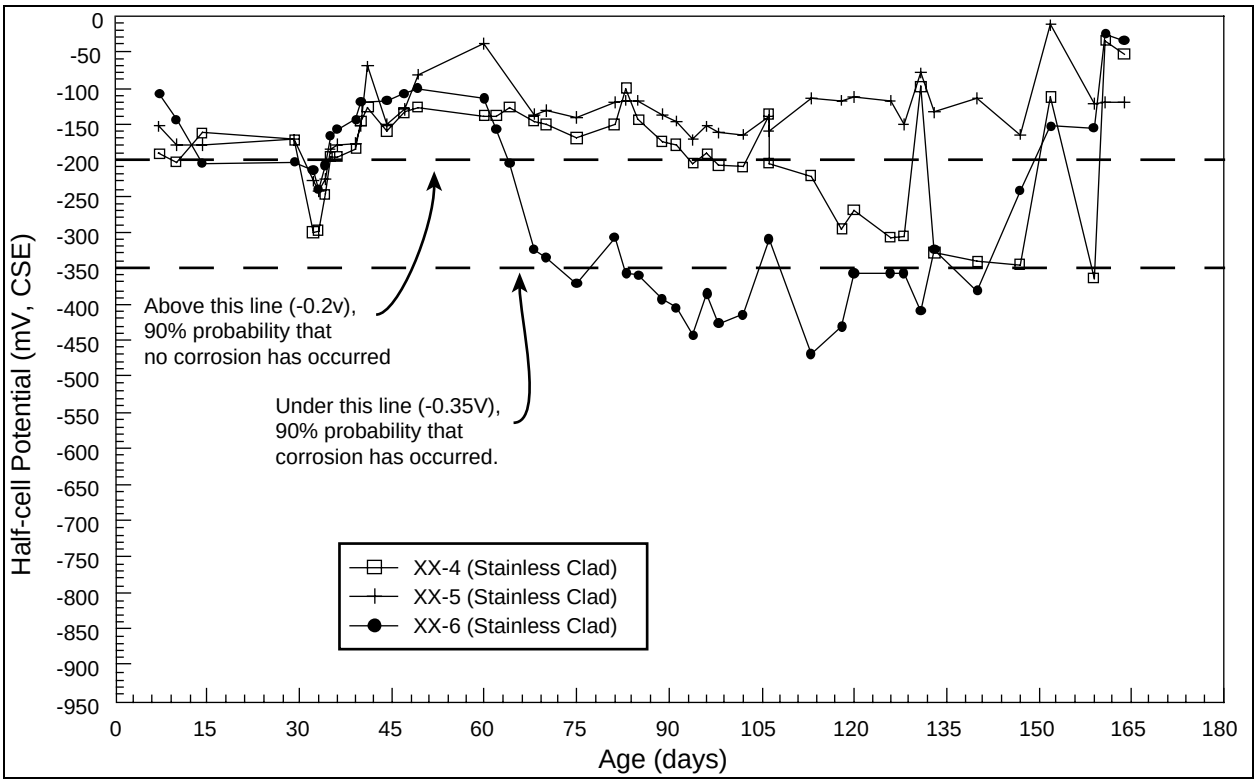

Figure 18. Half-cell potentials of stainless clad steel bars in chloride ponding at 40–43ºC.

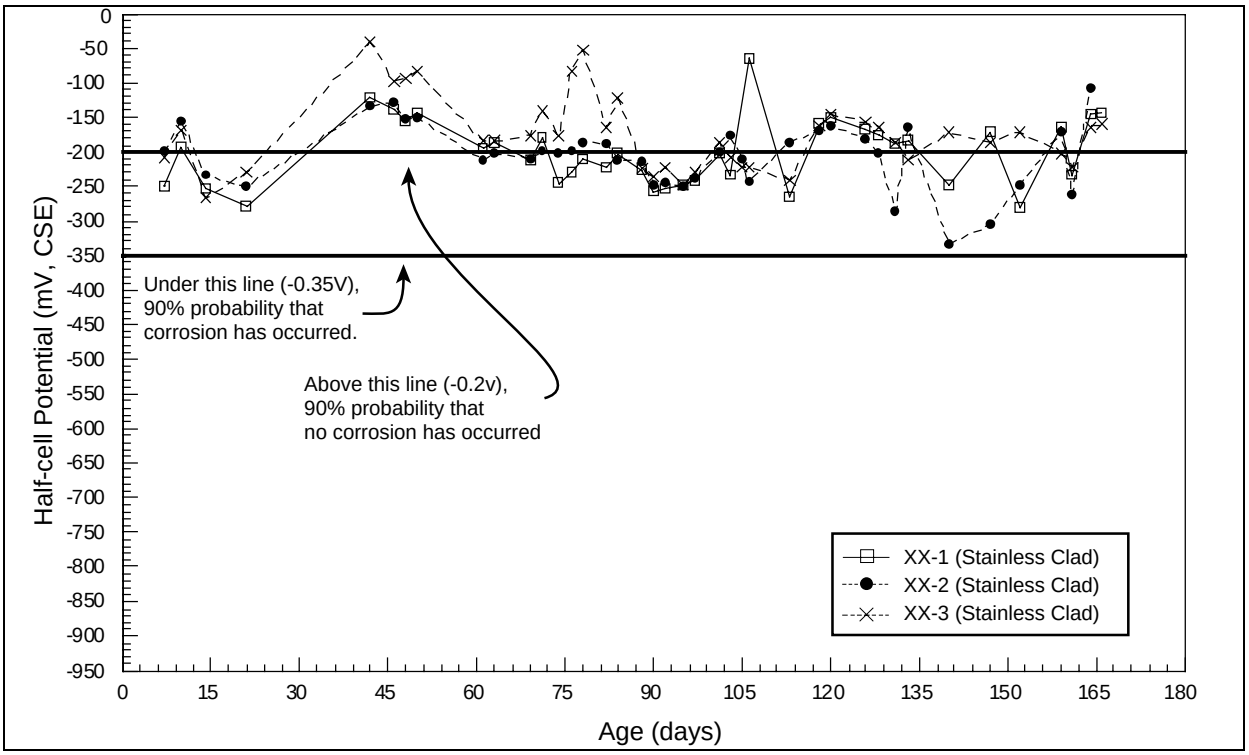

Figure 19. Half-cell potentials of stainless clad steel bars in chloride ponding at 4.4ºC.

As discussed in Section 1.1.1, compared to reinforcing steel in concrete structures in which the steel is completely encased in concrete, the initiation period may be greatly reduced in the case of steel dowels due to the easier access of aggressive agents to the bars.

At 4.4ºC (Figure 13), potentials moved to the active corrosion zone after about 30 days for RS-7 and RS-9, and not until 75 days for RS-8. It is interesting to notice that for some specimens corrosion was initiated earlier for carbon steels in the 4.4ºC room than those in 40–43ºC. The reason may be the difference in oxygen availability at different temperatures. The higher the temperature, the lower the oxygen solubility is in water. For instance, oxygen solubility in saltwater is about 11.7 mg/L at 4ºC, and the value drops to 6.5 mg/L at 30ºC.

It is important to mention that the polystyrene foam sheet used to create the joints was removed after 30 days of age. After the polystyrene sheet was removed, corrosion was immediate for the carbon steel in the 4.4ºC room, which indicates that the pavement joint is the dominant access of chloride, oxygen, and water to the dowel surface. This suggests that joint sealing may potentially reduce the likelihood of or retard the rate of corrosion of dowels by limiting access of corrosive solutions. However, joints are typically only sealed at the surface and corrosive solutions may be able to enter the joint from the sides and bottom of the joint in addition to the surface.

For the epoxy-coated steel bars at high temperatures (40–43ºC) (see Figure 14 and Figure 15), the measured potentials for Specimens EX-4 and EX-5 experienced an abrupt decrease at around 40 days to approximately -650 mV in the high-corrosion risk region. Specimen EX-6, on the other hand, measured zero and stayed in the inactive region throughout the test.

For cold temperature specimens (4ºC), the measured potential of Specimen EX-9 remained at zero throughout the test, possibly indicating absence of defects in its epoxy coating or perhaps some problem with the electrical connection at the dowel. The potentials of Specimen EX-7 oscillated within the intermediate corrosion risk (uncertain) range, while Specimen EX-8 entered the high-corrosion risk region (< -350mV) at around 70 days. Note that, in Phase I of the study, the epoxy coating was not checked for defects before casting. This procedure was adopted in the second phase, as described in Section 2.2.

Both stainless hollow and stainless clad dowels (Figure 16 to Figure 19) generally had measured potentials above the -350 mV line at both test temperatures, indicating low probability of corrosion.

In the first phase, emphasis was placed on the determination of the initiation period based on the measurement of half-cell potentials over time. However, an LPR test to evaluate corrosion rate was also performed on the carbon and stainless steel dowels. Figure 20 shows the results obtained (specimens were stored at 40–43ºC). The slope of a polarized potential and corresponding current supply curve is the polarization resistance, *Rp*. Its value is inversely proportional to the corrosion rate (*i*) indicated in Stern-Geary relationship $i = B/Rp$, where *B* is a constant with the value from 25 mV to 56 mV. The corrosion rate of carbon steel can be 10 times as high as that of the stainless steel. Note that the corrosion rate of RS4 was low while its half-cell potential was located in the active corrosion region (<-350mV), indicating that the half-cell potential measurement is not a quantitative method. Results from the other two specimens (RS5 and RS6) matched the half-cell potential measurements well.

3.1.2 Visual Inspection

At the end of six months, the concrete beams were broken open and the dowels were retrieved and inspected. Figure 21 shows one of the concrete beams at the moment the dowel was being retrieved.

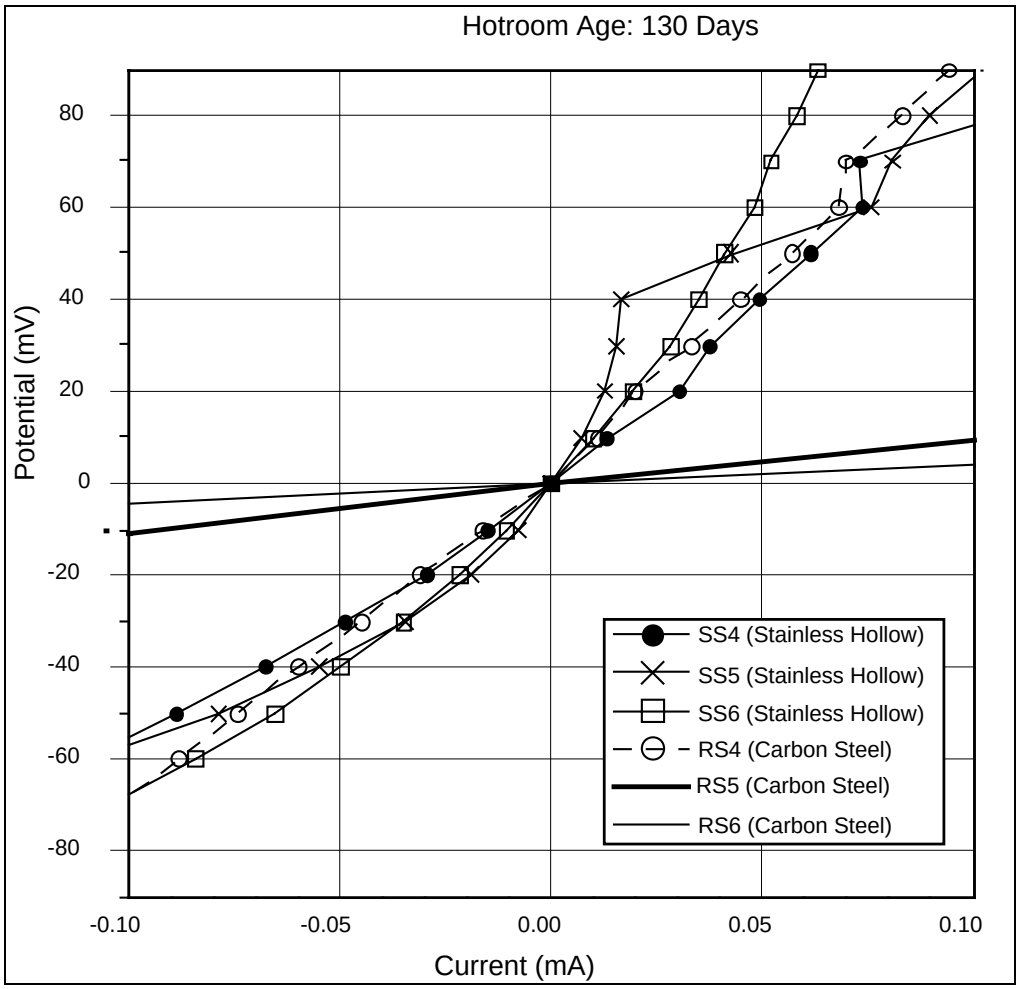

Figure 20. Linear polarization of the carbon and stainless steels at 40–43ºC.

For the carbon steels exposed to chloride ponding, corrosion products were distributed along the length and perimeter of the bars for both the cold and hot conditions, as shown in Figure 22. The epoxy-coated bars had localized corrosion mostly at the ends of the bars where the coating is the most vulnerable to damage. All the epoxy-coated bars exposed to Chloride ponding, except EX-9, were corroded at the ends, as shown in Figure 23. The results matched the half-cell potential in the sense that once corrosion occurred and the coating was lifted, the measured potential was not zero anymore. No visible corrosion was found on either stainless steel hollow bars or stainless clad bars, as can be observed in Figure 24 and Figure 25.

Figure 21. Extraction of dowels for visual inspection.

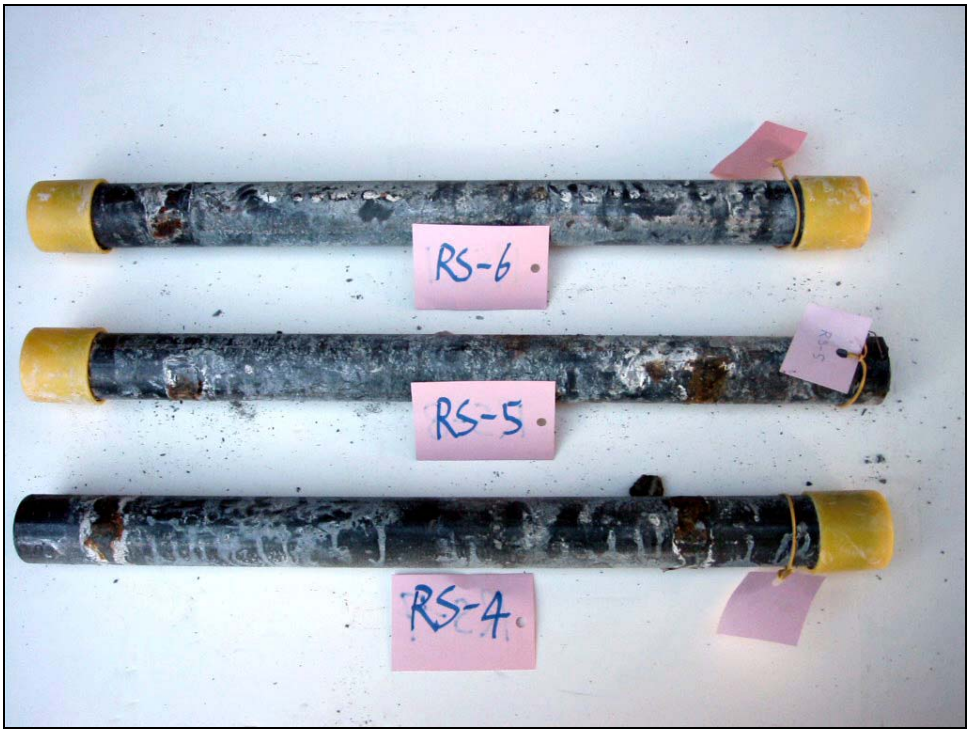

Figure 22. Corrosion along the carbon steel bars.

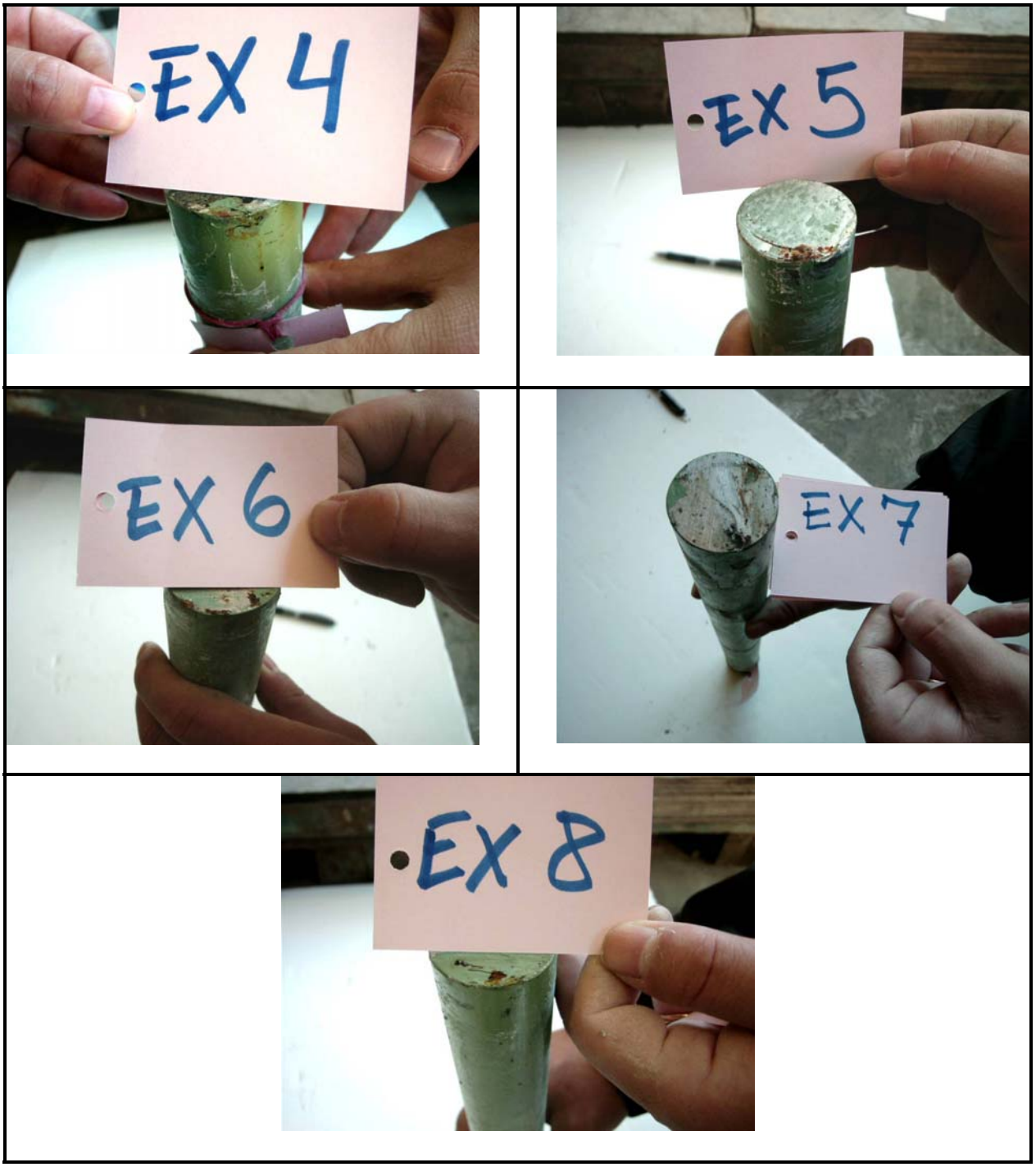

Figure 23. Corrosion on the epoxy-coated bars.

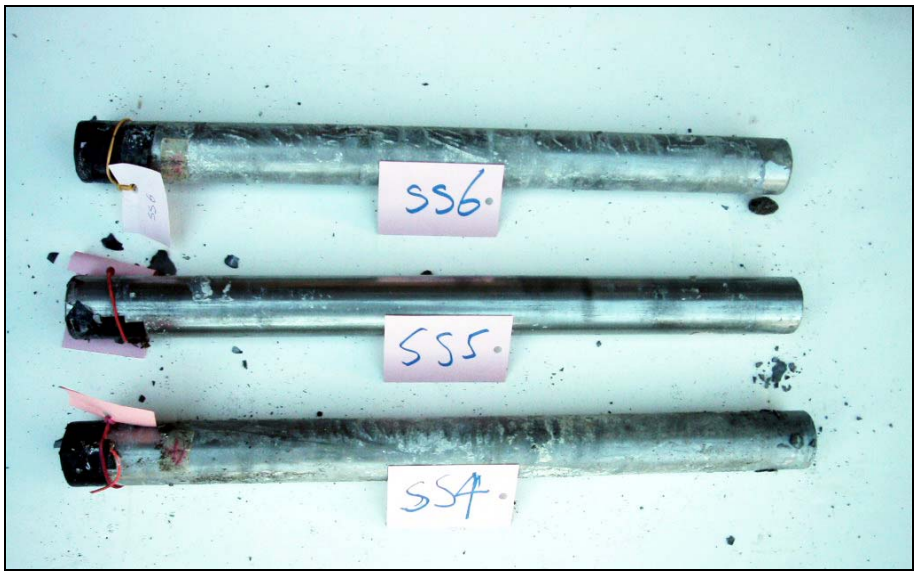

Figure 24. Appearance of stainless steel hollow bars after tests.

Figure 25. Appearance of stainless clad bars after tests.

3.2 Phase II Results

This section presents the results obtained in the second phase of the research, in which half-cell potential tests, Linear Polarization Resistance curves, visual inspections, chloride analyses and microscopic investigation were obtained at room temperature on the seven types of steel dowels investigated [carbon steel, microcomposite steel, stainless hollow, stainless clad, carbon steel coated with flexible epoxy (green colored), and carbon steel coated with non-flexible epoxies (purple and gray colored)].

3.2.1 Half-Cell Potential and Linear Polarization Resistance

In this section, individual graphs present the LPR results for each type of dowel investigated. The plots present the average results of four replicates normalized with respect to the half-cell value. Current density ($\mu A/cm^2$) and potential (mV) are given as variations from the values obtained at equilibrium, half-cell potential. Normalizing the data facilitates comparison among the different samples. Non-normalized results for each type of steel dowel are presented in Appendix B.

As described in Section 2.1, the slope of the curves ($\Delta E/\Delta i$) provides the value of the polarization resistance, *Rp*. Notice that the greater the slope, the more difficult the charge transfer across the metal/electrolyte interface, and therefore the corrosion current density is lower and, consequently, the corrosion reaction rate is slower.

Figure 26 to Figure 29 present the Linear Polarization Resistance plots for the carbon steel, microcomposite, hollow stainless steel, and stainless steel-clad bars, respectively. It can be seen that for the same variation in potential, carbon steel bars exhibit a much larger variation in the corrosion current density compared to the other materials. Consequently, the carbon steel samples will exhibit a smaller slope, smaller polarization resistance, and larger corrosion rate, followed by microcomposite steel, stainless steel-clad, and stainless steel hollow, respectively.

Figure 30 through Figure 32 present LPR plots for the epoxy-coated bars, respectively non-flexible (purple and gray) and flexible (green) epoxy coatings. Note that the LPR results obtained for the epoxy-coated bars are not to be interpreted quantitatively. In coated specimens, corrosion is not uniform. Rather, it is concentrated at localized defective areas (such as pinholes, voids, etc.). Given that epoxy is an electrical insulator, polarization only occurs at these defective areas, which cannot be accounted for in the calculation of the polarization resistance term. For this reason, R_p and i_{corr} calculations for epoxy-coated bars are not presented here.

As mentioned in Section 2, it has been assumed that the polarized area corresponds to the surface of the dowels exposed to the NaCl solution inside the fabricated joints. If the polarized area decreases in size, the corrosion current density (given in $\mu A/cm^2$) will increase.

The surface area used in the current density calculations was 7.18 cm^2, which corresponds to the dowel bar circumference (119.69 mm) multiplied by the thickness of the joint (6 mm). The microcomposite steel dowels had smaller diameter (1.25 in. or 31.75 mm), and the polarized area was thus 5.98 cm^2.

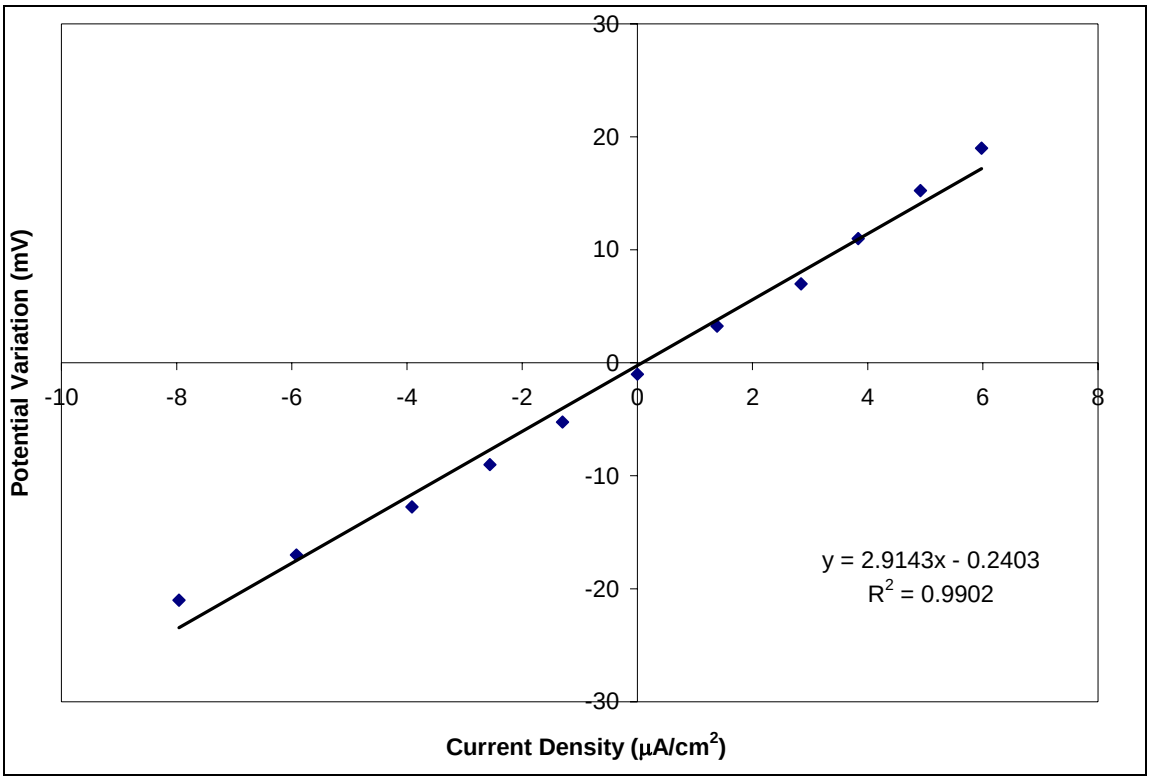

Figure 26. Linear Polarization Resistance results for carbon steel dowels.

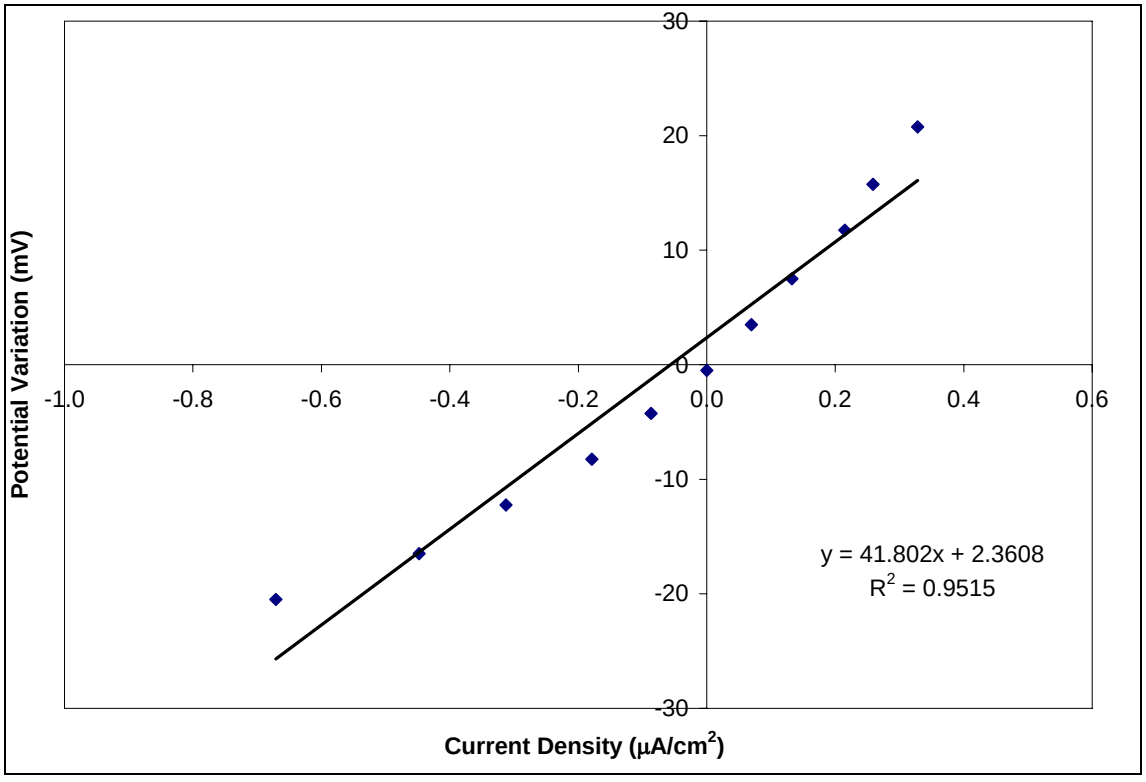

Figure 27. Linear Polarization Resistance results for microcomposite steel dowels.

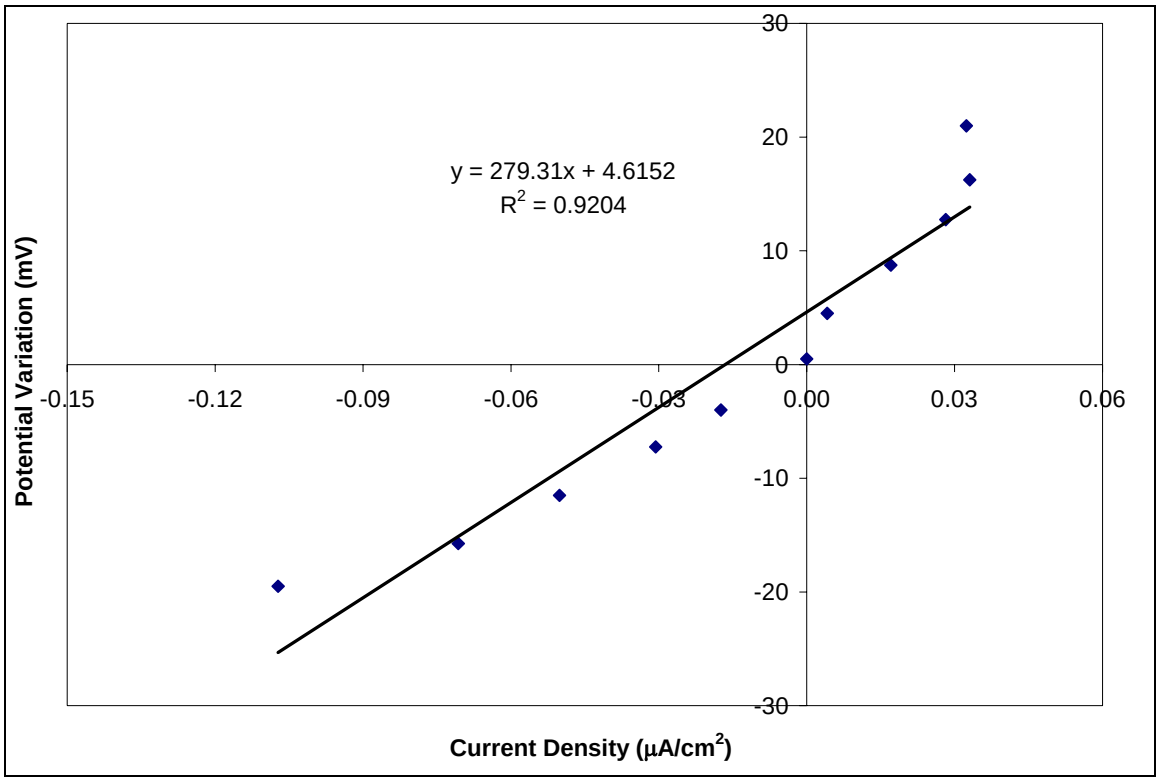

Figure 28. Linear Polarization Resistance results for stainless steel-clad dowels.

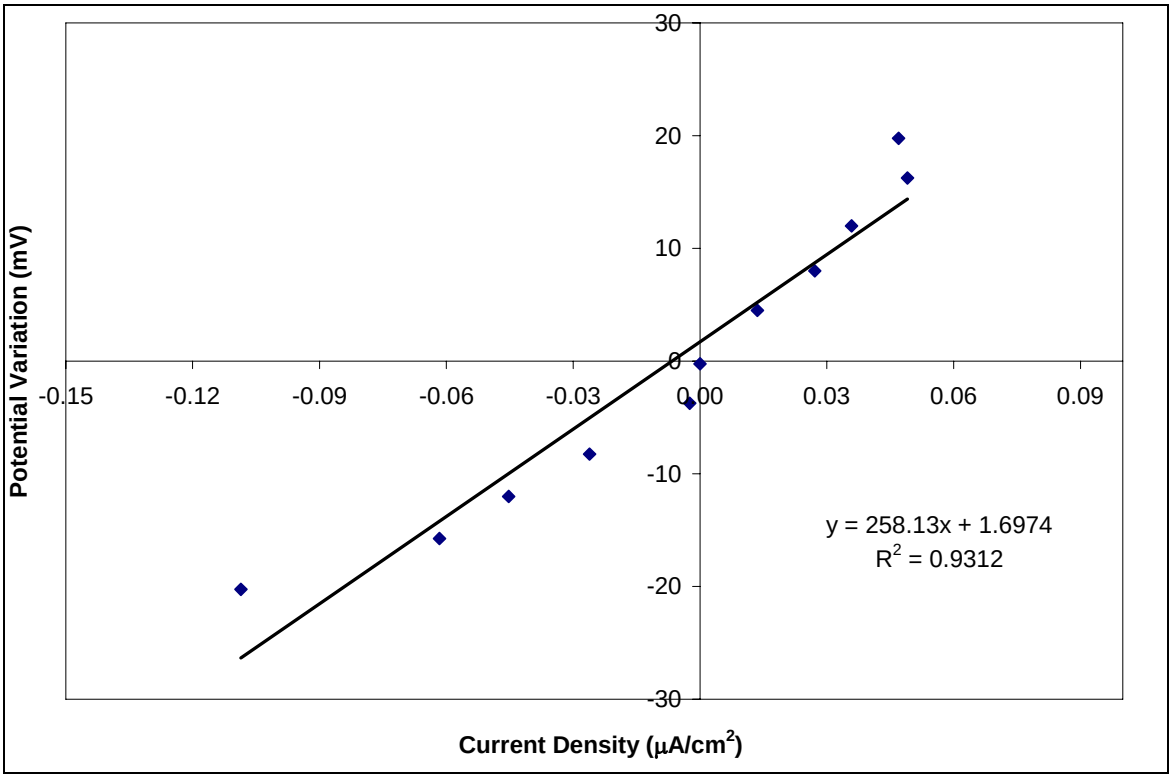

Figure 29. Linear Polarization Resistance results for stainless steel hollow dowels.

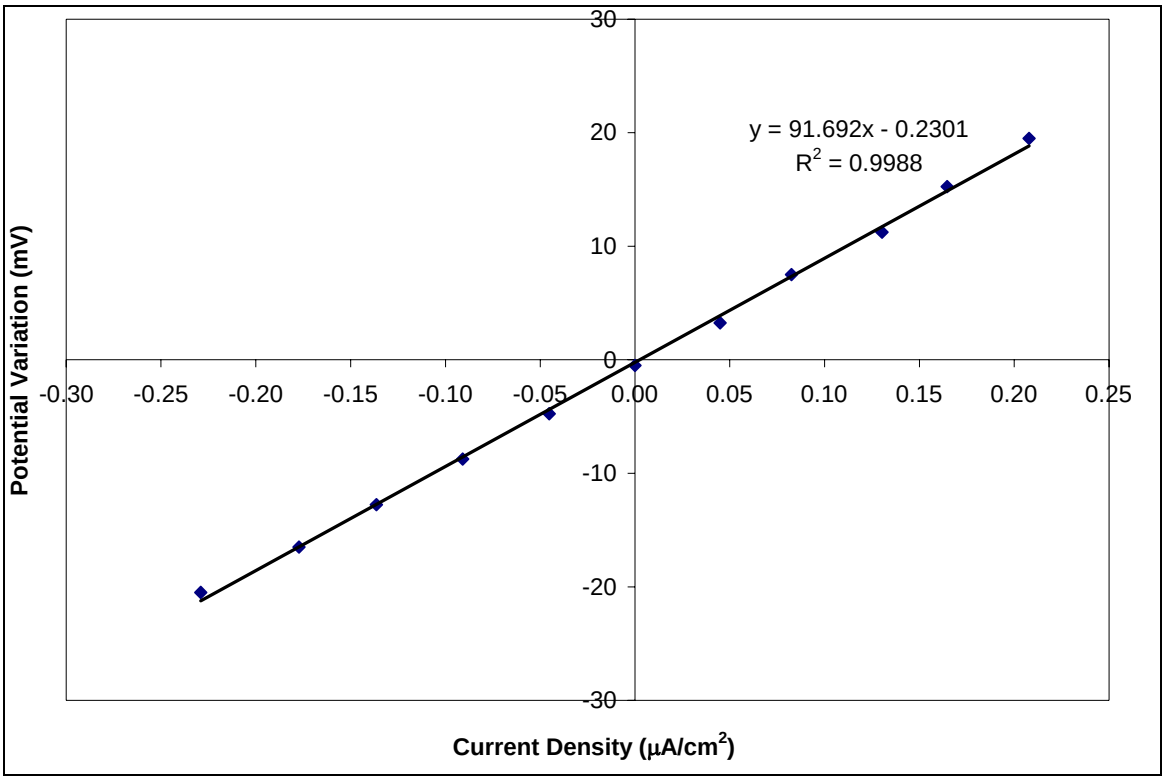

Figure 30. Linear Polarization Resistance results for non-flexible purple epoxy-coated dowels.

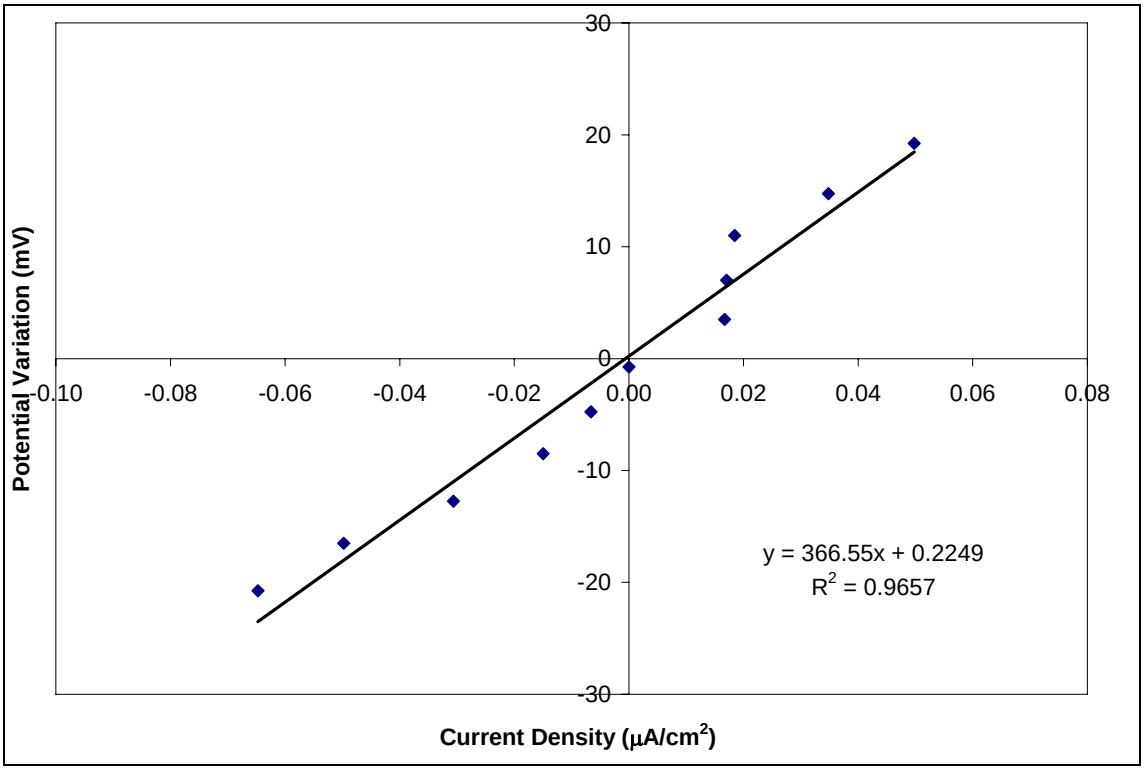

Figure 31. Linear Polarization Resistance results for non-flexible gray epoxy-coated dowels.

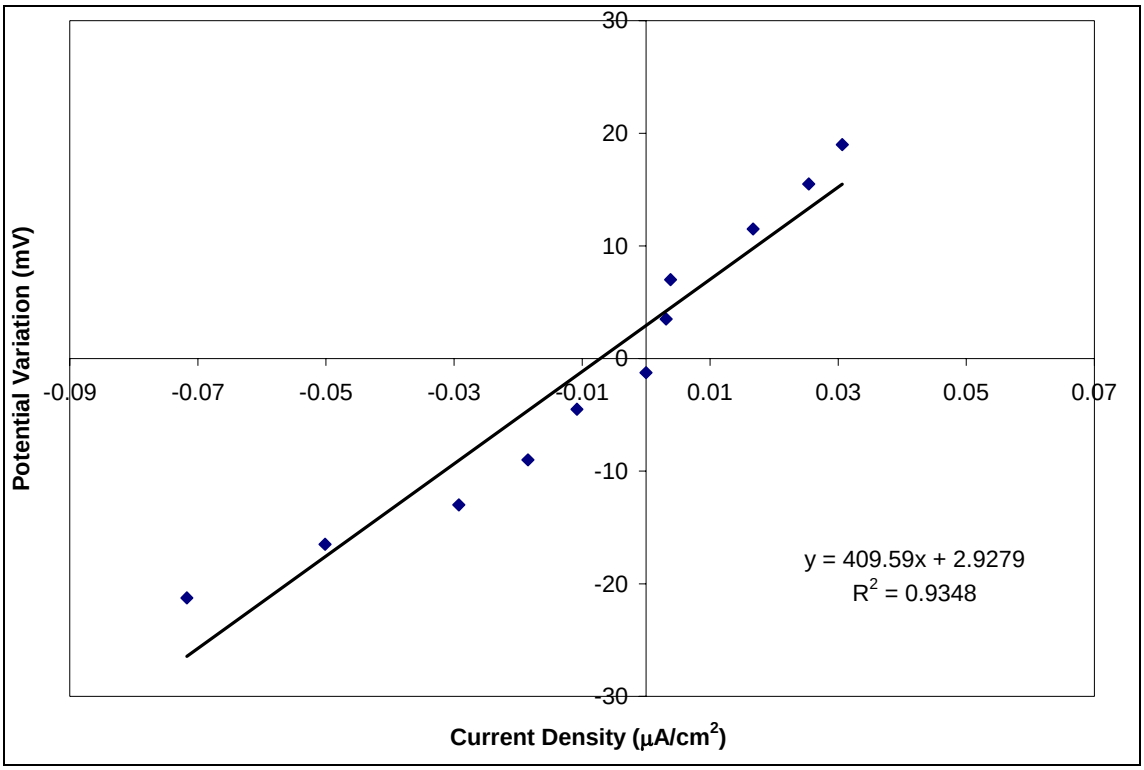

Figure 32. Linear Polarization Resistance results for flexible green epoxy-coated dowels.

The fact that electrical contact can be made between the reference electrode (copper/copper sulfate) and the working electrode (steel dowel), and that a half-cell potential can be measured for epoxy-coated bars, indicates the presence of defects in the coating. The Linear Polarization Resistance results may indicate the presence of corrosion in the defective areas, but an evaluation of the extent of corrosion must rely on visual inspections and microscopic investigations.

Figure 33 and Figure 34 present a comparison of the Linear Polarization Resistance results of various dowels. It can be easily seen that the carbon steel specimens performed much worse than the other dowels tested. On the other hand, it can be observed that the stainless steel hollow bars exhibited the best performance, followed by stainless steel-clad and microcomposite steel dowels. Table 4 summarizes the individual results obtained for each sample including half-cell potential, polarization resistance *(Rp)* and corrosion current density (i_{corr}). (Plots with calculations are presented in Appendix B.) The criteria used to interpret the results presented in Table 4 are per ASTM C876 and ASTM G59 and are presented in Table 1 and Table 2, respectively. Figure 35 presents a comparative summary of Linear Polarization Resistance and current density results.

Regarding the half-cell potential values, note that the stainless steel hollow and stainless steel-clad specimens are, on average, located in the uncertain corrosion region, while all the other samples are in the active corrosion region (refer to Table 1).

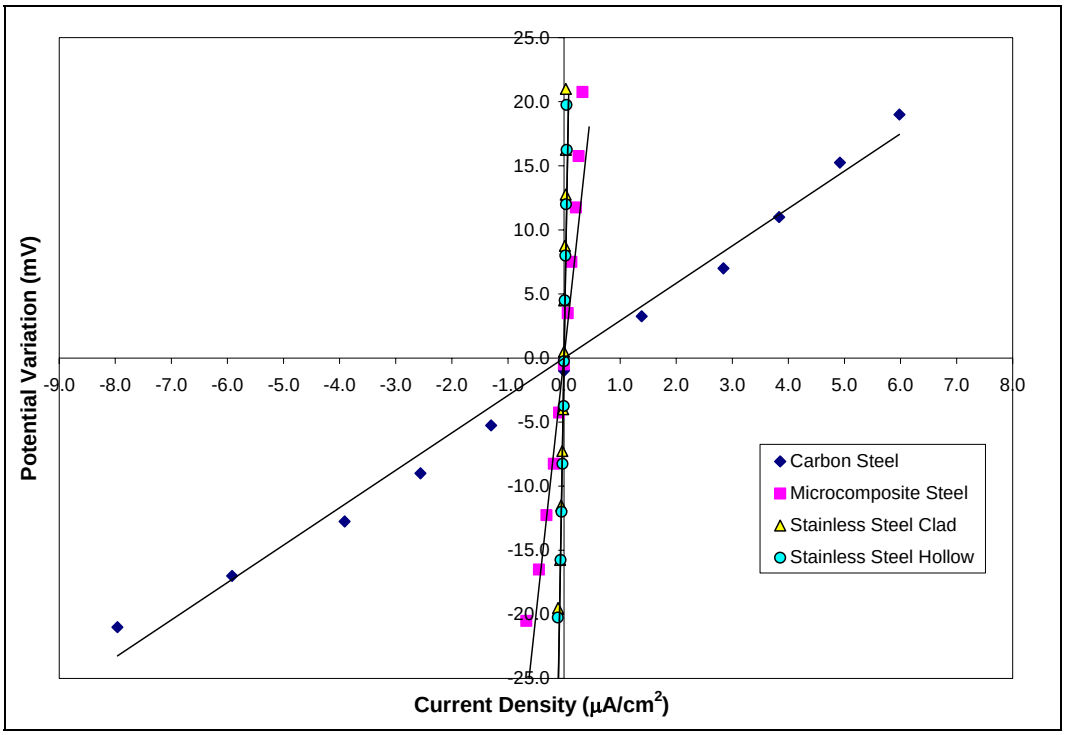

Figure 33. Summary plot showing the variation of potential and current density about the half-cell potential, for different dowels.

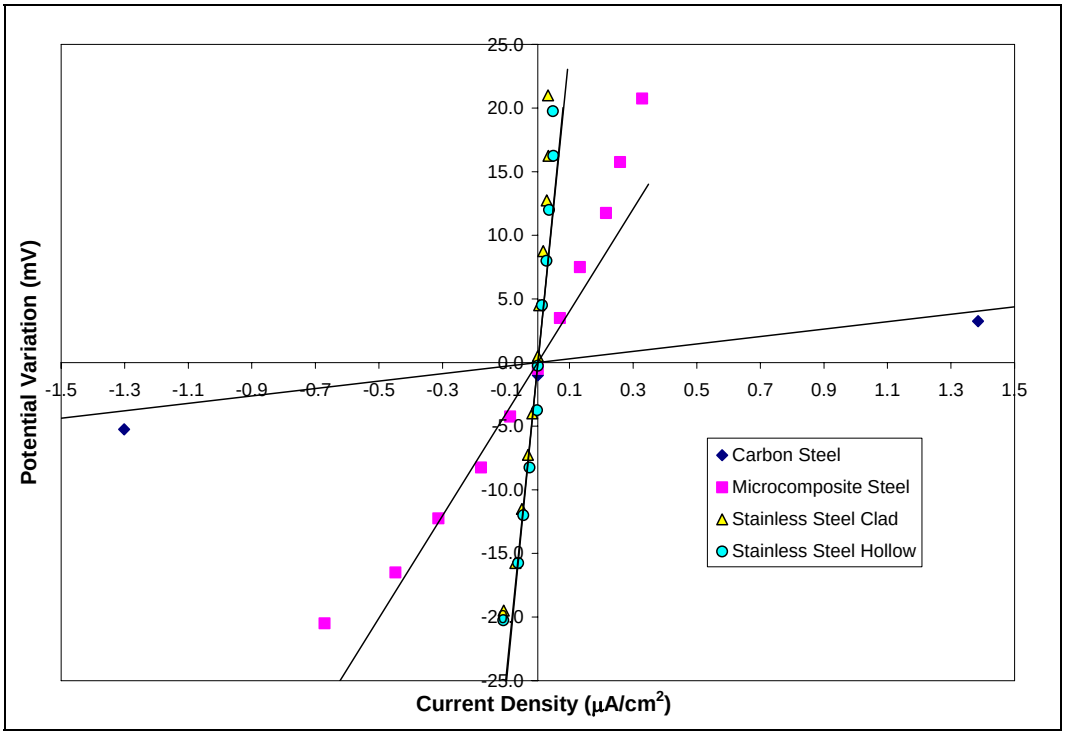

Figure 34. Detail of the region around the half-cell potential. The greater the slope, the higher the corrosion resistance.

Table 4. Summary Results of Half-Cell Potential, Polarization Resistance, and Corrosion Current Density

Specimen #		Half-Cell Potential (mV)	Polarization Resistance *(Rp)*	Corrosion Current Density (i_{corr})
Carbon steel	1	-602	1544.3	16.84
	2	-640	6066.5	4.29
	3	-694	2568.2	10.12
	4	-629	5410.8	4.81
	Avg.	-641.3	3897.5	9.01
	Std. Dev.	38.6	2183.2	5.84
Micro-composite steel	1	-567	23495	1.11
	2	-571	23146	1.12
	3	-292	367410	0.07
	4	-278	124620	0.21
	Avg.	-427.0	134667.8	0.63
	Std. Dev.	164.1	162343.7	0.57
Stainless clad	1	-286	311560	0.08
	2	-179	249520	0.10
	3	-216	361130	0.07
	4	-345	216530	0.12
	Avg.	-256.5	284685.0	0.09
	Std. Dev.	73.8	64414.8	0.02
Stainless hollow	1	-210	229850	0.11
	2	-569	192840	0.13
	3	-193	481700	0.05
	4	-320	233050	0.11
	Avg.	-323.0	284360.0	0.10
	Std. Dev.	173.4	132819.5	0.03
Purple epoxy coating (non-flexible)	1	-476	-	-
	2	-582	-	-
	3	-464	-	-
	4	-811	-	-
	Avg.	-583.3	-	-
	Std. Dev.	160.8	-	-
Gray epoxy coating (non-flexible)	1	-630	-	-
	2	-405	-	-
	3	-648	-	-
	4	-597	-	-
	Avg.	-570.0	-	-
	Std. Dev.	112.0	-	-
Green epoxy coating (flexible)	1	-420	-	-
	2	-760	-	-
	3	-558	-	-
	4	-643	-	-
	Avg.	-595.3	-	-
	Std. Dev.	143.2	-	-

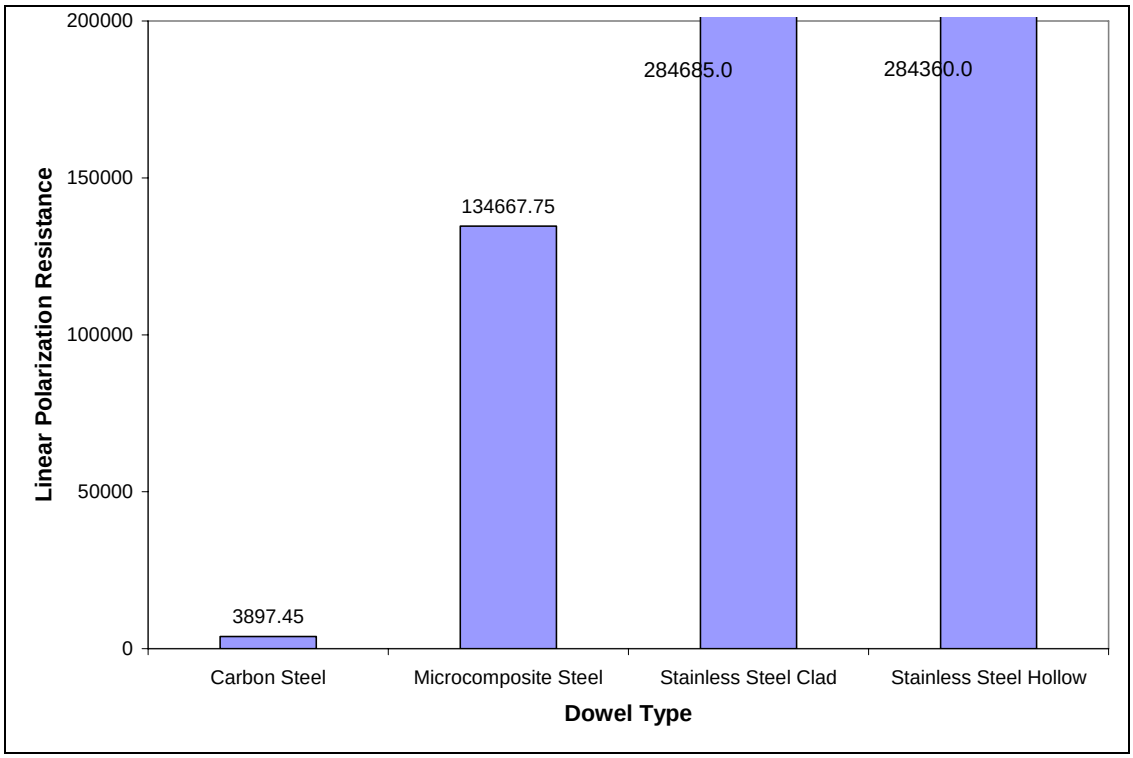

(a)

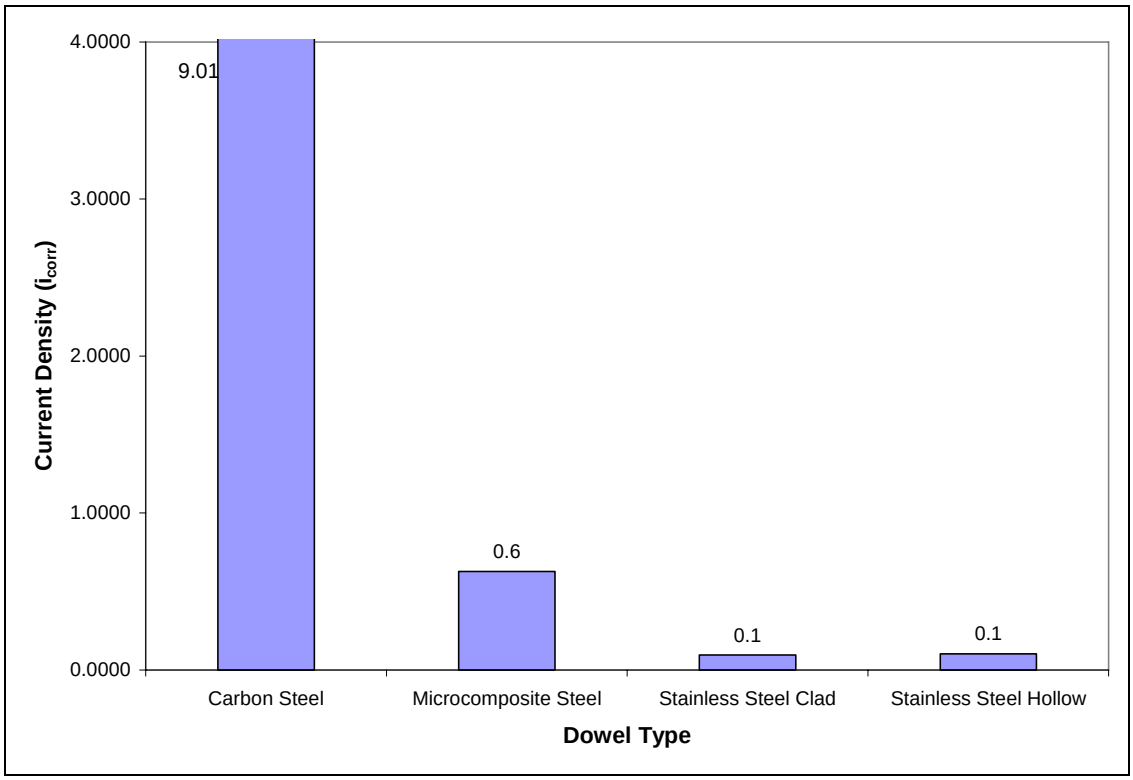

(b)

Figure 35. Comparative column plots showing average results of polarization resistance (*Rp*) and corrosion current density (i_{corr}) for non-coated dowels.

With respect to the average corrosion current densities, one can observe that the carbon steel dowels exhibit very rapid corrosion while microcomposite steel exhibits a moderate level of corrosion. Stainless steel-clad and stainless steel hollow dowels proceed at a low corrosion rate (refer to Table 1 and Table 2 for criteria used). Individual results show that two out of four microcomposite samples were in the "uncertain" corrosion region (as per half-cell potential results), and presented low corrosion rate.

The average values presented for the epoxy-coated bars also indicate a low corrosion rate and, in fact, visual inspection (Section 3.2.3) revealed no major signs of corrosion for these dowels, except at a few localized defective areas. However, LPR results for epoxy-coated bars cannot be interpreted quantitatively. As is further discussed in Section 3.2.4 (microstructural analysis), localized corrosion was identified at defects in the coating. Additional corrosion was also observed under the coating.

3.2.2 Statistical Analysis of Results

The Analysis of Variance (ANOVA) model was used to evaluate the results obtained and to verify if there is a statistically significant effect of the type of steel dowel on the parameters investigated. Basically, the Analysis of Variance table takes into account the effect of the factor(s) being studied and the variability of the experiments (i.e., the experimental error) to determine whether the results obtained are statistically significant at a confidence interval of 95 percent. The analysis is based on the so-called "F-test," in which the calculated value of the parameter F ("F_{calc}") is compared to the critical value "F_{crit}". If $F_{calc} > F_{crit.}$, it is said that the effect is statistically significant.

In the case of the research presented herein, the factor or independent variable being analyzed is the type of steel dowel, and the dependent variable is the experimental result obtained. Separated analyses were performed in order to evaluate the half-cell potential, Linear Polarization Resistance, and corrosion current density results as functions of the type of dowel. Table 5 through Table 8 present the ANOVA results obtained.

In these tables, *SS* means Sum of Squares, *df* is degrees of freedoms, and *MS* is the Mean Square. By comparing the F_{calc} and F_{crit} values obtained, one can observe that in all cases the type of steel dowel had a statistically significant effect ($F_{calc} > F_{crit}$) on the parameters studied.

Table 5. Analysis of Variance (ANOVA) of Half-Cell Potential Results of Non-Coated Samples

Material	**Count**	**Sum**	**Average**	**Variance**	**Std. Dev.**
Carbon steel	4	-2565	-641.3	1491.58	38.62
Microcomposite steel	4	-1708	-427.0	26920367	164.08
Stainless steel clad	4	-1026	-256.5	5449.67	73.82
Stainless steel hollow	4	-1292	-323.0	30064.67	173.39
ANOVA					
Source of Variation	***SS***	***df***	***MS***	F_{calc}	F_{crit}
Type of dowel	339527	3	113175.7	7.08	3.49
Error	191780	12	15981.65		
Total	531307	15			

Table 6. Analysis of Variance (ANOVA) of Half-Cell Potential Results of All Samples, Including Epoxy-Coated Bars

Material	**Count**	**Sum**	**Average**	**Variance**	**Std. Dev.**
Carbon steel	4	-2565	-641.3	1491.6	38.6
Microcomposite steel	4	-1708	-427.0	26920.7	164.1
Stainless steel clad	4	-1026	-256.5	5449.7	73.8
Stainless steel hollow	4	-1292	-323.0	30064.7	173.4
Purple (non-flexible) epoxy	4	-2333	-583.3	25864.9	160.8
Gray (non-flexible) epoxy	4	-2280	-570.0	12546.0	112.0
Green (flexible) epoxy	4	-2381	-595.3	20507.6	143.2
ANOVA					
Source of Variation	***SS***	***df***	***MS***	F_{calc}	F_{crit}
Type of dowel	541069	6	90178.14	5.14	2.57
Error	368535	21	17549.3		
Total	909604	27			

Table 7. Analysis of Variance (ANOVA) of Polarization Resistance (*Rp*) Results

Material	**Count**	**Sum**	**Average**	**Variance**	**Std. Dev.**
Carbon steel	4	15589.8	3897.45	4766409	2183.2
Microcomposite steel	4	538671	134667.8	2.64E+10	162343.7
Stainless steel clad	4	1138740	284685	4.15E+09	64414.8
Stainless steel hollow	4	1137440	284360	1.76E+10	132819.5
ANOVA					
Source of Variation	***SS***	***df***	***MS***	F_{calc}	F_{crit}
Type of dowel	2E+11	3	7.32E+10	6.08	3.49
Error	1+11	12	1.2E+10		
Total	4E+11	15			

Table 8. Analysis of Variance (ANOVA) of Corrosion Current Density (i_{corr}) Results

Material	**Count**	**Sum**	**Average**	**Variance**	**Std. Dev.**
Carbon steel	4	36.051	9.0127	34.162	5.845
Microcomposite steel	4	2.509	0.6273	0.320	0.566
Stainless steel clad	4	0.380	0.0949	0.000	0.021
Stainless steel hollow	4	0.413	0.1034	0.001	0.035
ANOVA					
Source of Variation	***SS***	***df***	***MS***	F_{calc}	F_{crit}
Type of dowel	229.78	3	76.59247	8.88	3.49
Error	103.45	12	8.621028		
Total	333.23	15			

3.2.3 Visual Inspection

After the electrical experiments were finished, one beam of each dowel type was cored at the joint in order to analyze the concentration of chlorides in the concrete surrounding the dowels. The remainder of the

specimens were cut open and broken to retrieve the dowels for visual inspection of the corroded areas. At this moment, specimens were selected for the microstructural SEM (Scanning Electron Microscope) analyses presented in Section 3.2.3.

Figure 36 through Figure 42 illustrate the general appearance of the inspected dowels. In general, carbon steel dowels exhibited generalized corrosion along the bars. Microcomposite steel dowels showed significantly less corrosion (as compared to carbon steel specimens). Stainless clad dowels had no visible corroded areas along the bars (corrosion was verified at the ends between the carbon steel core and outer stainless steel layer). Stainless hollow dowels showed basically no visible corrosion. Localized corrosion was verified in the defective regions on the epoxy-coated dowels, but no major signs of corrosion could be observed visually.

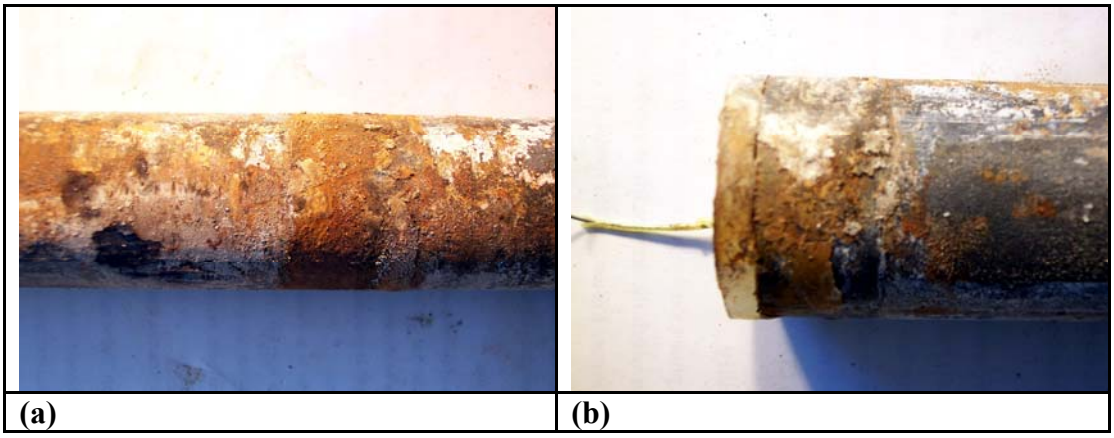

Figure 36. Carbon steel dowels. (a) Center region below joint; (b) End with electrical connection.

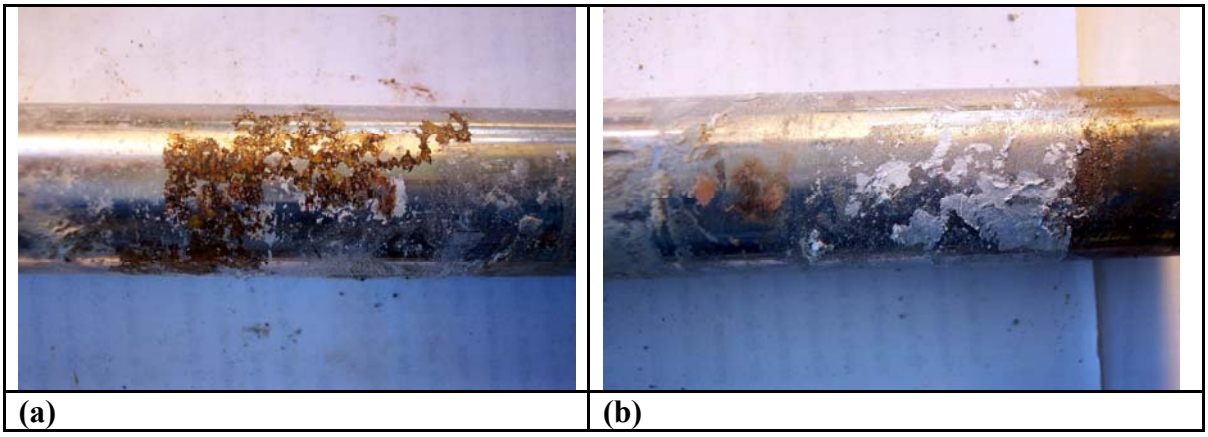

Figure 37. Microcomposite steel dowels. (a) General view of the center region below joint; (b) End region.

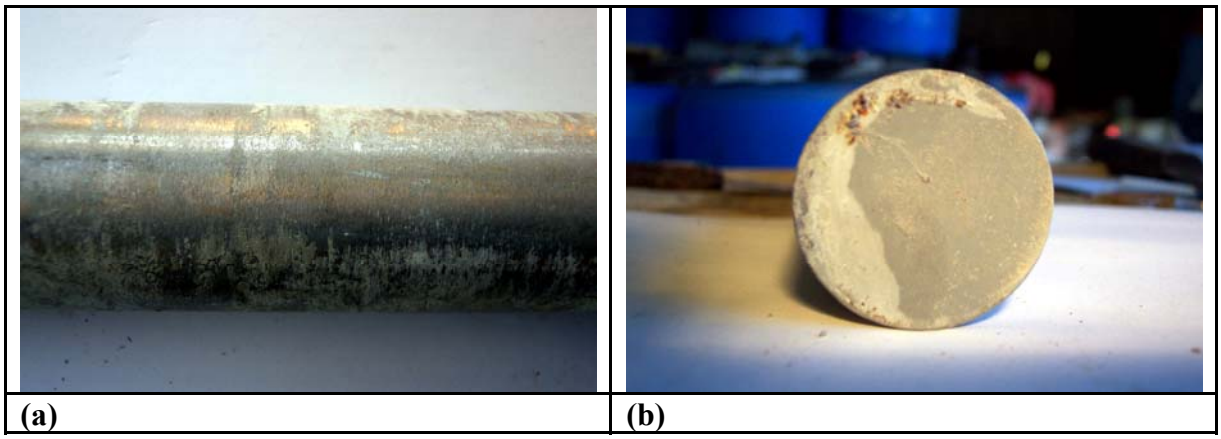

(a) (b)

Figure 38. Stainless clad dowels. (a) General view of the center region below joint; (b) End region showing corrosion between the carbon steel core and the stainless steel outer layer.

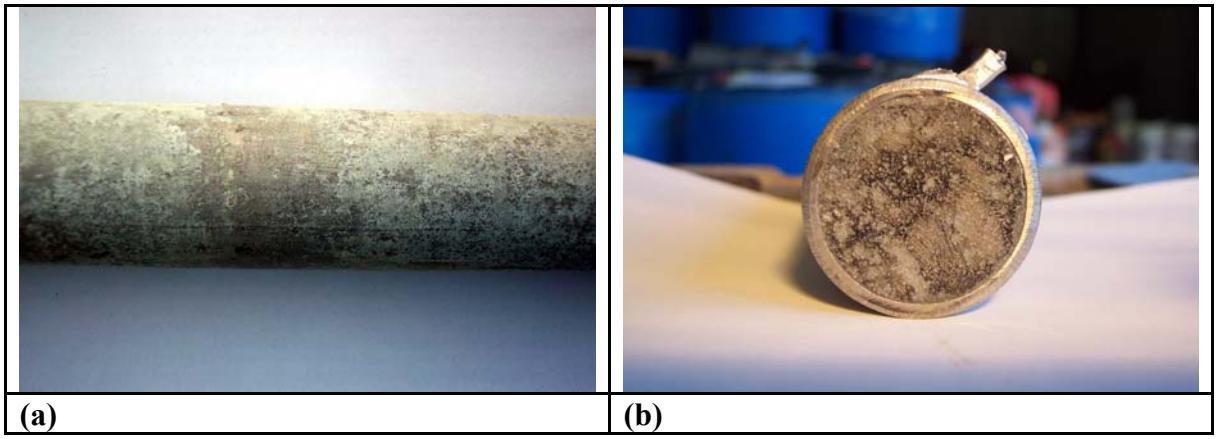

(a) (b)

Figure 39. Stainless hollow dowels. (a) General view of the center region below joint; (b) End region showing grouted core.

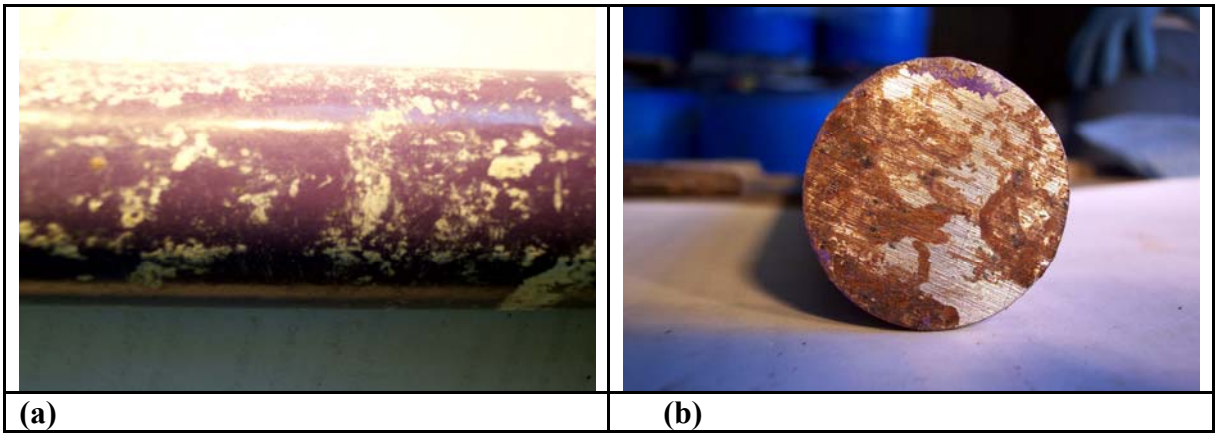

(a) (b)

Figure 40. Epoxy-coated dowel (purple). (a) General view of the center region; (b) Corrosion was verified at the end region, underneath the epoxy seal.

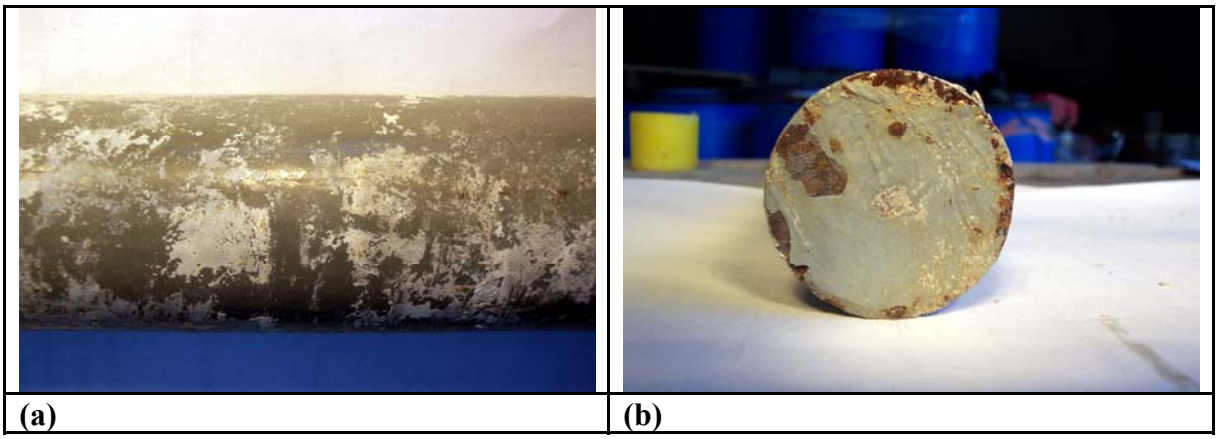

(a) (b)

Figure 41. Epoxy-coated dowel (gray). (a) General view of the center region; (b) Corroded edges at the end of dowels.

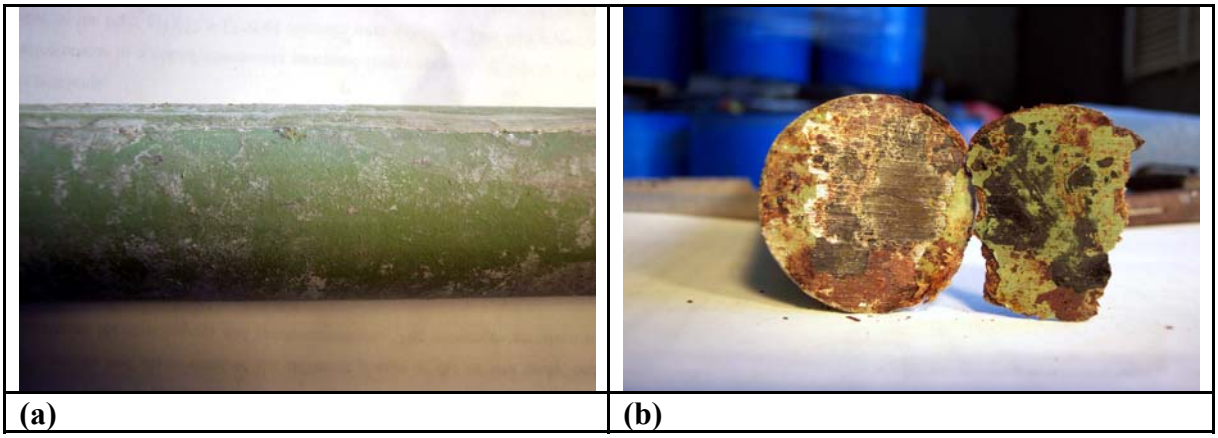

(a) (b)

Figure 42. Epoxy-coated dowel (green). (a) General view of the center region; (b) Corroded edges and corrosion underneath coating at the end of dowels.

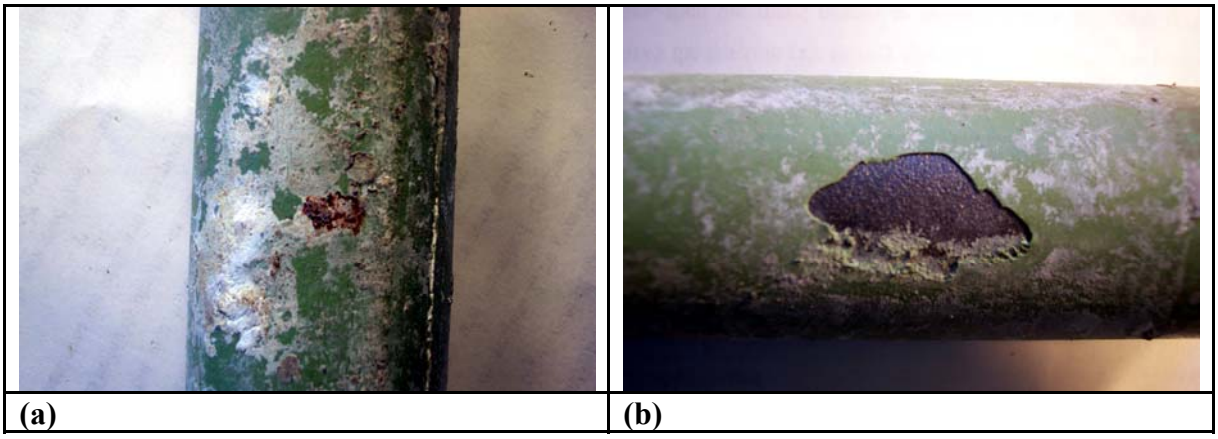

(a) (b)

Figure 43. Corrosion product concentrated in a defective area in the epoxy coating (a); part of the epoxy coating was removed in order to observe the state of the carbon steel beneath the coating (b).

As seen in Figure 36 through Figure 42, the carbon steel samples were heavily corroded. The microcomposite steel dowels exhibited less corrosion. The stainless steel-clad and stainless steel hollow dowels showed essentially no visible signs of corrosion. Defects were observed in the epoxy-coated bars and, as expected, localized corrosion in the defective regions was verified.

3.2.4 Microstructural Analysis of Corroded Areas

The microstructural investigation was performed with a digital Leo 430 Scanning Electron Microscope (SEM) using secondary electrons. The SEM imaging consists of bombarding the sample with an electron beam with sufficient energy to excite and eject secondary electrons, which are detected and recorded using a CCD camera.

In this study, samples of each corroded dowel type were collected during the visual inspection and then analyzed by SEM.

In the SEM microstructural analysis, preference was given to the inspection of the corroded areas in each sample (e.g., Figure 43a). In addition, selected regions such as the one illustrated in Figure 43b were also investigated. Figure 44 through Figure 50 present characteristic SEM pictures for each material investigated.

In general, the severity of the corrosion observed with the electron microscope matches the results anticipated by the electrical measurements and visual inspections. However, one should keep in mind that the microstructural investigation focused mostly on the corroded areas of each sample, and does not represent the general state of the dowel bars. The stainless steel-clad dowels, for example, exhibited excellent performance on the corrosion rate measurements, and no corrosion was identified by visual inspection; however, relatively severe localized corrosion was observed at the ends of the dowels close to the interface with carbon steel (see Figure 38b and Figure 47).

A similar situation was observed with the analysis of the epoxy-coated samples. It has been observed that the electrical measurements do not provide a reliable quantitative estimate of the corrosion state of such specimens, and in the visual inspection it was found that the bars were still in relatively good condition, especially compared to carbon steel dowels. However, several defects on the epoxy coating have been presented in this section, and the relation between defects and the occurrence of localized corrosion has been explored.

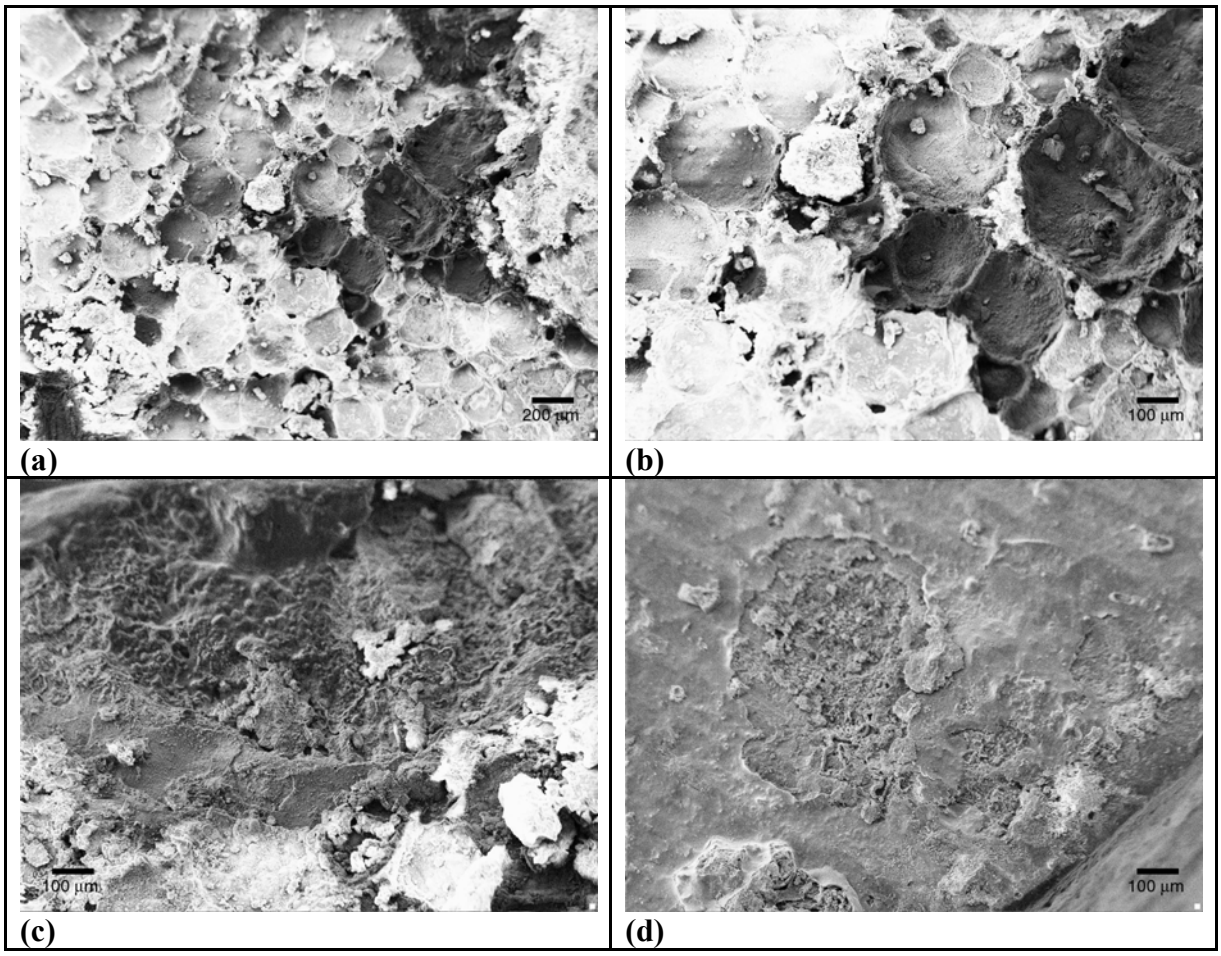

Figure 44. Carbon steel samples: (a) heavy corrosion along the dowel surface, magnification = 100×; (b) same region, 200×; (c) different region at the surface, 200×; and (d) corrosion at the bar end, 100×.

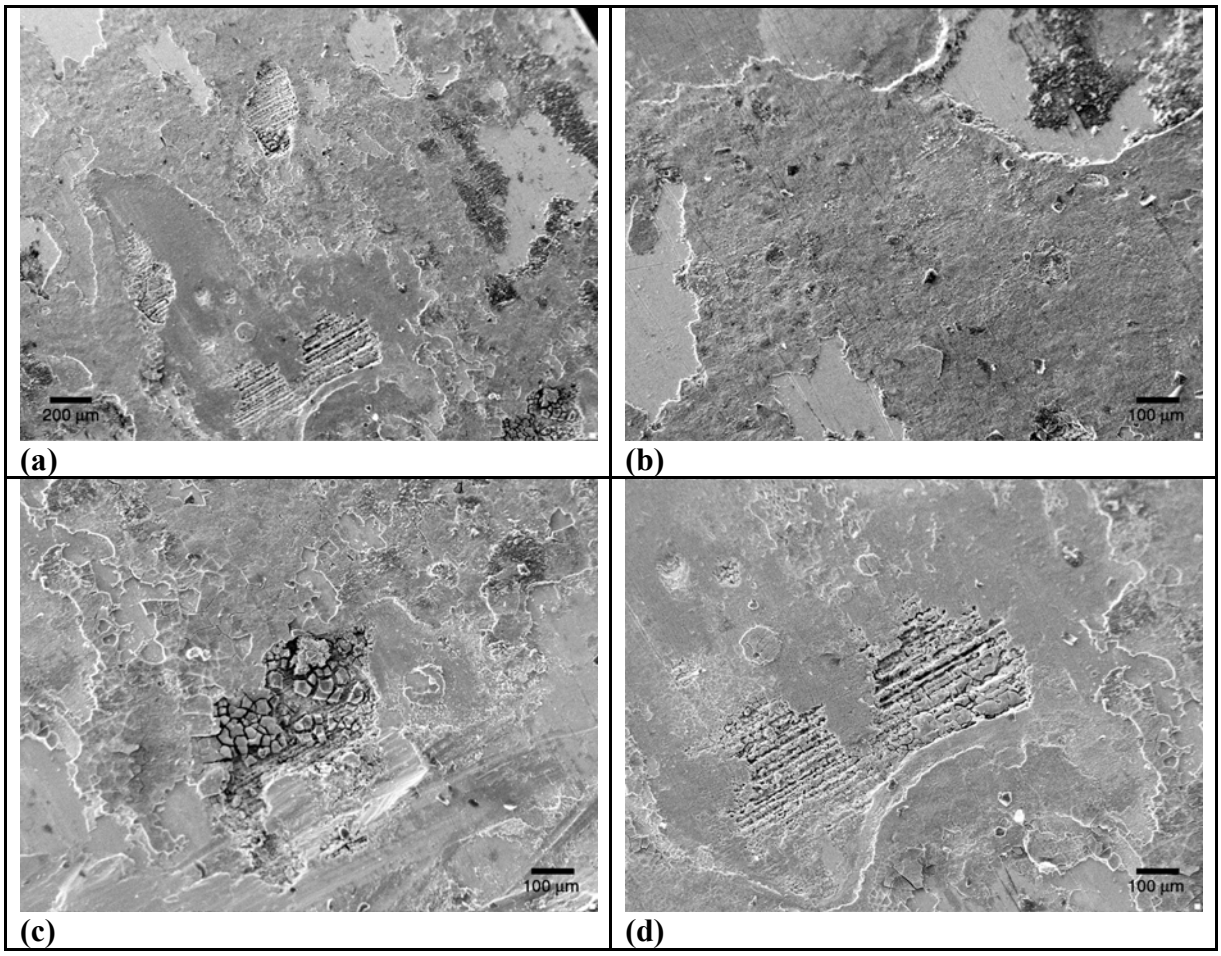

Figure 45. Microcomposite steel samples: (a) aspect of corrosion along at the surface, 100×; (b) same region, 205×; (c) and (d) details of characteristic corrosion sites, 205×.

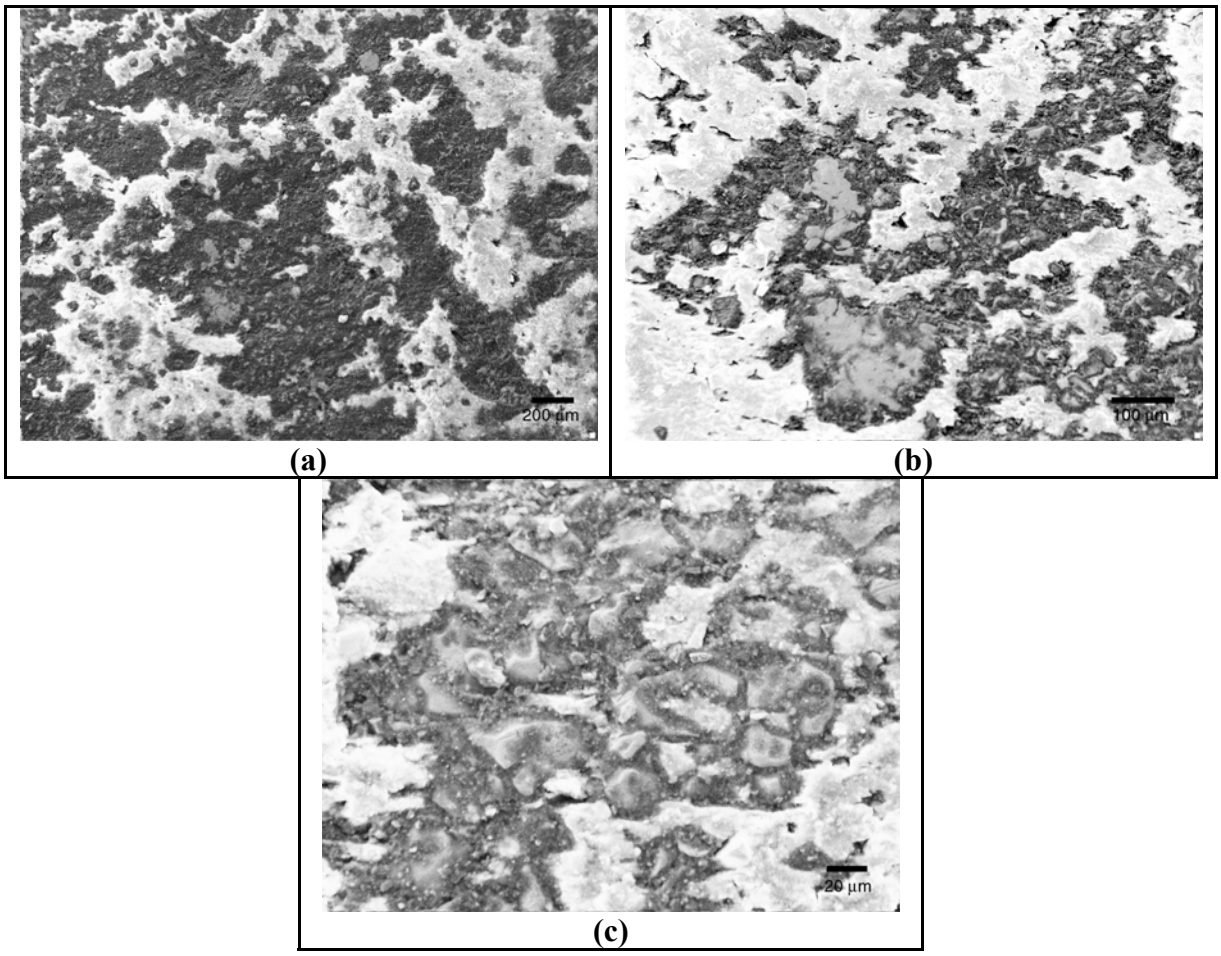

Figure 46. Hollow stainless steel samples: (a) view at the surface, 100×; (b) same region, 300×; and (c) detail of the surface condition, 1,000×. The surface appears rough, but no signs of corrosion damage were observed.

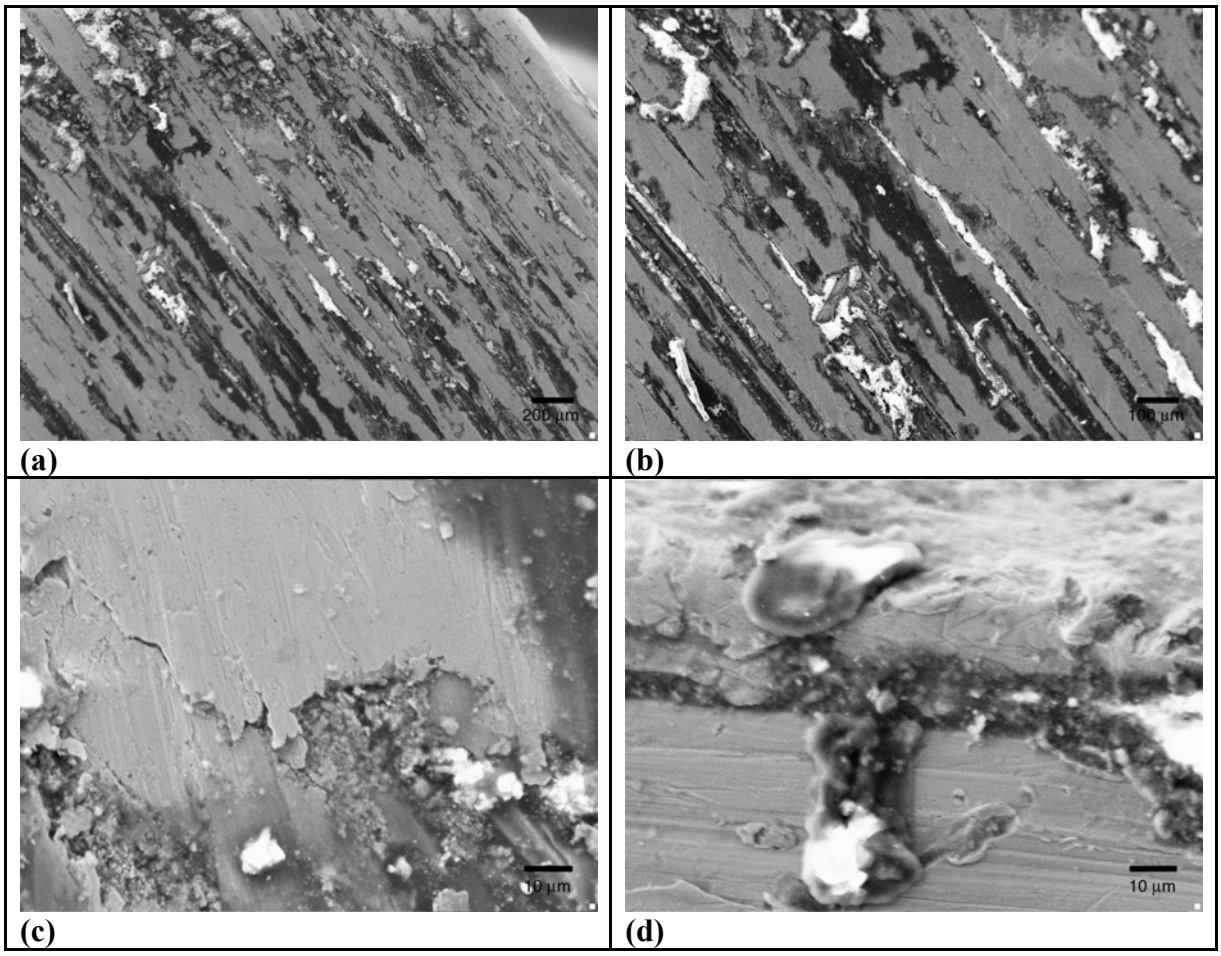

Figure 47. Stainless steel-clad samples: (a) aspect of corrosion along the surface, in a region close to the end of the dowel, 100×; (b) zoom around same region, 200×; (c) details of corrosion at the surface, interface between sound and corroded area, 2,390×; and (d) detail of corrosion at an edge, 2,320×.

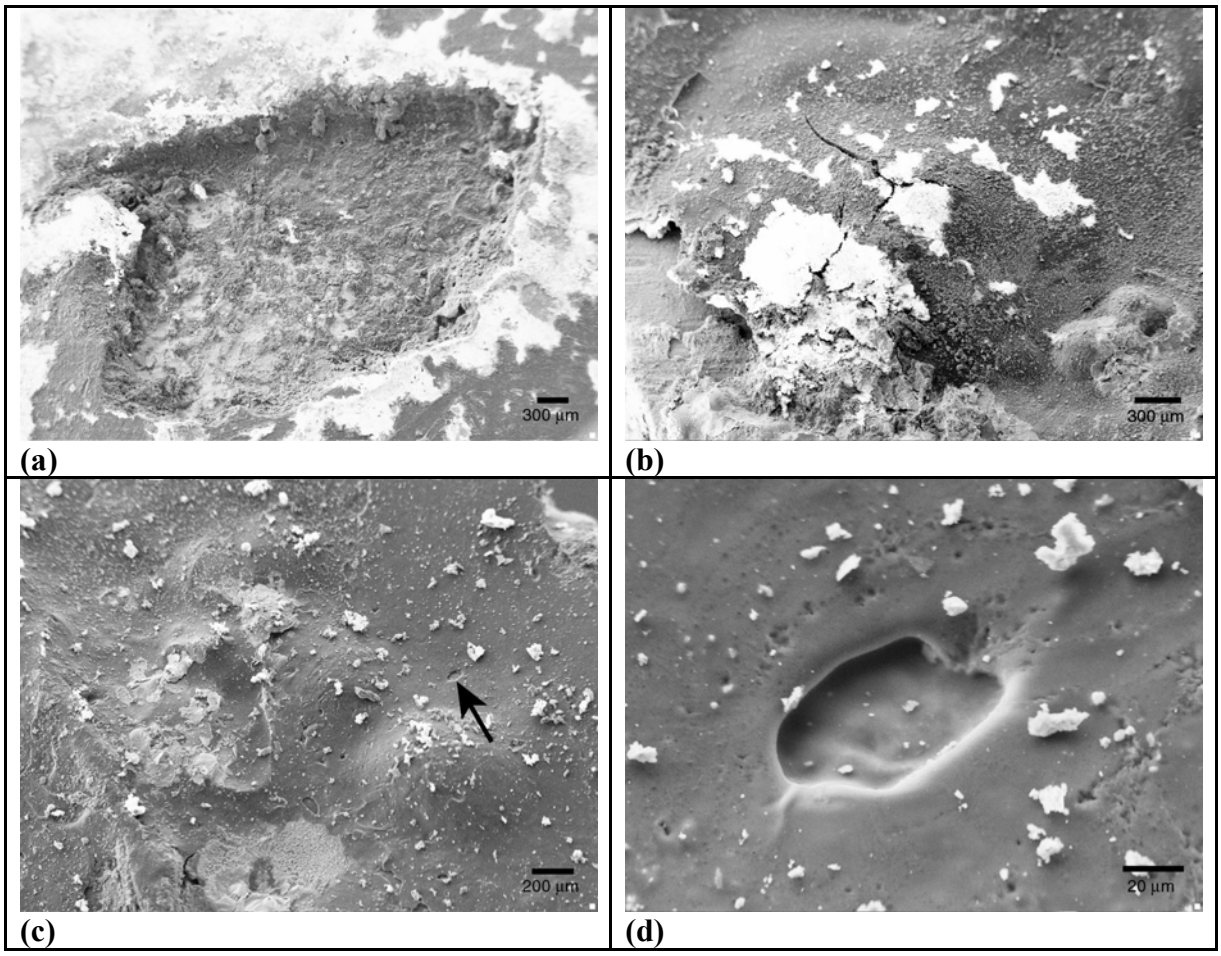

Figure 48. Gray epoxy-coated samples: (a) view of a defect in the coating, with corroded area inside, 50×; (b) another region, at an edge, where coating is lifted 75×; (c) general view of the surface, 100×; and (d) detail of a pinhole present in image (c) (see arrow), 1,500×.

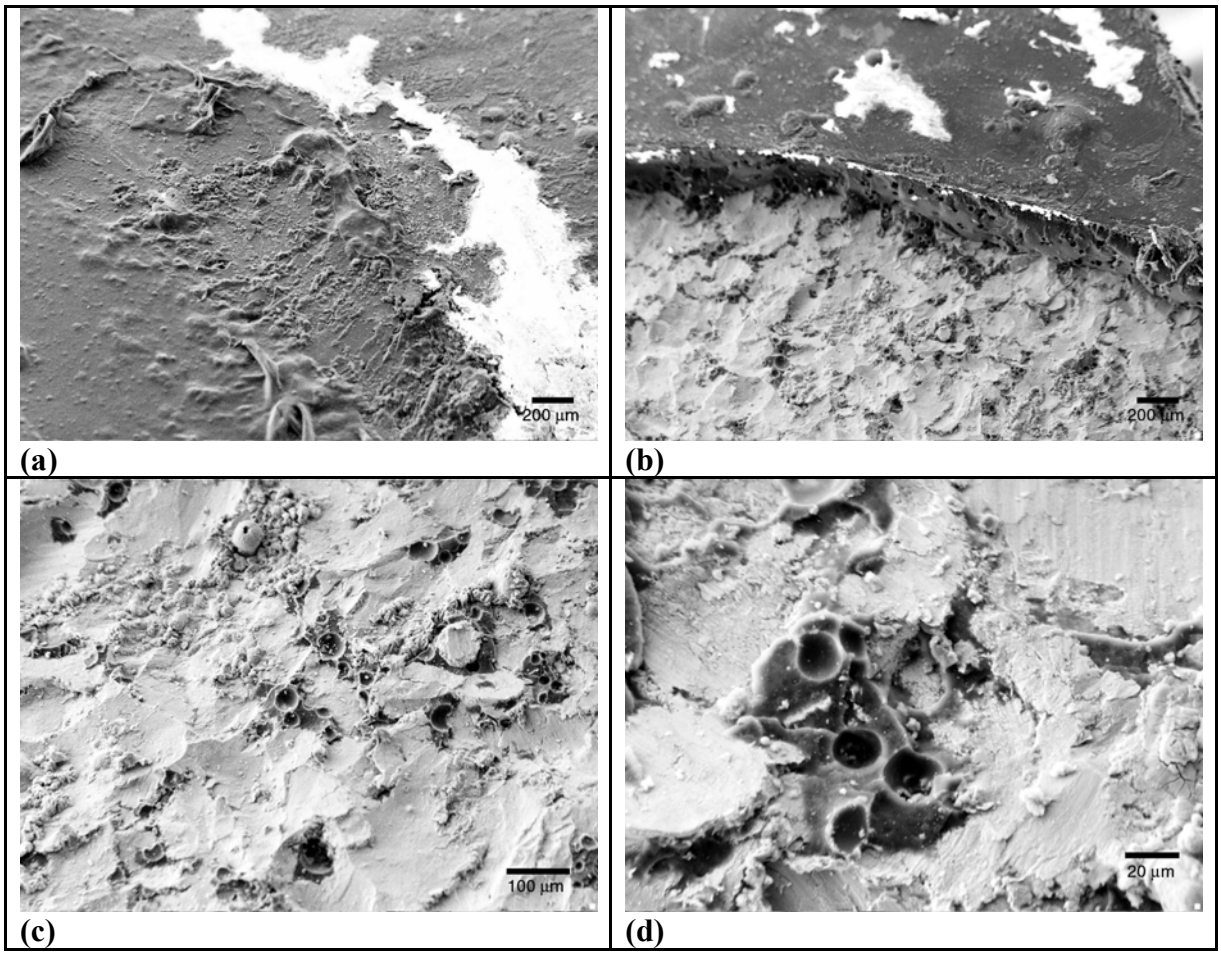

Figure 49. Green epoxy-coated samples: (a) general view of the surface, 100×; (b) region where part of the epoxy coating was removed, 100×; (c) condition of the steel underneath the epoxy, 302×; and (d) detail of corroded area and pits present under the coating, 1,330×.

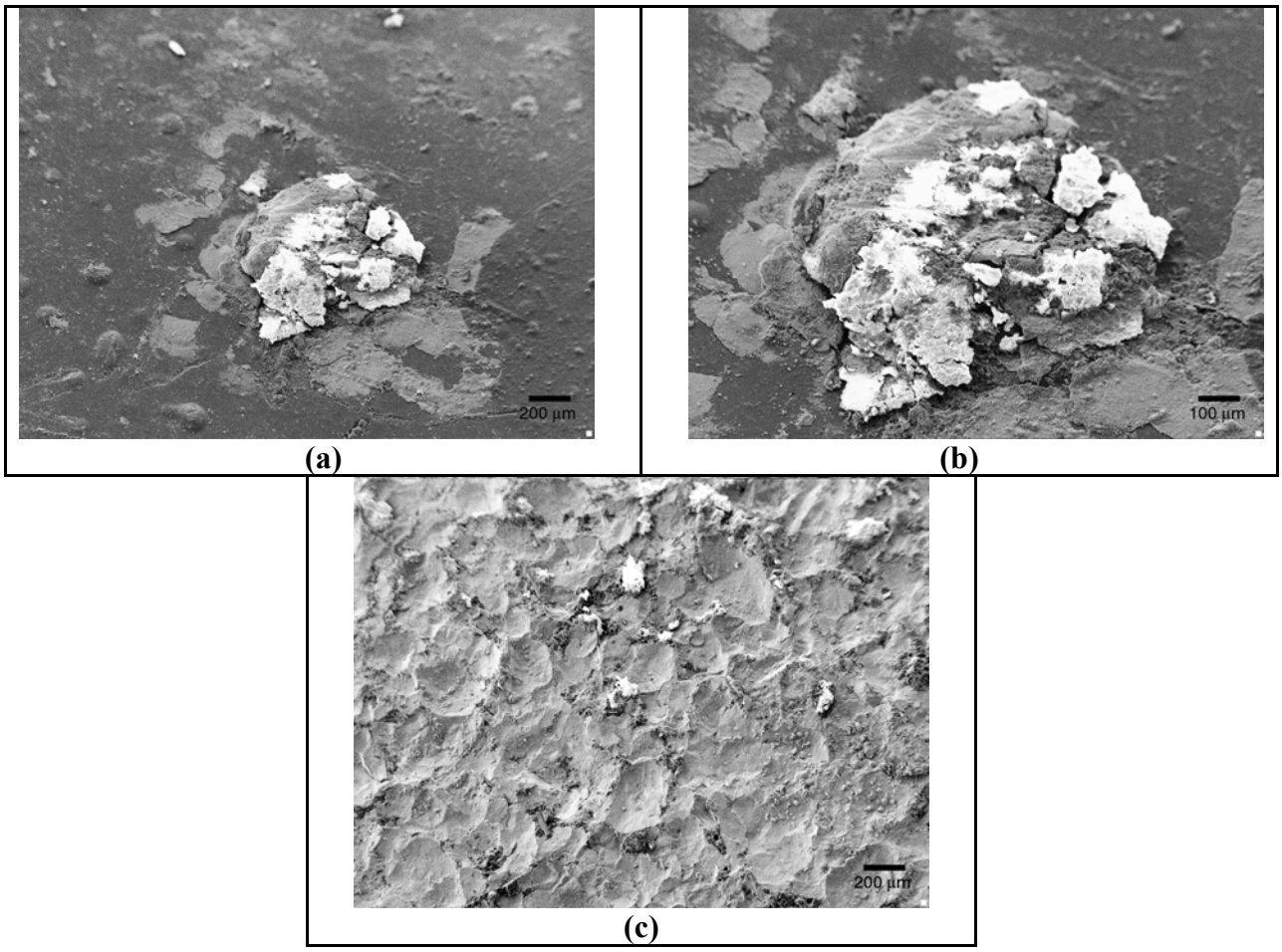

Figure 50. Purple epoxy-coated samples: (a) general view of the surface with corrosion products accumulated in a holiday, 100×; (b) zoom in the same region, 200×; and (c) condition of the steel underneath the epoxy, 200×.

3.3 Phase III Results

Six cores from the WSDOT slabs extracted and transported to California were also tested in the Caltrans laboratory. Ten cores extracted from the corners of in-service pavements (two from each of five locations in Washington State) were submitted to Construction Technology Laboratories, Inc. for testing as well. The chloride contents of the concrete at different depths of the cores were compared between the laboratory specimens and the field slabs to compare the severity of the laboratory chloride environment to that of the field slabs. This comparison helps to relate the results from the accelerated laboratory testing to the long-term field conditions.

3.3.1 Extracted WSDOT Pavement Slabs

This section presents the results and discussion of half-cell potential tests, LPR experiments, chloride analyses, and visual inspection performed on the slabs from the WSDOT dowel bar retrofit project on Interstate 90.

3.3.1.1 Half-Cell Potential and Linear Polarization Resistance

Figure 51 through Figure 53 present the results of LPR tests done on the extracted WSDOT slabs. In these plots, the current density (in μA/cm^2) is plotted versus potential (in mV), and the X-axis crosses the Y-axis at the half-cell potential value. The slope of the curves (ΔE/Δi) provides the value of the polarization resistance (*Rp*), with flatter slopes indicating faster corrosion rate. The location of specimens A, B, and C are illustrated in Figure 54.

Although the polarization resistance appears to be large when estimated by the Linear Polarization Resistance method (which would lead to a small corrosion current density), it is important to highlight that accelerated, localized corrosion may occur at defects and/or underneath the epoxy coating. One has to keep in mind that this corrosion detection technique cannot be interpreted quantitatively for epoxy-coated rebar, since in this case corrosion is most likely localized at the coating holidays (pinholes, voids, etc.). Given that epoxy is an electrical insulator, polarization occurs only at very small areas (defective areas) that cannot be accounted for in the calculation of the polarization resistance term.

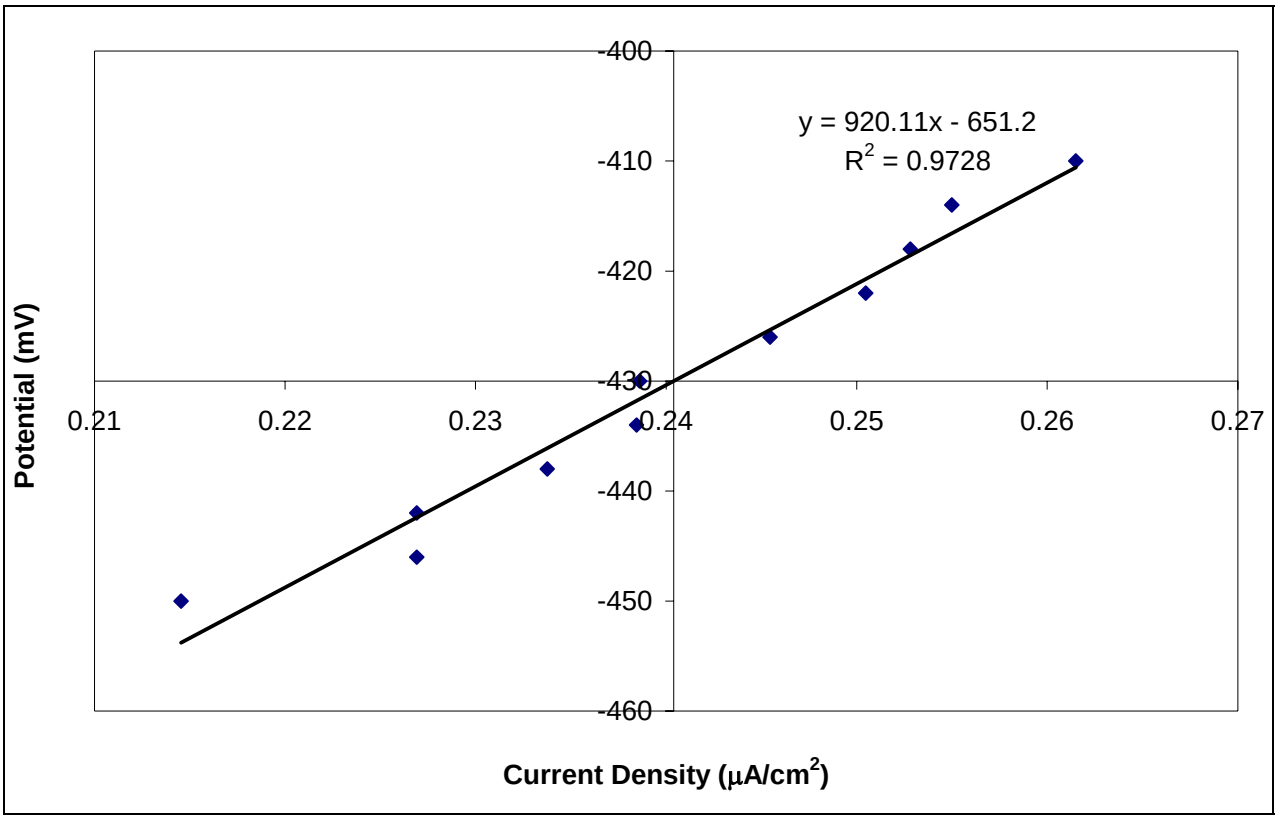

Figure 51. Linear Polarization Resistance, WSDOT slab, Specimen A.

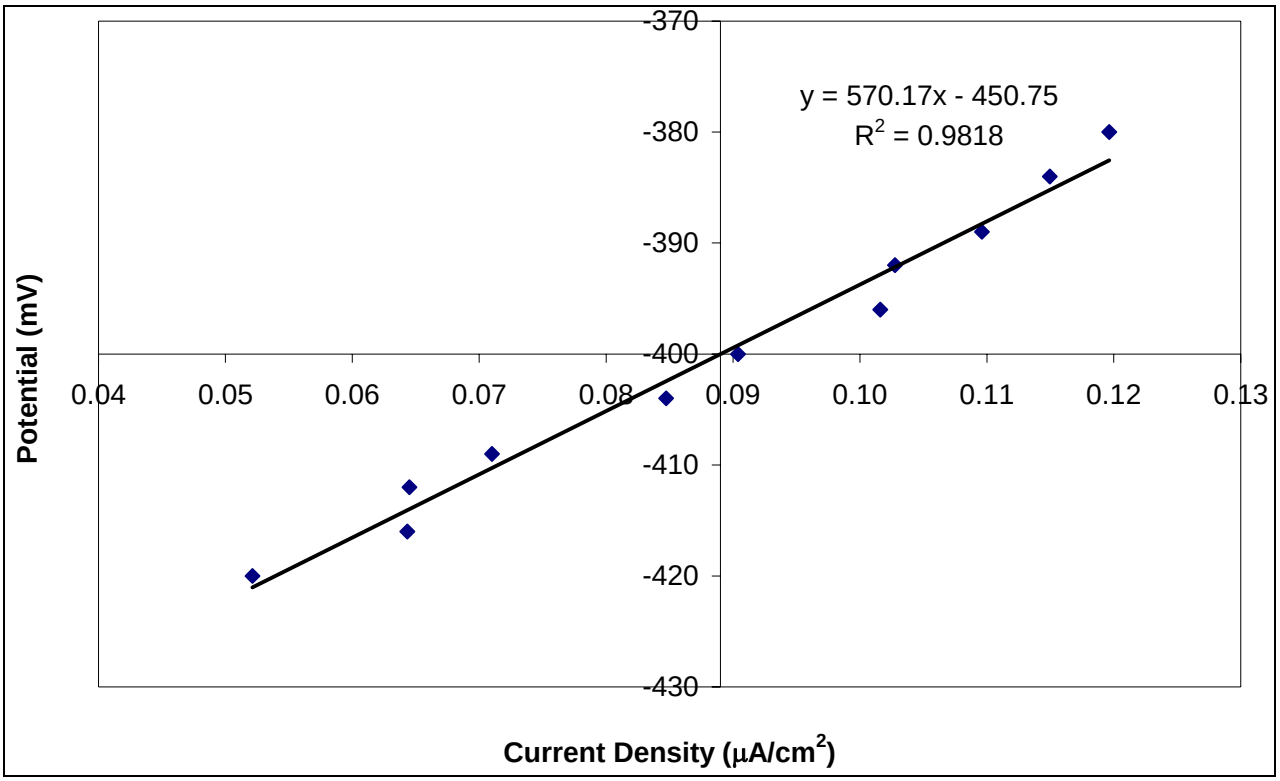

Figure 52. Linear Polarization Resistance, WSDOT slab, Specimen B.

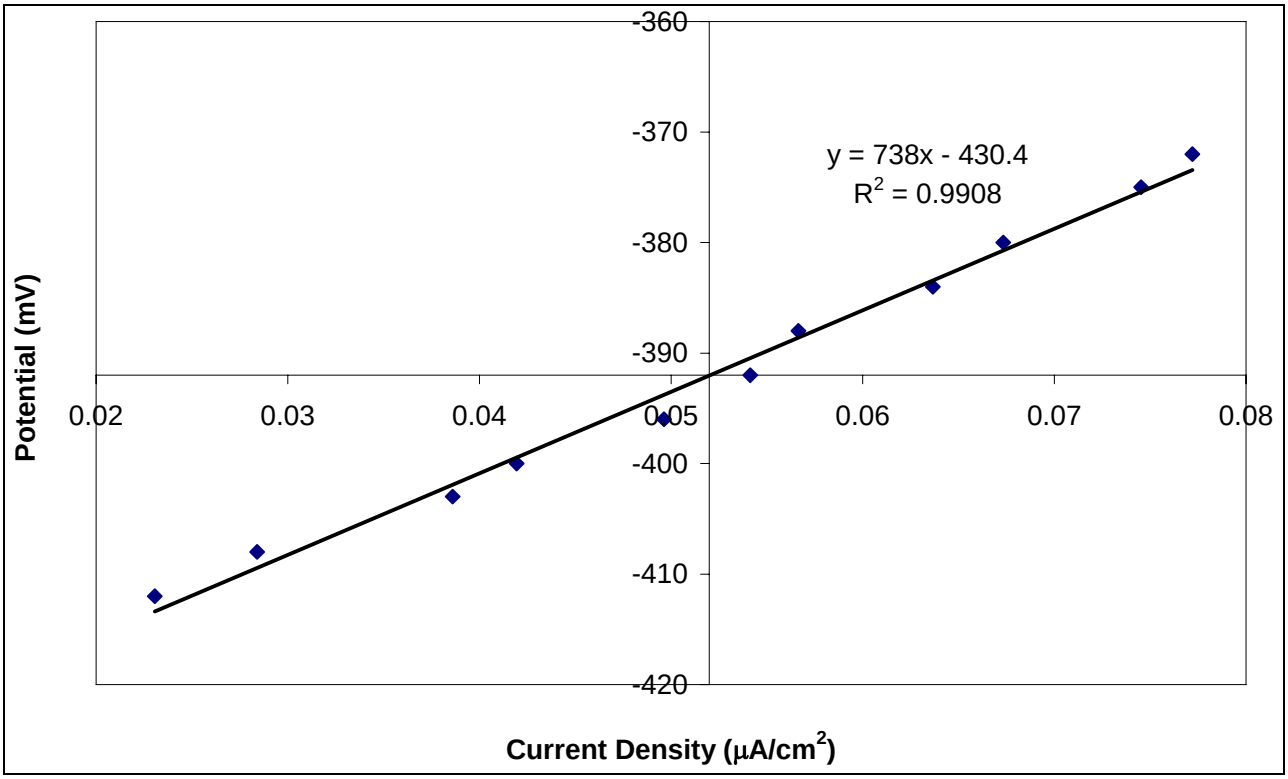

Figure 53. Linear Polarization Resistance, WSDOT slab, Specimen C.

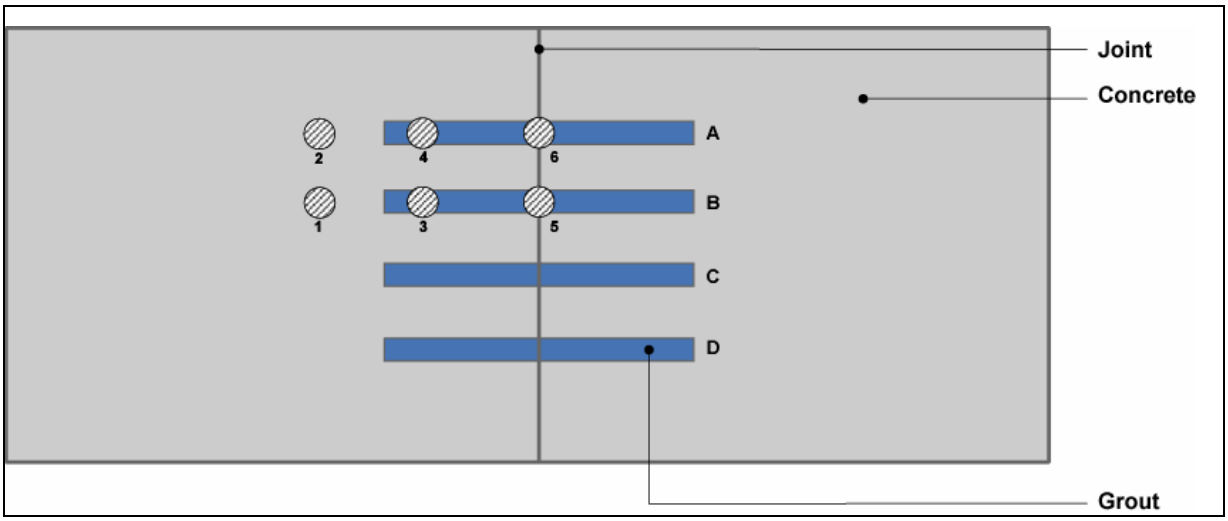

Figure 54. Samples extracted from the WSDOT pavement slab for chloride analyses.

Regarding the half-cell potential results, one can observe that the different dowels presented similar values (respectively -430mV, -400mV, and -392mV), being all located in the high probability of corrosion region (Table 1).

3.3.1.2 Visual Inspection

Figure 55 shows the interior of a core hole located at the joint immediately after coring. The top of the corroded dowel can be observed at the bottom of the hole. After scraping away some of the loose epoxy coating, a considerable amount of corrosion product was found. The core was removed using water for cooling the core bit, however, no time was permitted for corrosion to occur because of the coring water.

The coring also revealed that one of the retrofit dowel bars was not centered over the transverse joint, and only extended approximately 100 mm into the slab on one side of the joint. It is certain that this misplacement of the dowel contributed to the low load transfer efficiency (LTE) of the joint. It is likely that the observed corrosion, and presence of the weak layer of corrosion product between the concrete and the dowel also contributed to the loss of LTE.

3.4 Analysis of Chloride Contents

As mentioned in Section 2.6, several chloride analyses were performed on concrete cores cut from: (1) extracted WSDOT pavement slabs, (2) near-joint corners of in-service slabs at five different locations in Washington State, and (3) the laboratory beams from Phase II testing exposed to 3.5% NaCl solution. Such chloride profiles are used to evaluate the concentration of chlorides in the region surrounding the steel dowels, particularly in the vicinities of the open joints, and to compare field and laboratory exposure conditions.

3.4.1 Chloride Analyses from WSDOT Slab Extracted from Interstate 90

Six samples were obtained from the extracted WSDOT slabs from Interstate 90 for chloride analyses. Cores 1 and 2 were made through the concrete only; cores 3 and 4 were cut through the retrofit grout and the end of the dowel, and cores 5 and 6 were obtained at the joint through grout and the dowel. The samples were submitted to the Caltrans chemistry laboratory for the analyses to be performed.

Core 4 (grout) could not be completely removed on the same day due to problems with the coring machine, and was left out of the analyses. Results for Core 3 (Figure 58) showed that the concentration of chlorides in this region was low, and attention was focused on the study of chloride concentrations in the jointed region.

Figure 55. View of the interior of a recently made core hole showing corrosion products underneath the epoxy coating.

Figure 56 through Figure 60 show the chloride profiles obtained for this pavement slab. The pavement was built in 1964, and deicing salts were applied 120–150 days per year, with each icy day typically having at least two applications. Details of location, salt usage, and joint sealing practices are presented in Table 9 (SR-90 MP 76.88, extracted slab).

The steel dowels are located approximately at 3 in. depth. It can be noticed that the chloride concentration at this depth is around 1.0 lb./cu. yd., which is near the chloride threshold for regular carbon steel found in the literature (*10*). Notice that sometimes a smaller concentration may be verified at the top layer due to Cl- being "washed out" by surface water.

Figure 58 shows a profile of the chloride concentrations on the grout used for the dowel-bar retrofit, which was done in 1994. Even approximately 10–11 years after the project, one can observe that the concentration of Cl^- ions is considerably below the minimum value to initiate corrosion, even for regular unprotected carbon steels. However, in Figure 59 and Figure 60 it can be seen that the chloride concentrations close to the joint are significantly higher, reaching values as high as 11.38 lb./cu. yd. along the profile and 8.43 lb./cu. yd. in a region close to the dowel (Figure 60).

The results presented in Figure 56 through Figure 60 indicate that the chloride ions can more easily penetrate the grout through the open joint. Thus, at the joint, easier access and accumulation of chlorides results in higher localized concentrations close to the dowels. It is important to notice that in this case the chloride ions do not infiltrate the concrete (or grout) from the top, but instead they migrate through the open joint to the dowel.

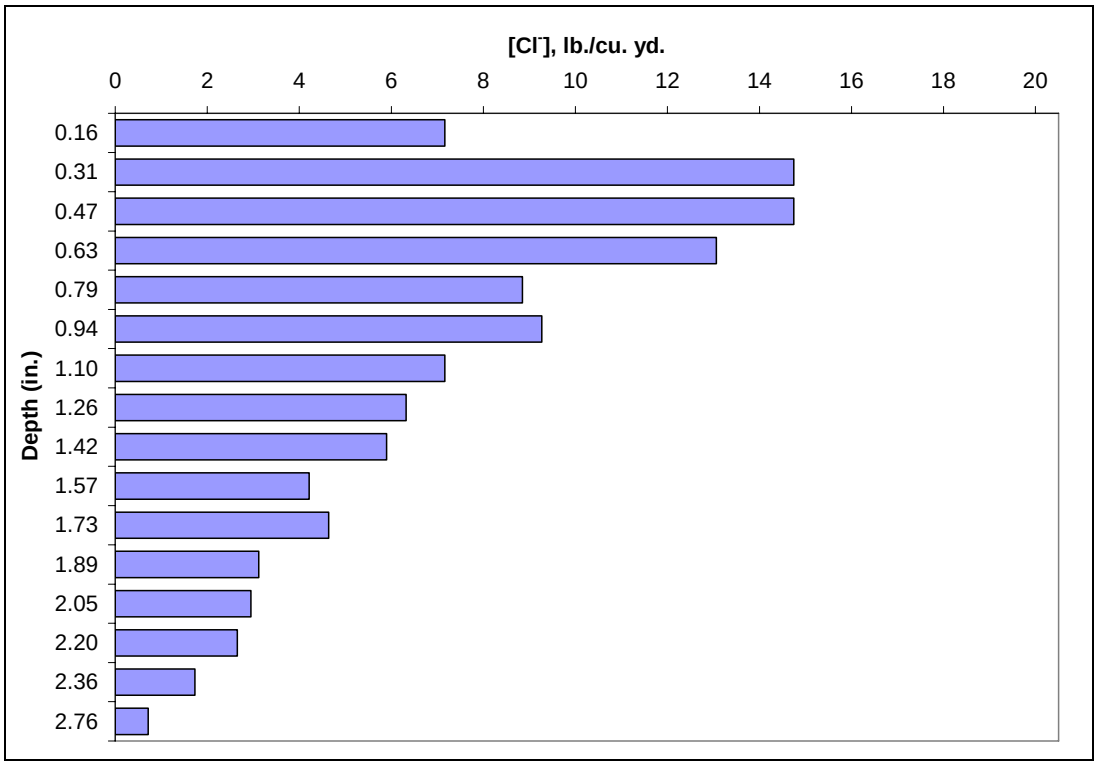

Figure 56. Chloride profile of the slab concrete (Core #1).

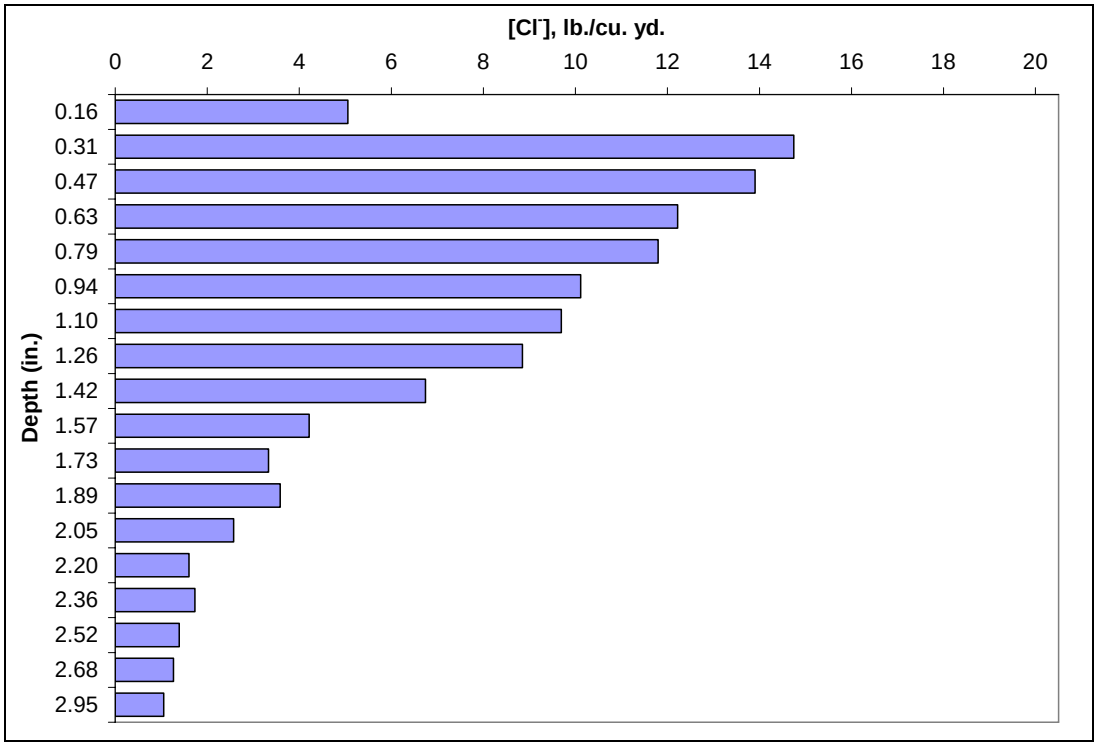

Figure 57. Chloride profile of the slab concrete (Core #2).

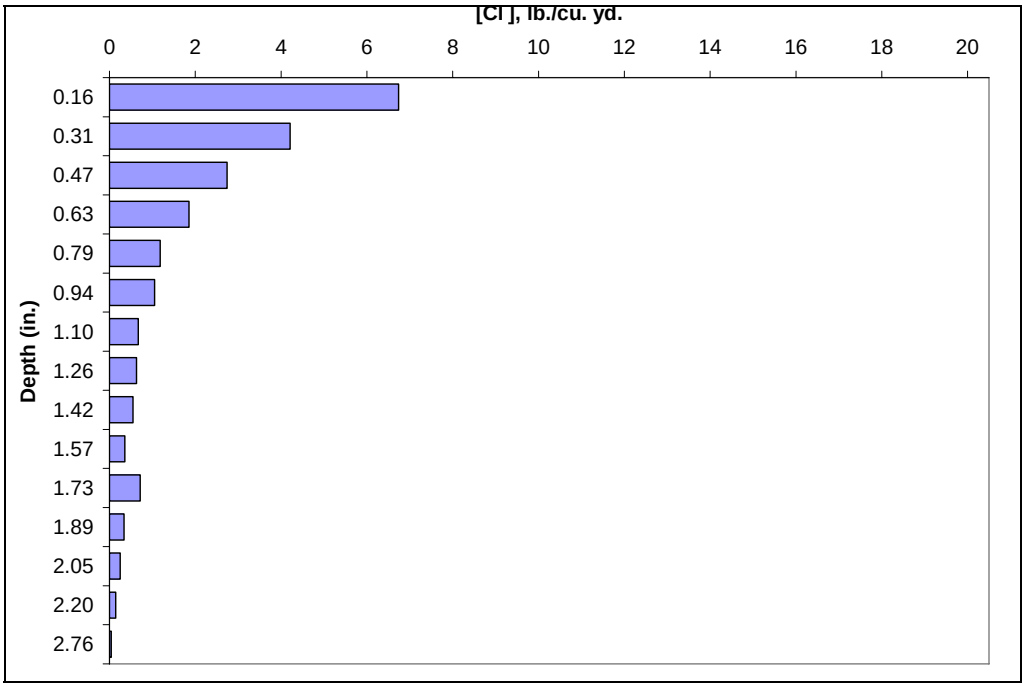

Figure 58. Chloride profile of the grout used for dowel bar retrofit (Core #3).

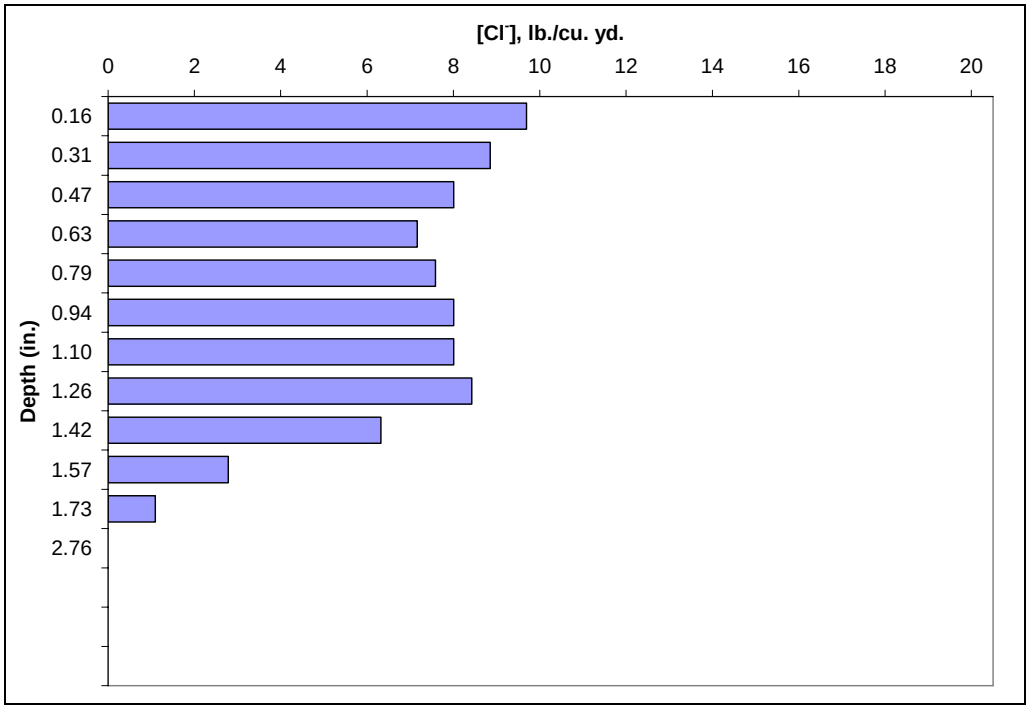

Figure 59. Chloride profile of the grout around the pavement joint (Core #5).

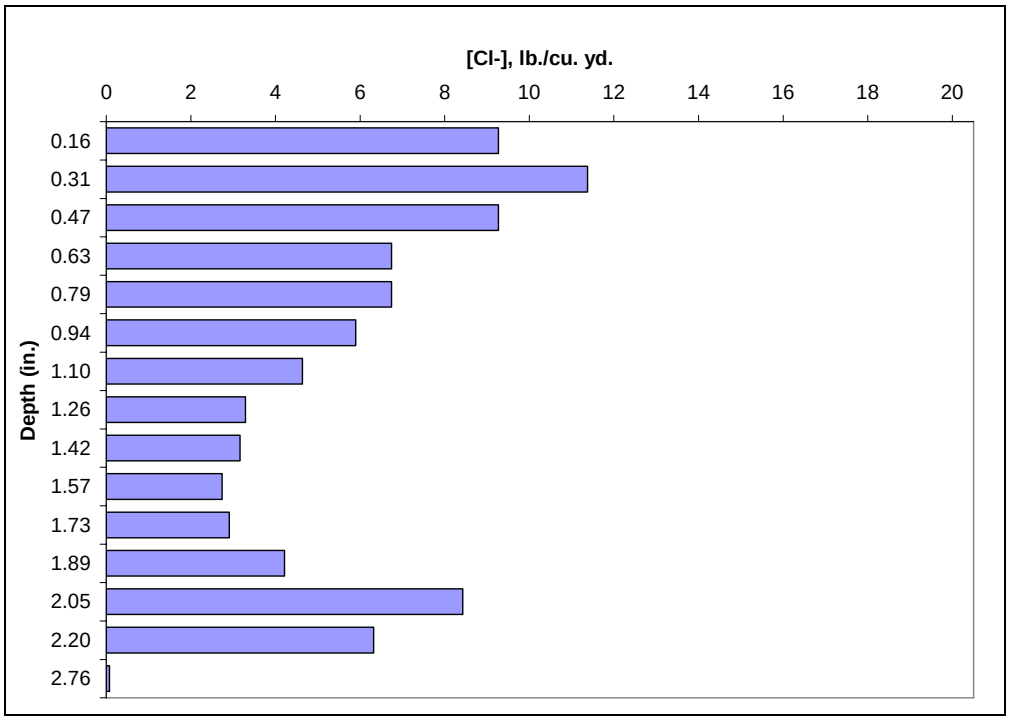

Figure 60. Chloride profile of the grout around the pavement joint (Core #6).

3.4.2 Chloride Analyses of Cores from WSDOT Pavements in Various Locations

This section presents the results of the chloride analyses performed on cores extracted from slab corners, next to the transverse joint of in-service slabs at five different locations in Washington State. These cores were extracted by WSDOT and tested for chloride content by Construction Technology Laboratories, Inc. for comparison with the laboratory results. Table 9 describes the locations from which cores were extracted, including years of construction and salt usage and joint-sealing practices. Figure 61 through Figure 65 present the chloride concentration profiles for the different locations described in Table 9. The error bars represent minimum and maximum values obtained at each location.

It is interesting to notice that the concentration of 1.0 lb./cu. yd., regarded as the chloride threshold for carbon steel, is exceeded in nearly all cases, except for the samples from Wapato

Table 9. Samples Extracted from In-Service Pavements for Chloride Analyses (Information Provided by WSDOT)

Route Number	Location (MP)	Year	Depth (in)	Salt Usage	Joint Sealing
I-90	76.88 (extracted slab)	1964	9	Up until the early 1980's, rock salt was used approximately 120-150 days per year at a typical rate of 180 pounds per mile using a 5:1 ratio (1 scoop of salt to 5 scoops of sand). Each day typically had at least two applications. Salting typically occurs from mid November to mid April. From the early 1980's to 1997 or so, rust inhibitor type deicers/salts have been used. Since 1997 or so liquid magnesium chloride has been used at a typical rate of 35 gallons per mile with a range of 15 to 50. The average rate seems to be coming down with the use of better flow controls.	Sawed and sealed during initial construction with a rubberized joint sealer product called "Seal Target 164." Joint sealed during 1994 DBR with rubberized joint sealant.
I-5	166.00 (Downtown Seattle)	1967	9	No data yet.	Sawed and sealed during initial construction with a rubberized joint sealer product called "Seal Target 164." No sealing since original construction.
I-90	91.324 (Elk Heights)	1967	9	See I-90 above. Same.	Sawed and sealed during initial construction with a rubberized joint sealer product called "Seal Target 164." Joint sealed during 1994 DBR with rubberized joint sealant
I-90	61.304 (Price Creek)	1959	9	See I-90 above. Same.	Sawed and sealed during initial construction with a rubberized joint sealer product called "Seal Target 164." Joint sealed during 1997 DBR with rubberized joint sealant.
SR 82	10.617 (Military Road)	1971	9	Same as I-90 above except that the use of rock salts was about 100 days per year. Most days had two applications. Rust inhibitor deicers/salts were used from the early 1980's to 1997 or so. Since 1997 liquid magnesium chloride has been used at the typical rates reported above.	Sawed and sealed during initial construction with a rubberized joint sealer product called "Seal Target 164." Joint sealed during 1997 DBR with rubberized joint sealant.
SR 82	43.524 (Wapato)	1981	9	Same as I-90 above, however the applications of rock salt were about 60-70 days per year until about 1985. Each day often had two applications. Rock salt was used at a 15:1 to a 20:1 blend. From 1985 to about 2000 rust inhibitor salts were used at the same rate. Since 2000, magnesium chloride has been used.	Sawed and sealed during initial construction with a rubberized joint sealer product called "Seal Target 164." No sealing since original construction.

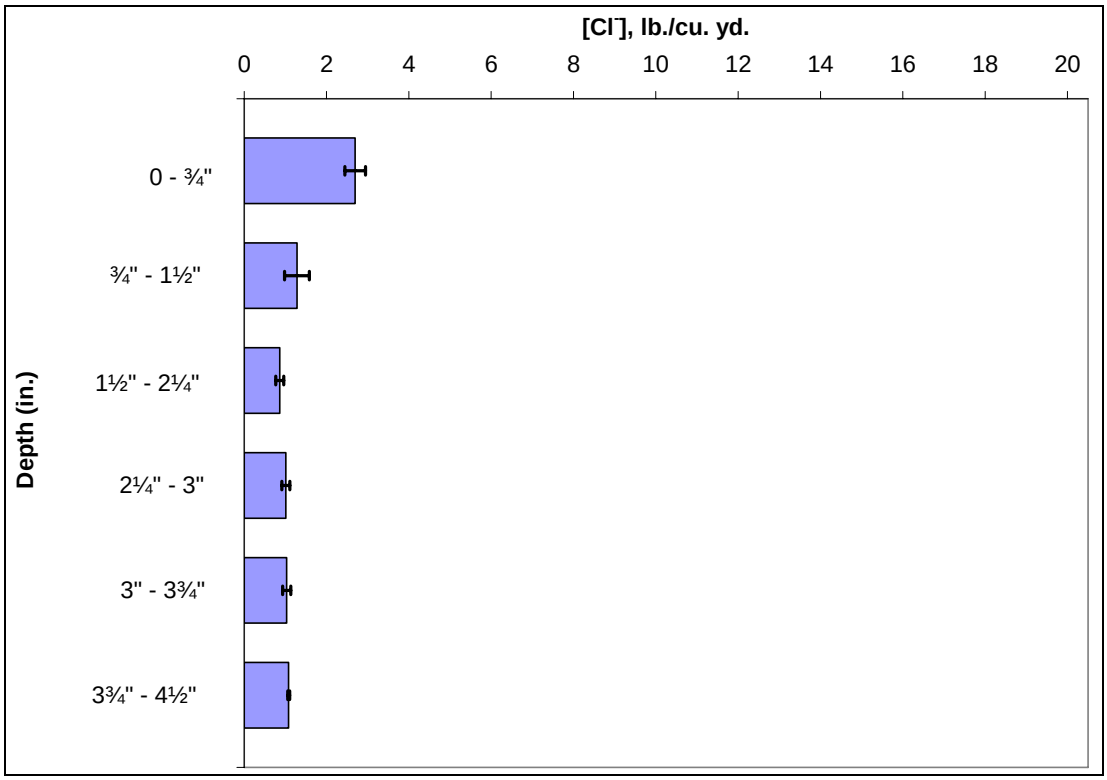

Figure 61. Chloride profile for I-5 MP 166.00 (downtown Seattle).

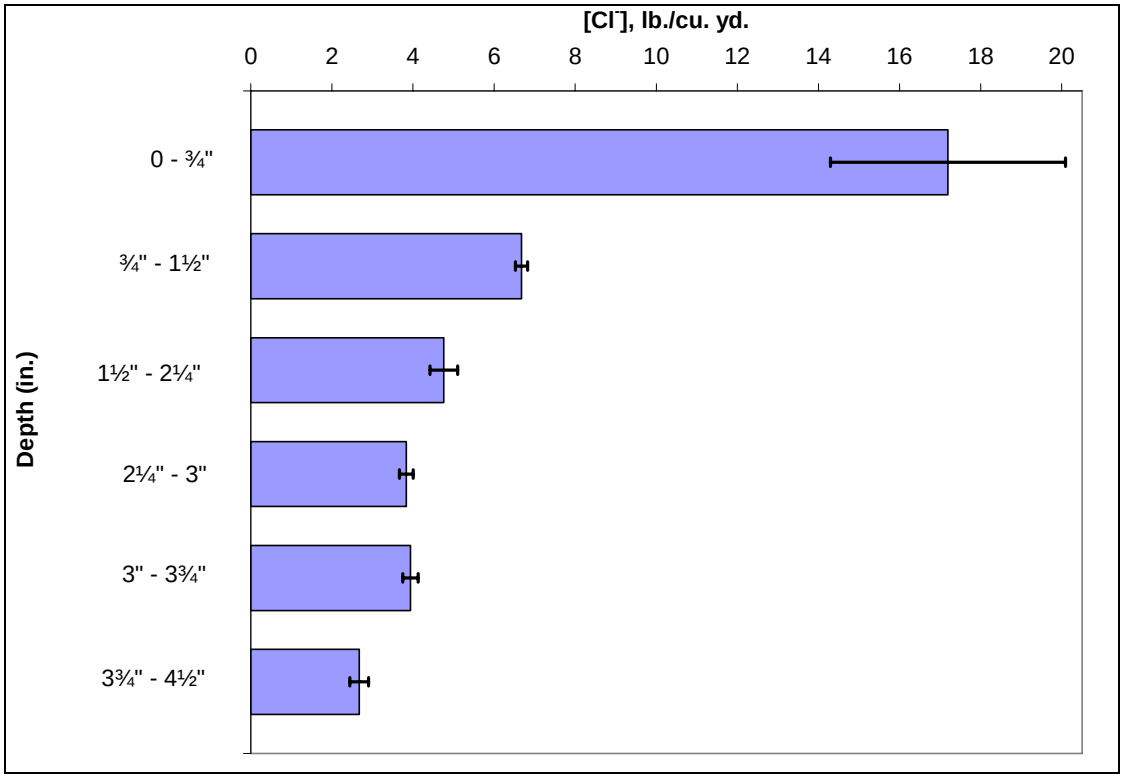

Figure 62. Chloride profile for I-90 MP 91.324 (Elk Heights).

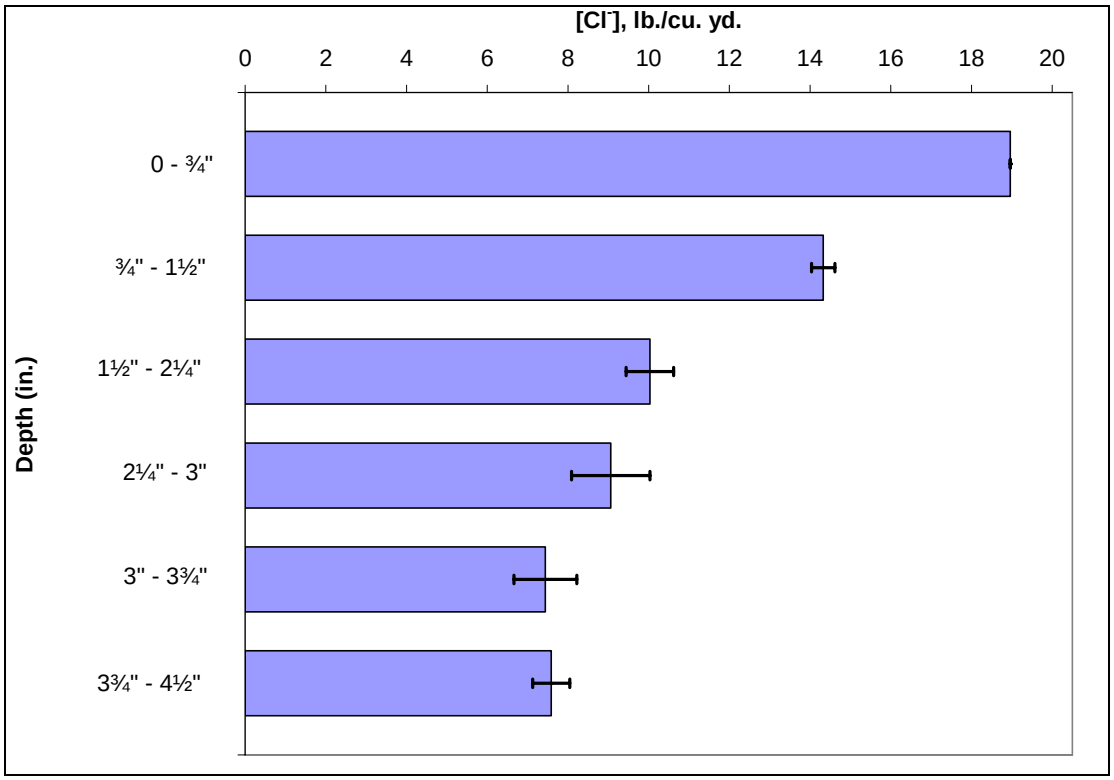

Figure 63. Chloride profile for I- 90 MP 61.304 (Price Creek).

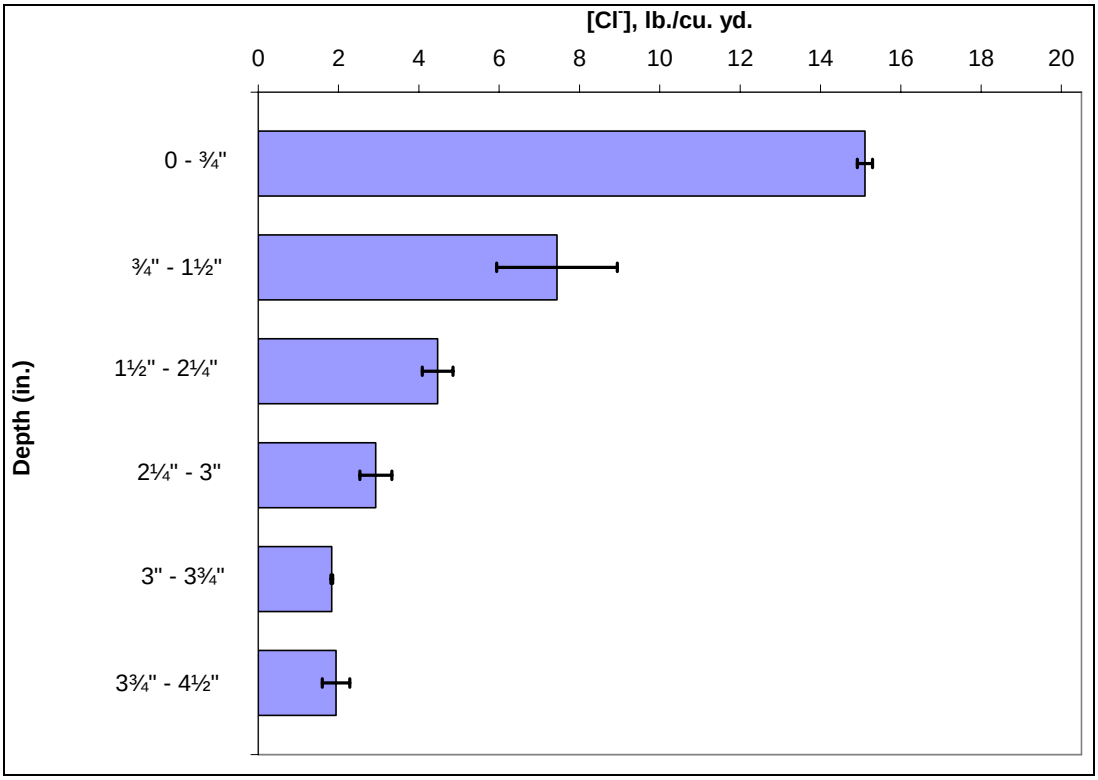

Figure 64. Chloride profile for SR 82 MP 10.617 (Military Road).

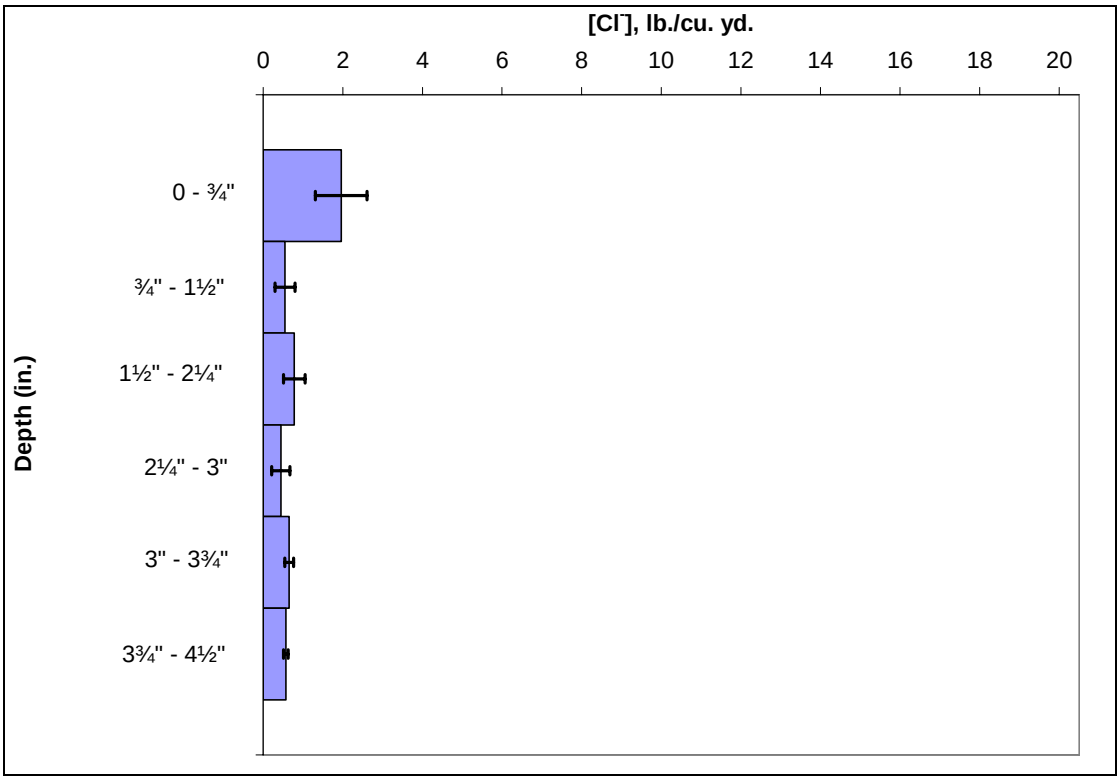

Figure 65. Chloride profile for SR 82 MP 43.524 (Wapato).

(Figure 65), which is a more recently built pavement where deicing salts were applied only 60-70 days/year at lower rates. Even so, at this location [Cl^-] reached 0.6–0.7 lb./cu. yd. On the other hand, only the older pavement built in 1959 (Figure 63), which was exposed to two daily applications of deicing salts for 120–150 days/year, reached a concentration that was high enough to overcome the chloride threshold of 7.7 lb/cu. yd. found in the references for the microcomposite steel *(8-10)*.

3.4.3 Chloride Analyses from Laboratory Samples

As described in Section 2.6, cylindrical cores were extracted from the laboratory concrete beams at the central, jointed region. The laboratory specimens were subjected to wet-and-dry cycles with a 3.5% NaCl solution, which is typically used to simulate seawater, over an 18-month period. The extracted samples were shipped to the Caltrans chemistry laboratory where the chloride analyses were performed. Figure 66 through Figure 71 present the results from these analyses.

In general, it can be seen that the chloride concentrations are much more constant along the depth profile compared to situations in which the chloride has to diffuse through the concrete (e.g., Figure 57 and Figure 58) or migrate through a narrow joint (e.g., Figure 60 and Figure 63). This is due to the fact that in the laboratory specimens, a large (approximately 6 × 50 mm) open joint was cast above the dowels.

In addition, it was verified that the use of a 3.5% NaCl solution may lead to high chloride concentrations, as compared to the results obtained in the field specimens, greatly accelerating the corrosion process. As a result of this aggressive environment, corrosion could be observed in nearly all samples after only 18 months of exposure, except for the stainless clad and stainless hollow specimens. Comparatively, based on the previous results, it can certainly be said that the corrosion resistance of carbon steels is considerably lower than that of microcomposite steels, which in turn are less corrosion-resistant than stainless hollow and stainless steel-clad dowels. However, one should keep in mind that the chloride concentration

analyses indicate that the actual field conditions and local environment should be taken into account when choosing the appropriate material for a given project.

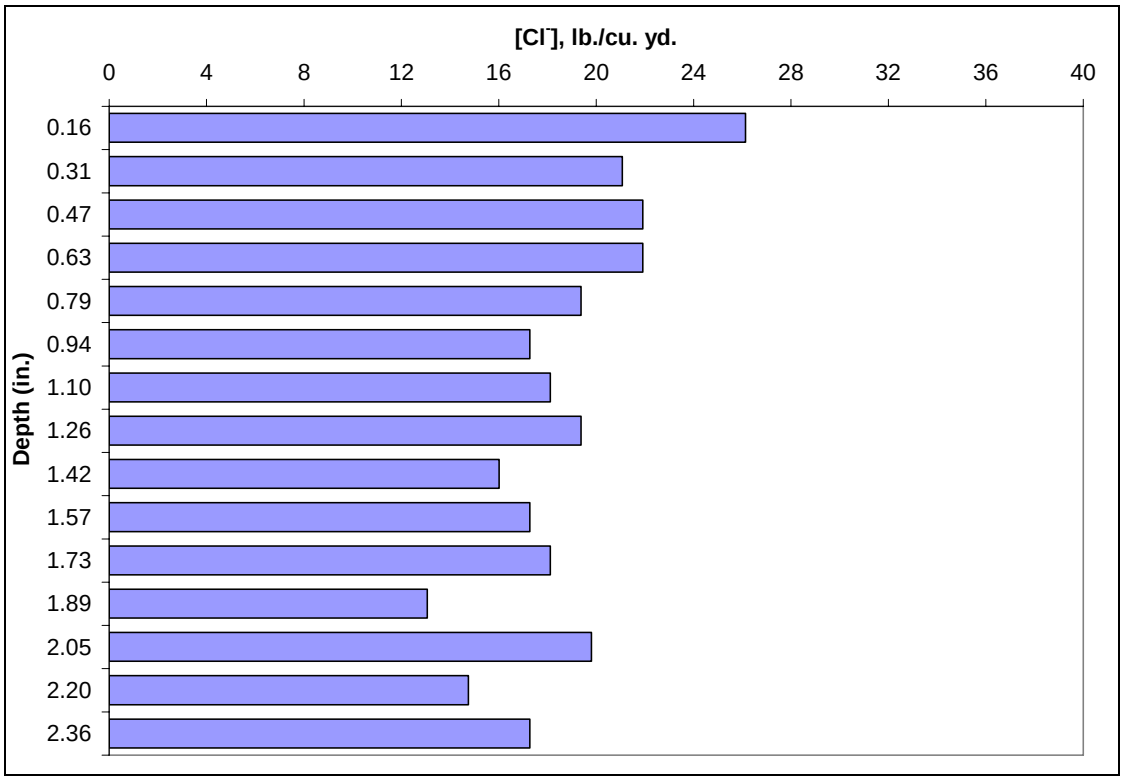

Figure 66. Chloride profile on the concrete of a carbon steel specimen.

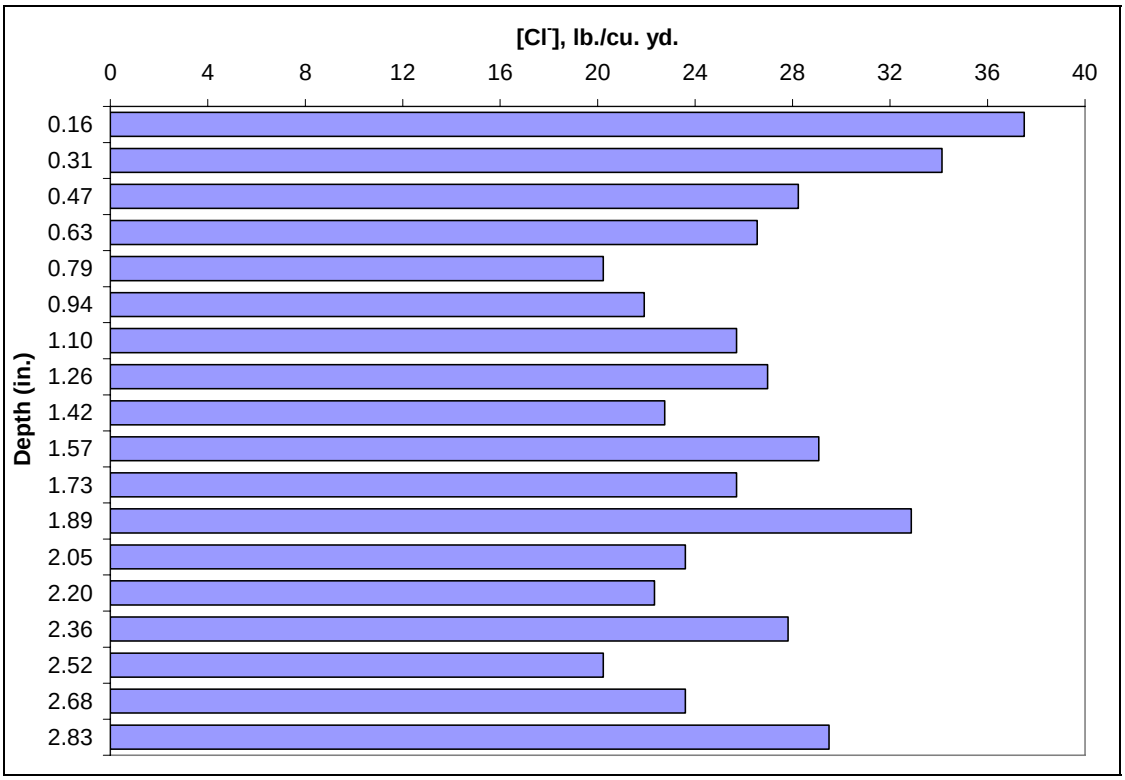

Figure 67. Chloride profile on the concrete of a stainless clad specimen.

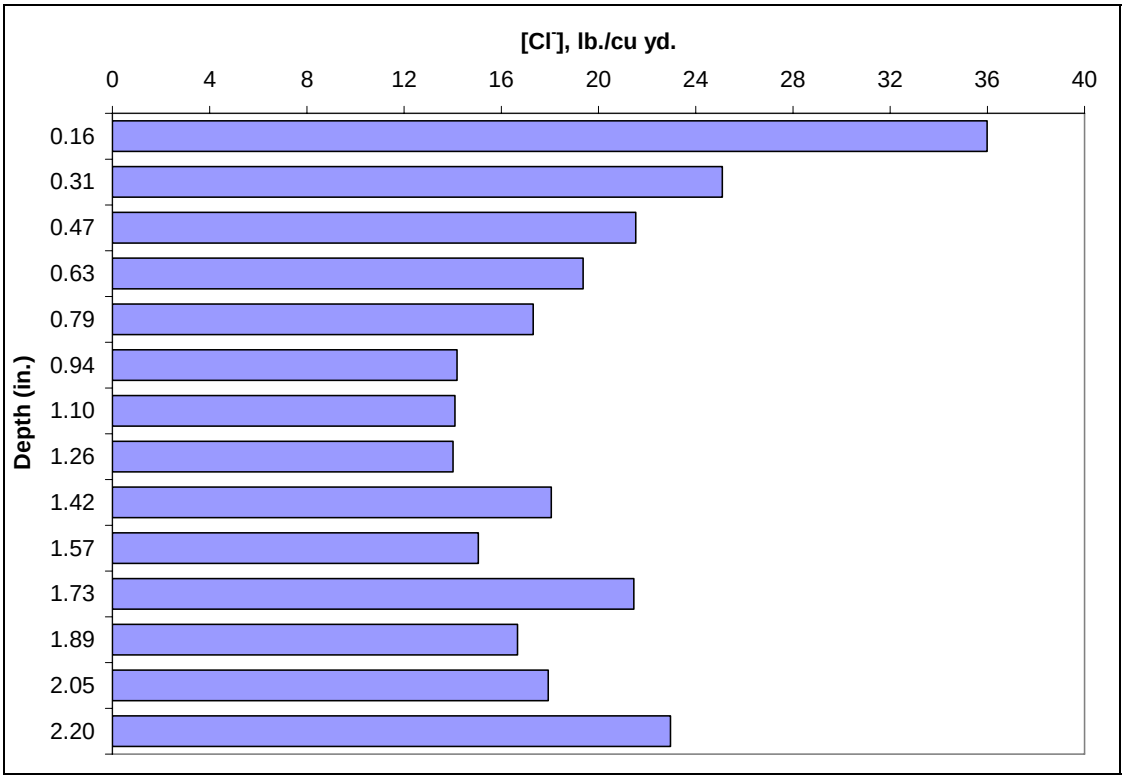

Figure 68. Chloride profile on the concrete of a stainless hollow specimen.

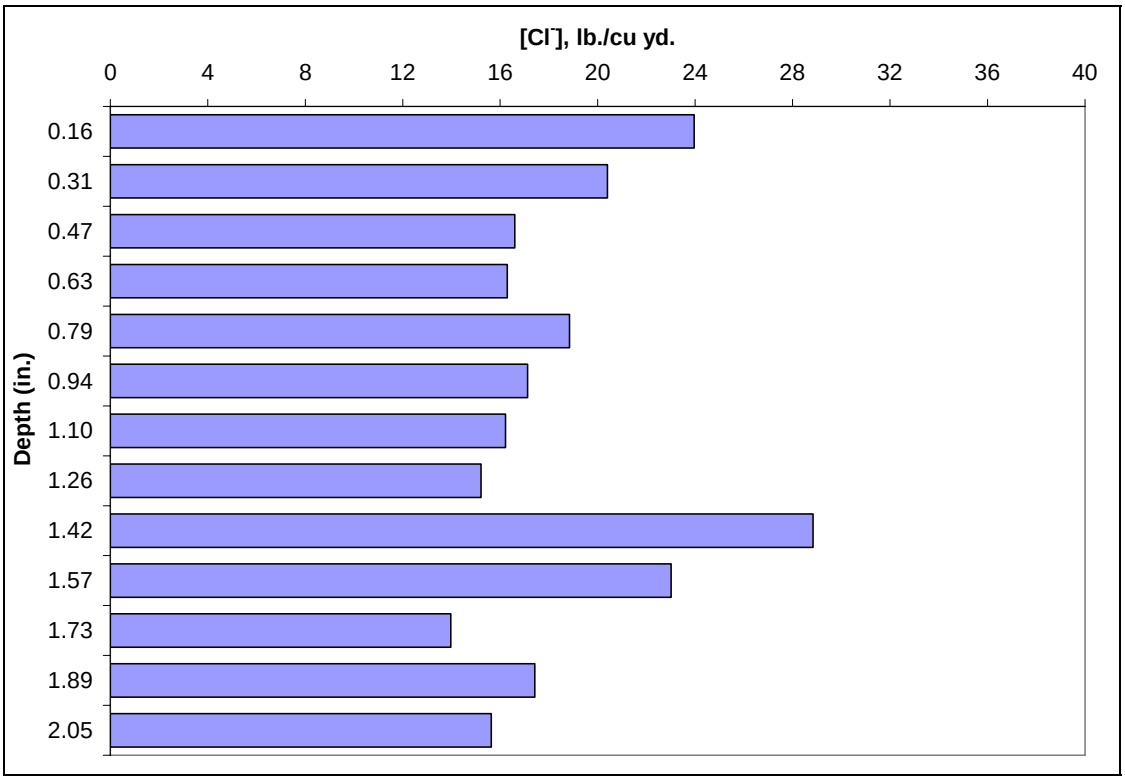

Figure 69. Chloride profile on the concrete of a flexible (green) epoxy-coated specimen.

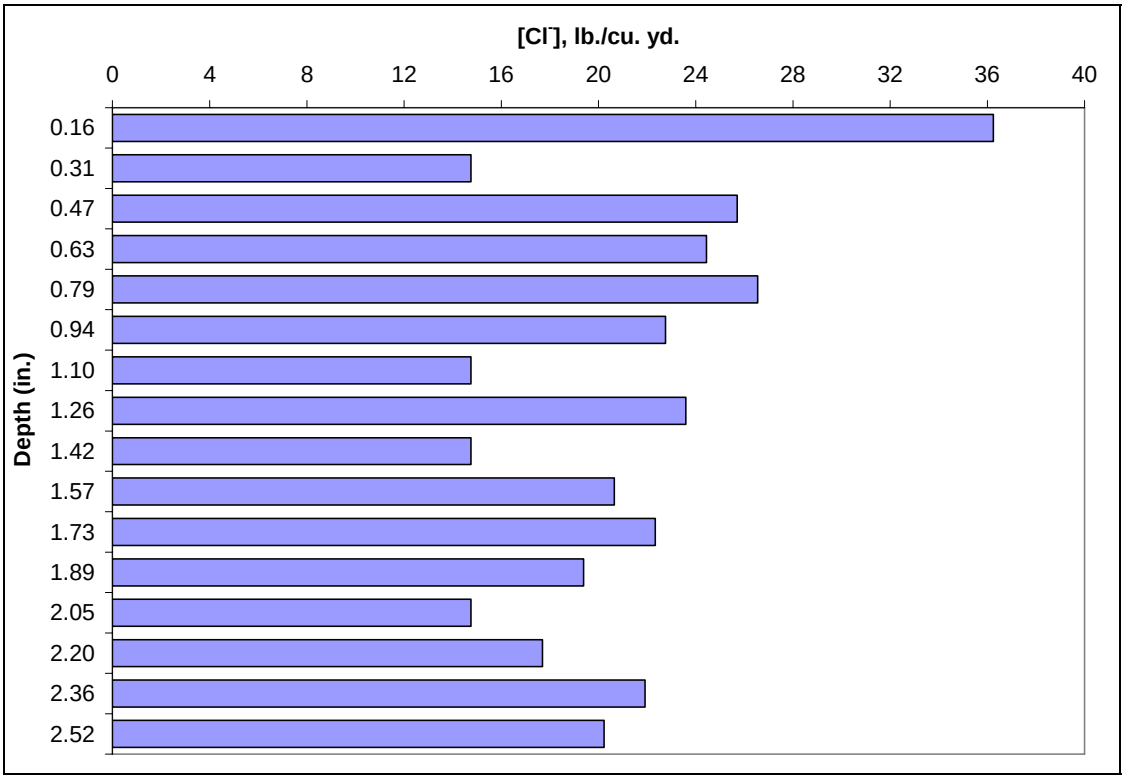

Figure 70. Chloride profile on the concrete of a non-flexible (purple) epoxy-coated specimen.

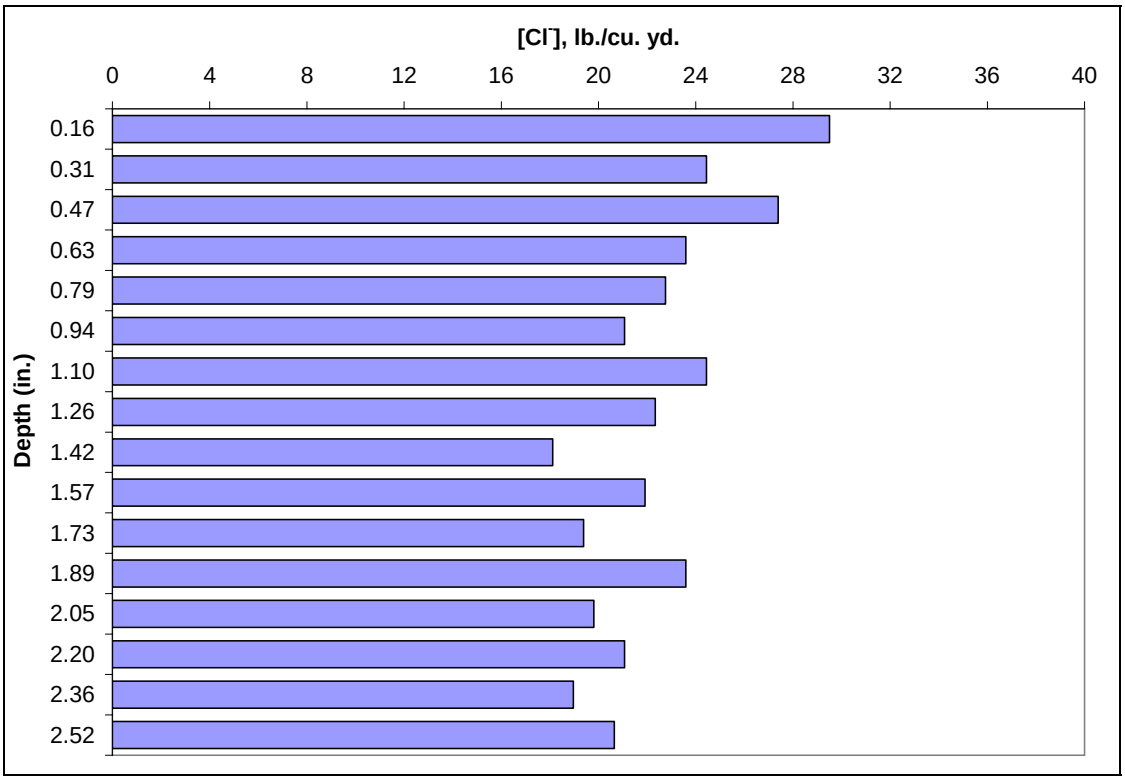

Figure 71. Chloride profile on the concrete of a microcomposite steel specimen.

4 CONCLUSIONS AND RECOMMENDATIONS

This study investigated through the use of accelerated laboratory tests the corrosion performance of several types of steel dowels cast in concrete beams. The accelerated testing consisted of ponding water with a chloride solution on the top of the beams and including a "joint" in each beam that provided direct access to a short segment of the dowels. No force loading was applied to the beams. Results are presented from the tests.

Conclusions are based on the results of half-cell potential tests, LPR curves, visual inspections, and microscopic investigations by Scanning Electron Microscope (SEM), all of which are presented in this report.

4.1 Phase I Testing Conclusions

The following conclusions are from the Phase I testing consisting of the placement of four types of dowels (carbon steel, epoxy-coated steel, stainless steel hollow, and stainless steel-clad) cast in concrete beams with joints in different corrosive environments, and evaluation using half-cell potential tests for corrosion initiation and visual inspection at the completion of testing.

1. Carbon steel dowels present the shortest corrosion initiation period — when chlorides have direct access to the bar through the joint, the initiation stage can be disregarded and the corrosion propagation phase begins immediately. Epoxy-coated dowels increased the initiation period considerably, while the stainless hollow and stainless clad dowels provided the highest resistance to the onset of corrosion.
2. From the visual inspections after six months of cyclic ponding, it was observed that the carbon steel dowels present uniform corrosion along the bar, while the epoxy-coated dowels had localized corrosion at defects mostly at the ends of the bars where the coating is most vulnerable to damage. No visible corrosion was found on either the stainless steel hollow bars or stainless clad bars.

4.2 Phase II Testing Conclusions

The following conclusions are based on the Phase II laboratory testing in which seven types of dowels [carbon steel, microcomposite steel, stainless steel hollow, stainless steel-clad, carbon steel coated with flexible epoxy (green colored), and carbon steel coated with non-flexible epoxies (purple and gray colored)] were cast in concrete beams with joints in different corrosive environments. These specimens were evaluated for corrosion resistance using half-cell potential tests, Linear Polarization Resistance curves, visual inspections, chloride analyses, and microscopic investigations.

1. In coated specimens, such as the epoxy-coated specimens included in this study, corrosion is not uniform, but is instead concentrated at localized defective areas (such as pinholes, voids, etc.). Given that epoxy is an electrical insulator, polarization happens only at very small areas (defective areas) that cannot be accounted for in the calculation of the polarization resistance term. Therefore, the epoxy-coated dowels cannot be quantitatively evaluated with the other dowels and must be evaluated qualitatively.
2. The carbon steel dowels exhibited the lowest values of polarization resistance (R_p) and consequently have the smallest resistance to charge transfer across the interface, and are therefore expected to have the fastest rate of corrosion propagation
3. Microcomposite steel dowels exhibited polarization resistance *(R_p)* approximately 35 times greater than carbon steel dowels, while stainless clad and stainless hollow bars had about 73 times greater polarization resistance. Notice that R_p is inversely proportional to the corrosion current density, and thus to the corrosion rate (see Equations A1 and A2 in Appendix A). This indicates that the microcomposite steel dowels exhibit much greater resistance to corrosion propagation than carbon steel dowels, but not as much as the stainless clad and hollow bars.

4. Based on corrosion current density results, it was verified that the carbon steel dowels exhibited very rapid corrosion, while microcomposite steel exhibited a moderate level and stainless steel-clad and stainless steel hollow proceeded at a low corrosion rate.
5. Visual inspections of the corroded dowels revealed heavy and mostly uniform corrosion along the carbon steel dowels, light corrosion in the microcomposite steel dowels, and no visible corrosion in the stainless steel-clad and stainless steel hollow bars. For the epoxy-coated dowels, the visual inspections generally revealed that visible corrosion was not widespread, but did occur at a few localized defective areas, generally at holidays and at the edges of the bar ends. No significant difference was observed on the performance of non-flexible and flexible epoxy-coated dowels.
6. In general, the microscopic investigation by SEM matches well the results anticipated by the electrical measurements and visual inspections. However, the analysis has focused mostly on the corroded areas of each sample, and revealed corroded areas that were not visible to the naked eye.
7. Statistical analyses of the results show that, in all cases, the type of steel dowel has a statistically significant effect on the quantitative parameters studied (i.e., half-cell potential, polarization resistance, and corrosion current density).

4.3 Conclusions from Phase III Testing

The following conclusions are drawn from the Phase III evaluation of the WSDOT dowel bar retrofit slabs extracted from the 40-year-old field section.

1. In the extracted slabs from which cores were taken at the joints, a considerable amount of corrosion product was verified by means of visual inspection. The corrosion occurred underneath the epoxy coating on the central region of the dowel beneath the joint. The corrosion is likely to have contributed to the loss of load transfer efficiency (LTE) of the joint because of the low-strength corrosion products at the interface between the concrete and the dowel. Lack of centering of one dowel over the transverse joint is also likely to have contributed to the low LTE.
2. Half-cell potential and Linear Polarization Resistance results match the visual observations, indicating the presence of active corrosion.

4.4 Conclusions from Chloride Analysis

The following conclusions are made regarding the relationship among the concentrations of chlorides in the laboratory samples, extracted WSDOT field slabs, and cores extracted from slabs in various locations in Washington State:

1. Chloride concentrations close to the pavement joints are significantly higher than in other regions of the pavement. At the joint, easier access and accumulation of chlorides leads to higher, localized concentrations.
2. When a joint is present, the chloride ions do not reach the dowel through the concrete (or grout) from the top, rather, they migrate through the open joint to the dowel.
3. In the field experiments, it was verified that the chloride threshold for carbon steel was exceeded in five out of six projects.
4. In the laboratory samples, with open joints located above the dowels, the chloride concentrations are more constant along the depth profile, as compared to field conditions in which the chloride has to diffuse through the concrete or migrate through a narrower joint.
5. The use of a 3.5% NaCl solution for laboratory experiments may lead to considerably high chloride concentrations, as compared to the results obtained in the field specimens, greatly

accelerating the corrosion process. As a result of this aggressive environment, corrosion could be observed in nearly all samples in only 18 months of exposure.

6. Laboratory results can be used to comparatively evaluate the corrosion resistance of different materials exposed to the same aggressive environment. However, the chloride concentration analyses indicate that the actual field conditions and local environment should be taken into account when choosing the appropriate material for a given project.

4.5 Recommendations

The following recommendations are based on the conclusions presented above.

1. The presence of ponding water-induced corrosion at the ends of and along the length of cast-in concrete dowels indicates that chlorides can pass all the way from the joint to the dowel ends along the horizontal interface between the dowel and the concrete, or through the concrete. For this reason it is recommended that uncoated carbon steel dowels not be used.
2. Epoxy dowels present some risk of corrosion, primarily localized at holidays and the ends. Based on this finding, it is recommend that:
    1. Quality control checks to control holidays should be implemented.
    2. Bar ends should be coated with epoxy, and care must be taken with epoxy-coated dowels during shipping, storage, and installation. Corrosion will be exacerbated if the bar ends are not coated (observed on various Caltrans construction sites) or if the coated ends are damaged during storage, transport, and installation.
3. It is recommended that the use of stainless steel-clad, hollow stainless steel, or microcomposite steel dowels be considered for locations with high risk of high chloride exposure (such as on mountain passes and marine environments), where exposure to corrosive water is anticipated. The selection of a specific corrosion-resistant dowel should be based on further field investigations and cost differences.
4. It is recommended that a field study be performed at several mountain pass locations to measure the chloride content of snowmelt after sand/salt application for comparison with the chloride content of the solution used in the laboratory testing in Phases I and II. The results of this study should be used to further refine the risk assessment in these critical locations.

5 REFERENCES

1. Harvey, J. T., Ali, A., Hung, D., Uhlmeyer, J., Popescu, L., Bush, D., Grote, K., Lea, J., and Scheffy, C.. Construction and Test Results from Dowel Bar Retrofit HVS Test Sections 553FD, 554FD and 555FD: US 101, Ukiah, Mendocino County. Draft report prepared for the California Department of Transportation. Pavement Research Center, Institute of Transportation Studies, University of California. February 2003.
2. Bentur, A., Diamond, S., and Berke, N. S. *Steel Corrosion in Concrete*. E&FN Spon, 1997.
3. Mehta, P. K. and Monteiro, P. J. M. C*oncrete: Structure, Properties and Materials.* 3rd Edition, McGraw Hill, 2006.
4. Davids, W. G., Wang, Z. M. ., Turkiyyah, G., Mahoney, J.,and Bush, D. "3D Finite Element Analysis of Jointed Plain Concrete Pavement with EverFE2.2." *Transportation Research Record 1853*, TRB, National Research Council, Washington, D.C., 2003, pp 92-99.
5. Mack, J. W. "Dowel Retrofit Restores Pavement Load Transfer." RP335PAmerican Concrete Paving Association, Skokie IL, 1995.
6. Tuutti, K. *Corrosion of Steel in Concrete.* Stockholm, Sweeden. Swedish Cement and Concrete Research Institute, 1982.
7. Pavement Systems Limited LLC. *Climatic Database for Integrated Model (CDIM).* Software, version 1.0. Prepared for California Department of Transportation under contract to University of California Partnered Pavement Research Center. Bethesda, MD. April, 2004.
8. Trejo, D.; Radhakrishna, P. "Accelerated Chloride Threshold Testing: Part II – Corrosion Resistant Reinforcement." *ACI Materials Journal*, 101 (1). 2004. pp.57-64.
9. Broomfield, J. P. *Corrosion of Steel in Concrete: Understanding, Investigation and Repair.* E&FN Spon, 1997.
10. Trejo, D.; Radhakrishna, P. *Evaluation of the Critical Chloride Threshold for Different Steel Reinforcement Types.* TEES/MMFX Final Report. Texas Engineering Experiment Station, Texas A&M University, March 2005.
11. Carino, N. J. "Nondestructive Techniques to Investigate Corrosion Status in Concrete Structures." *Journal of Performance of Constructed Facilities*, 13 (3). 1999. pp.96-106.
12. Trejo, D.; Radhakrishna, P. "Accelerated Chloride Threshold Testing: Part I – ASTM A 615 and A 706 Reinforcement." *ACI Materials Journal*, 100 (6). 2003. pp.519-527.

APPENDIX A: Detection Techniques

Half-Cell Potential

The standard test method for half-cell potential measurements is described in ASTM C876 (1997). The test apparatus (illustrated in A1) consists of an external electrode (half cell)[1], connecting wires, and a high impedance voltmeter (impedance >10MΩ). The high impedance voltmeter is used so that there is a very little current through the circuit.

The half-cell potential measurement has been widely used in the field, due to its simplicity and general agreement that this technique does indicate the existence of active corrosion along the steel reinforcement in concrete.

Note that one terminal of the voltmeter must be connected to the reinforcement, that is, physical access to the reinforcement must be provided, so it is usual practice to break away the concrete cover to enable the electrical contact to be made.

When active corrosion is present, current flows through the concrete between the anodic and cathodic sites due to the migration of ions, and this current is accompanied by an electrical potential field surrounding the corroding bar. Also, once the metal used for the half-cell electrode (silver, mercury, or copper) has a more positive standard potential than iron, the external electrode will be the cathode in the circuit (Figure A1).

[1] The most commonly used electrodes are: silver/ silver chloride (Ag/AgCl), mercury/mercury oxide (Hg/HgO) and copper/copper sulfate ($Cu/CuSO_4$). In laboratory, it is more common to measure potentials with a *calomel* electrode (mercury/mercury chloride).

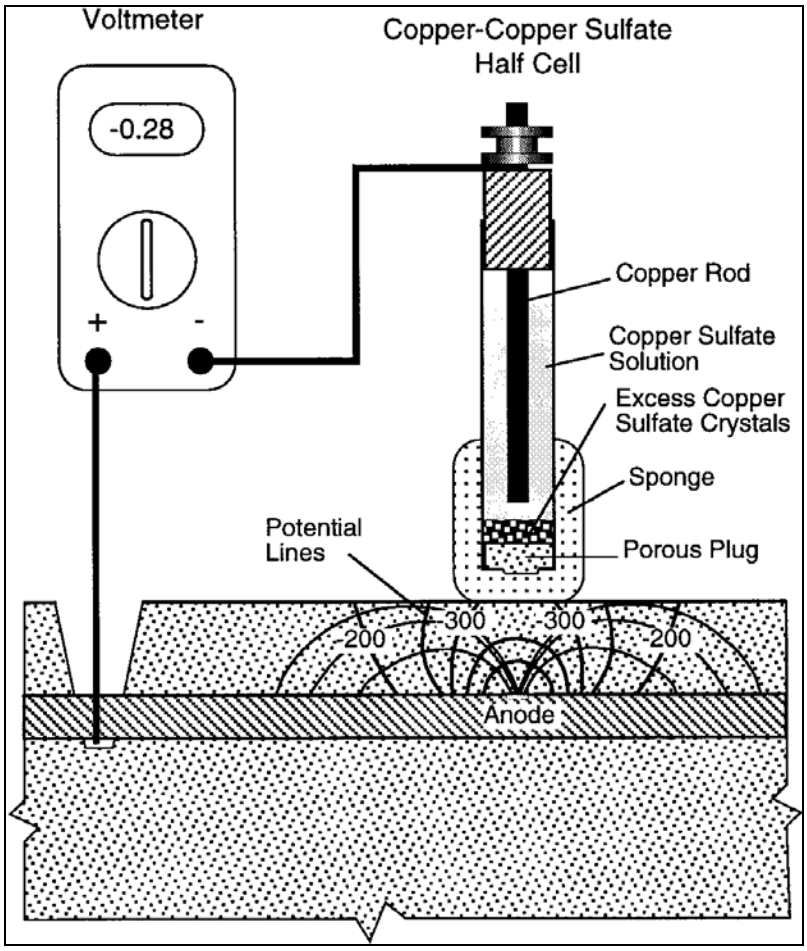

Figure A1. Apparatus for half-cell potential measurement, described in ASTM C876.

So, if the bar is corroding, the excess electrons in the bar will tend to flow from the bar (anode) to the half-cell (cathode). Because of the way the terminals of the voltmeter are connected, the voltmeter indicates a negative voltage. A more negative voltage reading is interpreted to mean that the embedded bar has more excess electrons and, therefore, there is a higher likelihood that the bar is corroding. The half-cell potential measurements are indicative of the probability of corrosion activity of the reinforcing steel located beneath the half-cell. *(11, 9)*

The appendix of ASTM C876 provides guidelines on interpreting results obtained through half-cell potential measurements. There are two basic techniques to evaluate the results: the numerical technique, in which the value of the potential is used as an indicator of the likelihood of corrosion activity (see Table A1); and the potential difference technique, in which the areas of active corrosion are identified on the basis of the potential gradients, constructed based on an equipotential contour plot.

Table A1. Relationship between Half-Cell Potential and Corrosion of Steel Embedded in Concrete (ASTM C876)

Half-Cell Potential (mV) *	**Interpretation**
> -200	Low probability (10%) of corrosion
-200 to -350	Corrosion activity (uncertain)
< -350	High probability (90%) of corrosion)

* Measurements made with a copper/copper sulfate electrode.

According to Carino, it is generally accepted that the potential difference technique is more reliable for identifying regions of active corrosion than is the use of numerical limits.(*11*) Thus, the half-cell potential method provides an indication of the likelihood of corrosion activity at the time of the measurement. However, it does not give any information on the rate of corrosion of the reinforcement.

Linear Polarization Resistance (LPR)

Several methods have been investigated for measuring the in-situ corrosion rate of steel embedded in concrete. Among these methods, Linear Polarization Resistance (LPR) appears to be gaining most acceptance.(*11*)

LPR is a well-established method for determining corrosion rate by using electrolytic test cells (ASTM G59). The technique involves measuring the change in the open-circuit potential of the electrolytic cell when an external current is applied to the cell. For a small perturbation about the open-circuit potential, there is a linear relationship between the change in applied current per unit area of electrode (Δi) and the change in the measured voltage (ΔE). The ratio $\Delta E/\Delta i$ is called the polarization resistance (Rp). The corrosion rate, expressed as the corrosion current density, is inversely related to the polarization resistance (ASTM G59), as showed in Equation A1.

$$i_{corr} = \frac{B}{R_P} \qquad \textbf{(A1)}$$

In this equation, i_{corr} is the corrosion current density (in A/cm^2), B is a constant (in V), and R_p is the polarization resistance (in Ω/cm^2). The constant B is a characteristic of the polarization curves, and a value of 26 mV is commonly used for steel that is actively corroding in concrete. The basic apparatus utilized is shown in Figure A2a.

One electrode is a reference half-cell, and the reinforcement is a second electrode called the working electrode. The third electrode is referred to as the counter electrode, and it supplies the polarization current to the bar. Supplementary instrumentation measures the voltages and currents during different stages of the test.

A major concern with this method is the uncertainty regarding the area of the steel bar that is affected by the current from the counter electrode. Usually it is assumed that the current flows in straight lines perpendicular to the bar and the counter electrode, and the affected bar area is taken as the bar circumference multiplied by the length of the bar below the counter electrode. In the laboratory experiments performed as part of this study, the counter electrode (CE) was placed above the joint, and therefore this concern is not justified. In this case, virtually all the current will flow through the NaCl solution present in the open joint, which represents a very low-resistivity path as compared to concrete.

Some guidelines have been developed to establish a relationship between corrosion current density and corrosion speed, as can be seen in Table A2.(*9*)

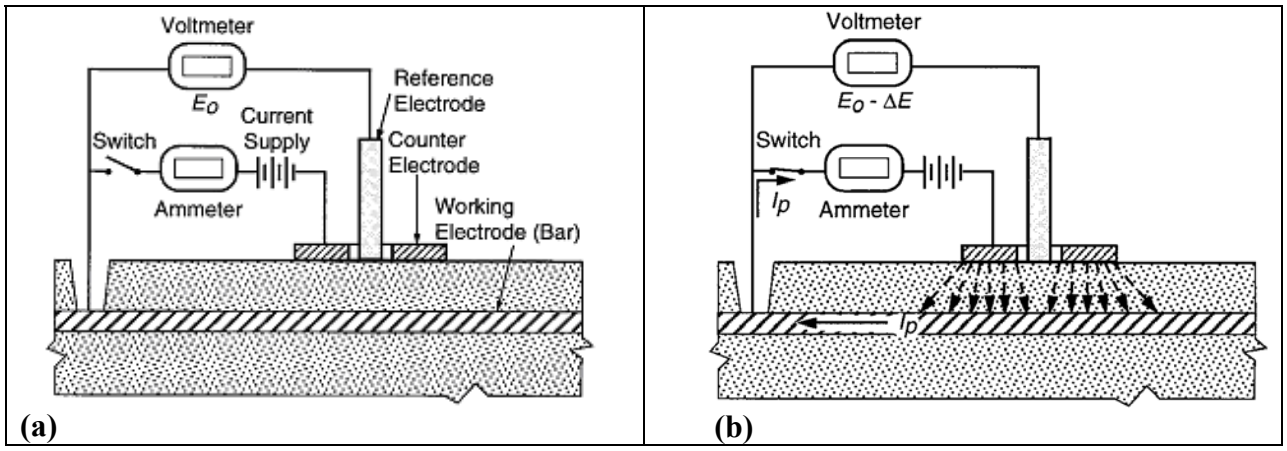

Figure A2. Three-electrode Linear Polarization Resistance method. (a) Measurement of the open-circuit potential (half-cell potential); (b) Current applied to the counter electrode to produce a small change in voltage E.(*12*)

Table A2 Relationship between Corrosion Current Density and Corrosion Speed

Corrosion Current Density (A/cm^2) *	Corrosion Speed
< 0.1	Negligible
0.1 – 0.5	Low
0.5 – 1.0	Moderate
> 1.0	High

*Measurements made with a guard electrode device.

Using Faraday's law, the corrosion current density (Equation A1) can be converted to metal loss. Faraday's law can be expressed as

$$m \quad \frac{M.i.t}{z.F} \qquad \textbf{(A2)}$$

In this equation, m is the mass of steel consumed, i is the current (in amperes), t is the time (in seconds), F is Faraday's constant (96500A), z is the ionic charge (equal to 2 for $Fe \quad Fe^{+2} + 2e^{-}$), and M is the atomic weight of the metal (equal to 56 g for Fe). This gives a conversion of 1 A.cm^2 = 11.6 m = 1.16*10^{-2} mm of steel section loss per year. It is important to note that this calculation assumes that corrosion is occurring uniformly on the bar, which is the typical condition when the corrosion is induced by a carbonation front. However, chloride-induced corrosion is associated with small, concentrated areas of corrosion. It has been reported that the depth of local pitting may be four to eight times the average depth of corrosion (*11*).

Physical Inspection

In addition to the electrochemical techniques, physical techniques have also found wide application for detecting corrosion in reinforced concrete. Physical methods such as visual inspection and others (e.g., stress wave techniques, magnetic methods, radar) can be used to detect deterioration of concrete or reinforcement loss by corrosion. Most of these techniques have been translated from concrete technology, where they were originally used for inspection of concrete degradation. Thus, most aim to detect corrosion from the identification of damage to concrete and other tests are usually needed to confirm the source and cause of the deterioration (*9*). In the present study, the concrete samples were broken apart and direct visual inspection was made of the corroded dowels.

APPENDIX B: Linear Polarization Results of Individual Specimens

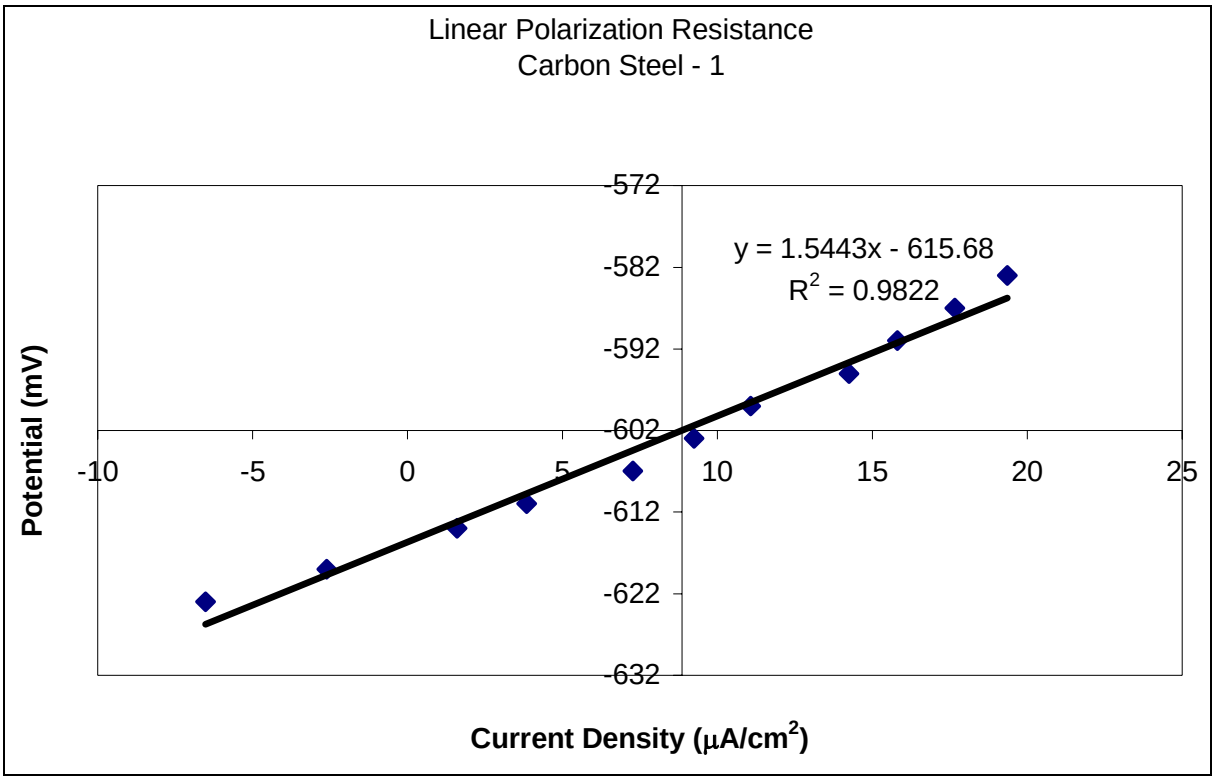

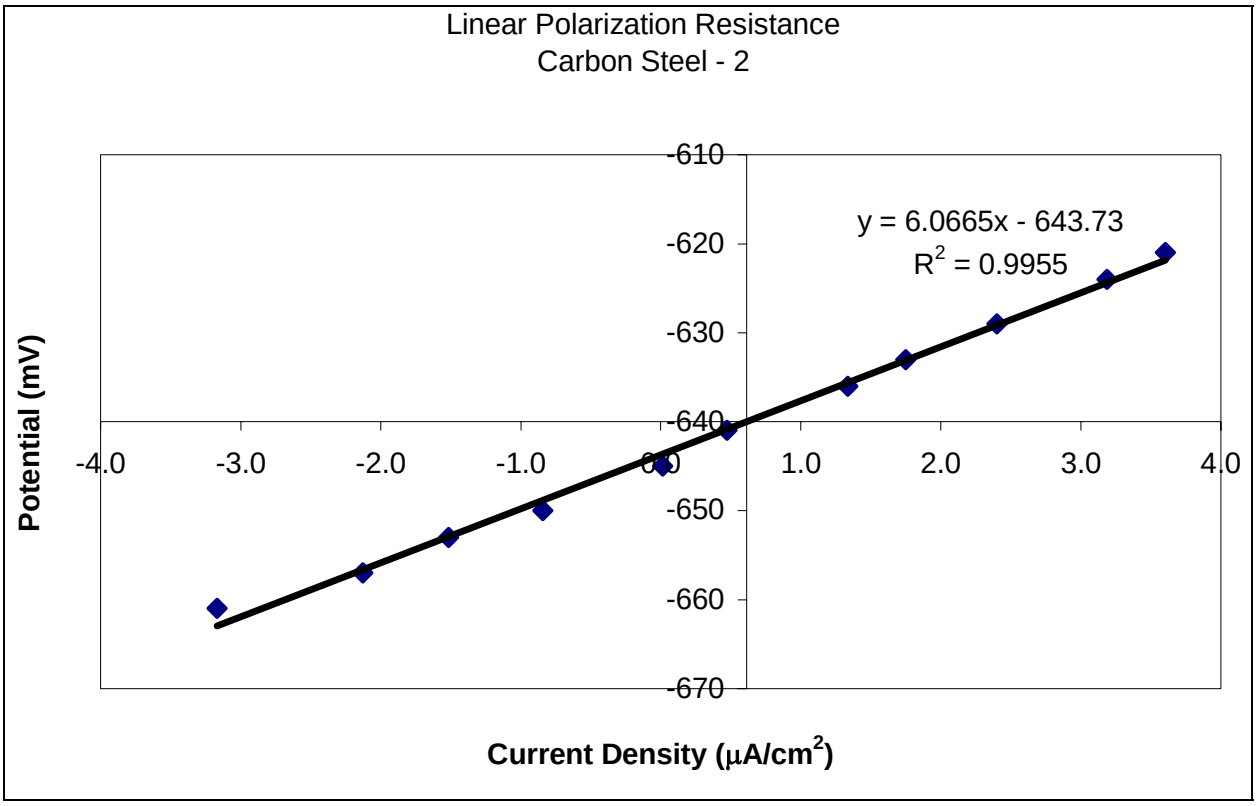
Linear Polarization Resistance
Carbon Steel - 2
y = 6.0665x - 643.73
R2 = 0.9955
Potential (mV)
-610
-620
-630
-640
-650
-660
-670
-4.0
-3.0
-2.0
-1.0
1.0
2.0
3.0
4.0
Current Density (µA/cm2)

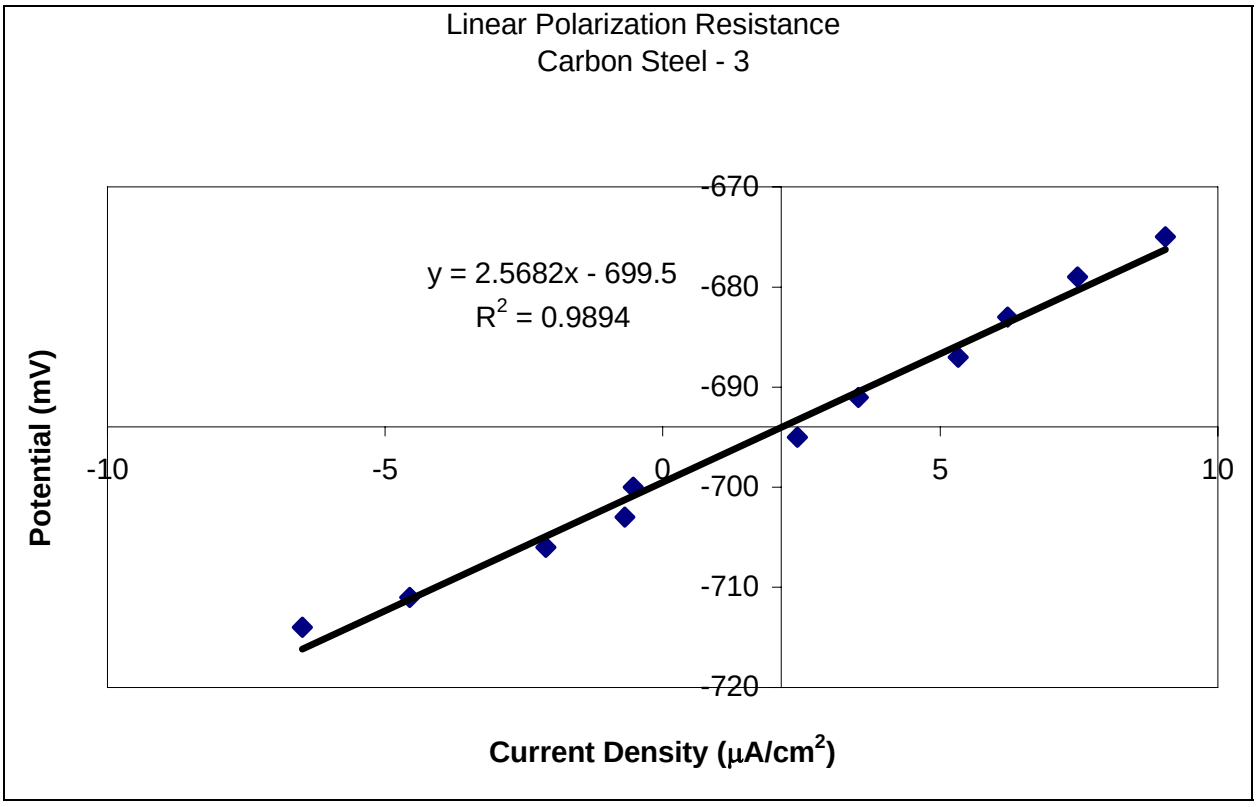
Linear Polarization Resistance
Carbon Steel - 3
y = 2.5682x - 699.5
R2 = 0.9894
Potential (mV)
-670
-680
-690
-700
-710
-720
-10
-5
0
5
10
Current Density (µA/cm2)

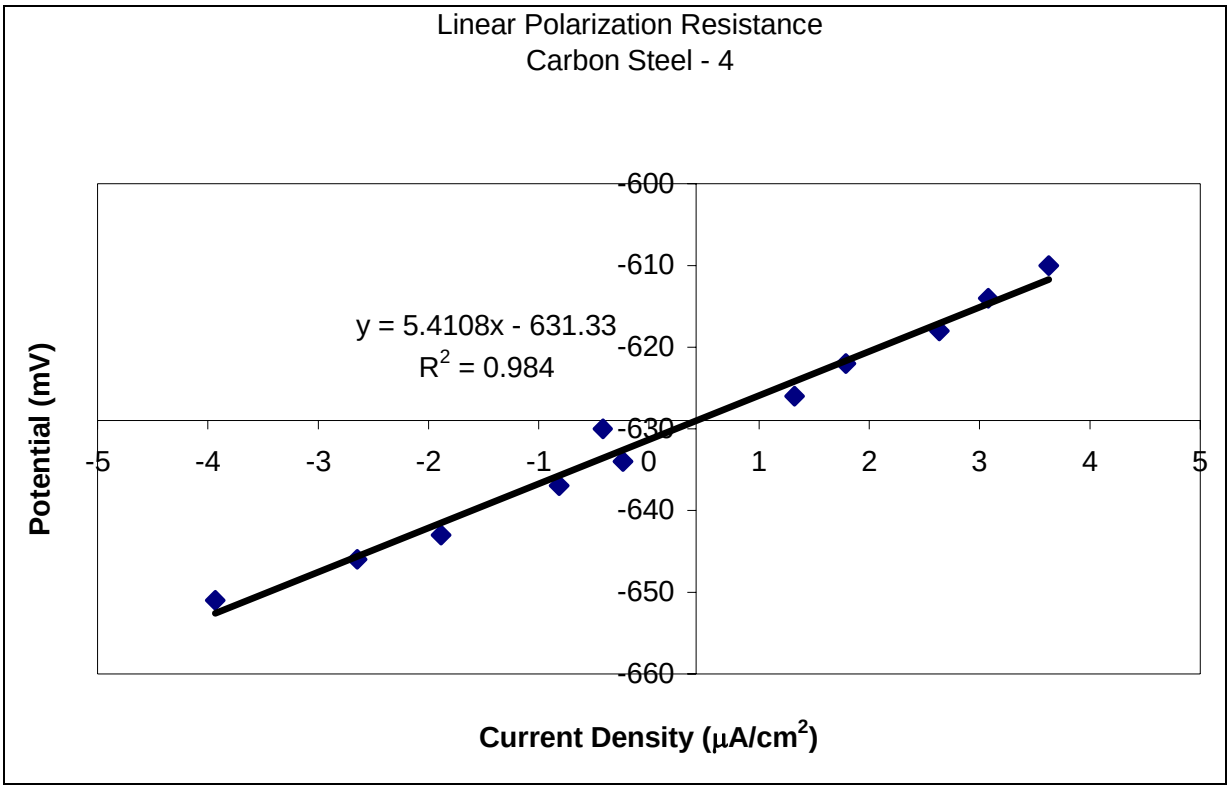
Linear Polarization Resistance
Carbon Steel - 4
y = 5.4108x - 631.33
R2 = 0.984
Potential (mV)
-600
-610
-620
-630
-640
-650
-660
-5
-4
-3
-2
-1
0
1
2
3
4
5
Current Density (µA/cm2)

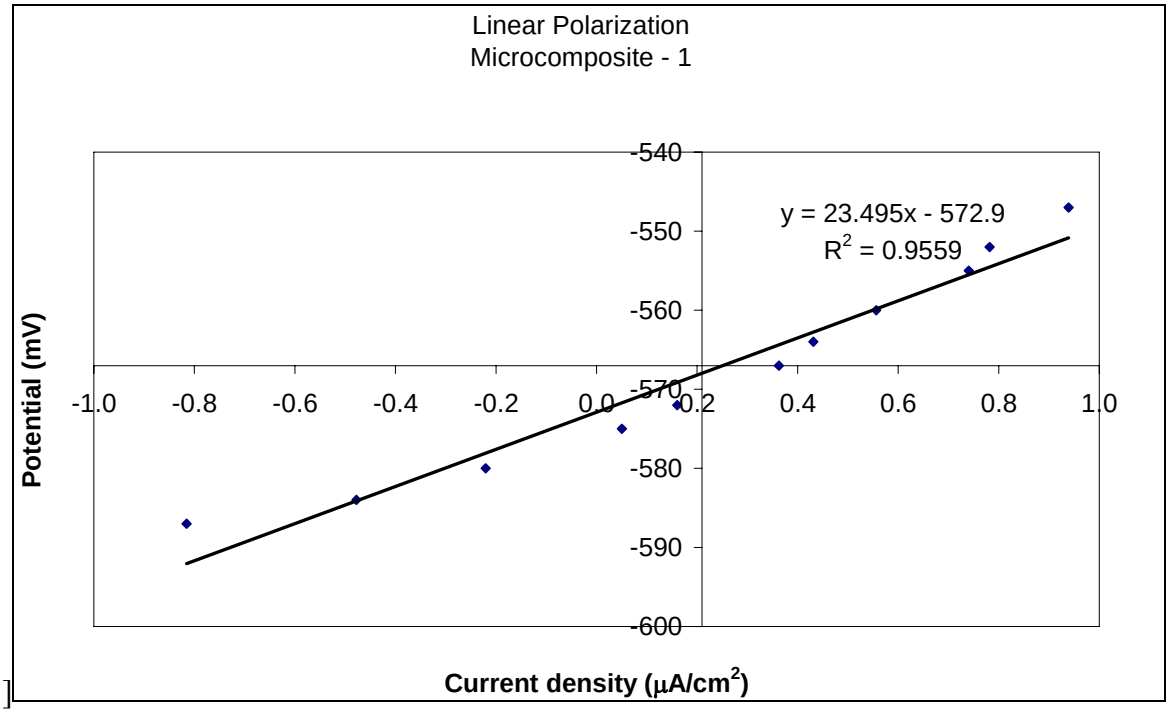
Linear Polarization
Microcomposite - 1
y = 23.495x - 572.9
R2 = 0.9559
Potential (mV)
-540
-550
-560
-570
-580
-590
-600
-1.0
-0.8
-0.6
-0.4
-0.2
0.0
0.2
0.4
0.6
0.8
1.0
Current density (µA/cm2)

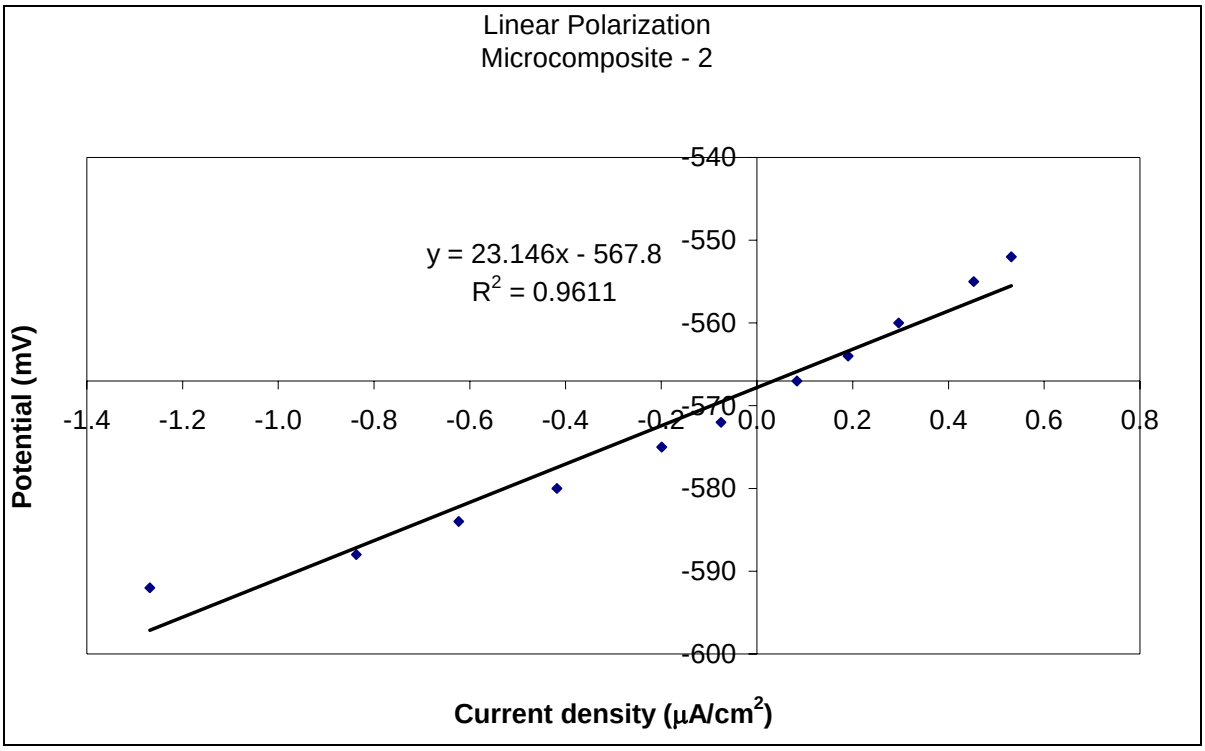
Linear Polarization
Microcomposite - 2
y = 23.146x - 567.8
R2 = 0.9611
Potential (mV)
-540
-550
-560
-570
-580
-590
-600
-1.4
-1.2
-1.0
-0.8
-0.6
-0.4
-0.2
0.0
0.2
0.4
0.6
0.8
Current density (µA/cm2)

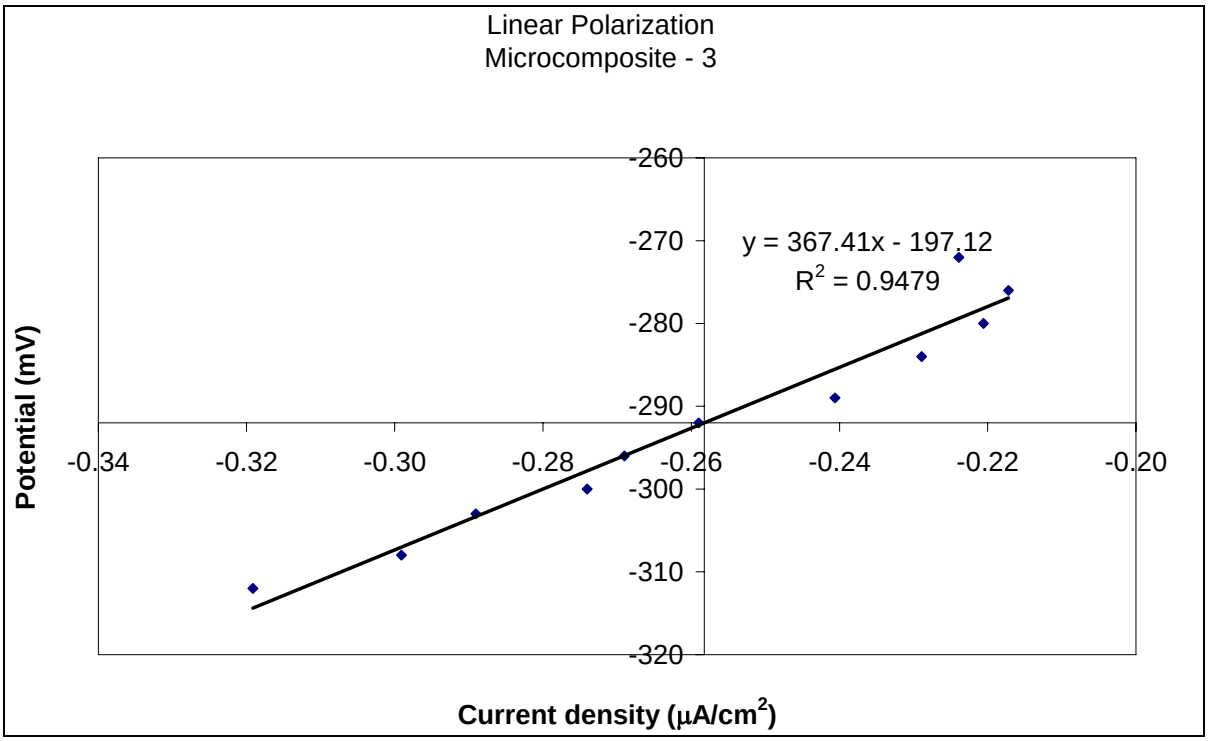
Linear Polarization
Microcomposite - 3
y = 367.41x - 197.12
R2 = 0.9479
Potential (mV)
-260
-270
-280
-290
-300
-310
-320
-0.34
-0.32
-0.30
-0.28
-0.26
-0.24
-0.22
-0.20
Current density (µA/cm2)

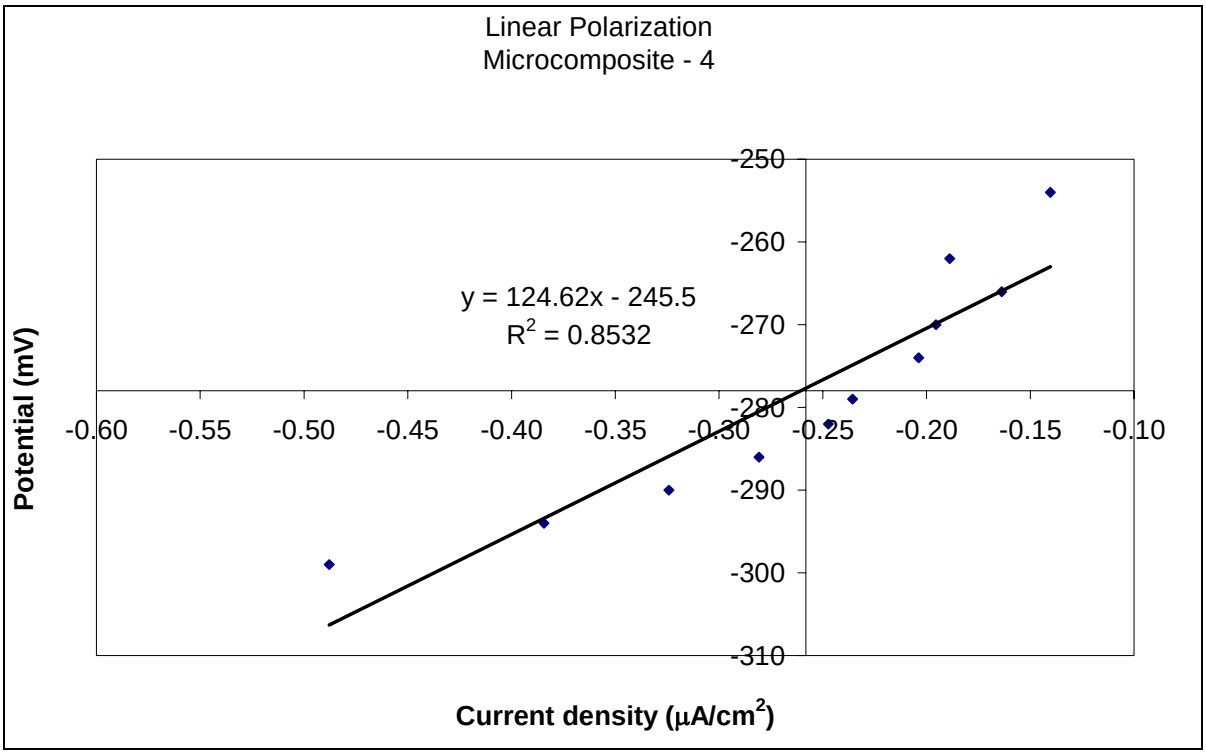
Linear Polarization
Microcomposite - 4
y = 124.62x - 245.5
R2 = 0.8532
Potential (mV)
-250
-260
-270
-280
-290
-300
-310
-0.60
-0.55
-0.50
-0.45
-0.40
-0.35
-0.30
-0.25
-0.20
-0.15
-0.10
Current density (µA/cm2)

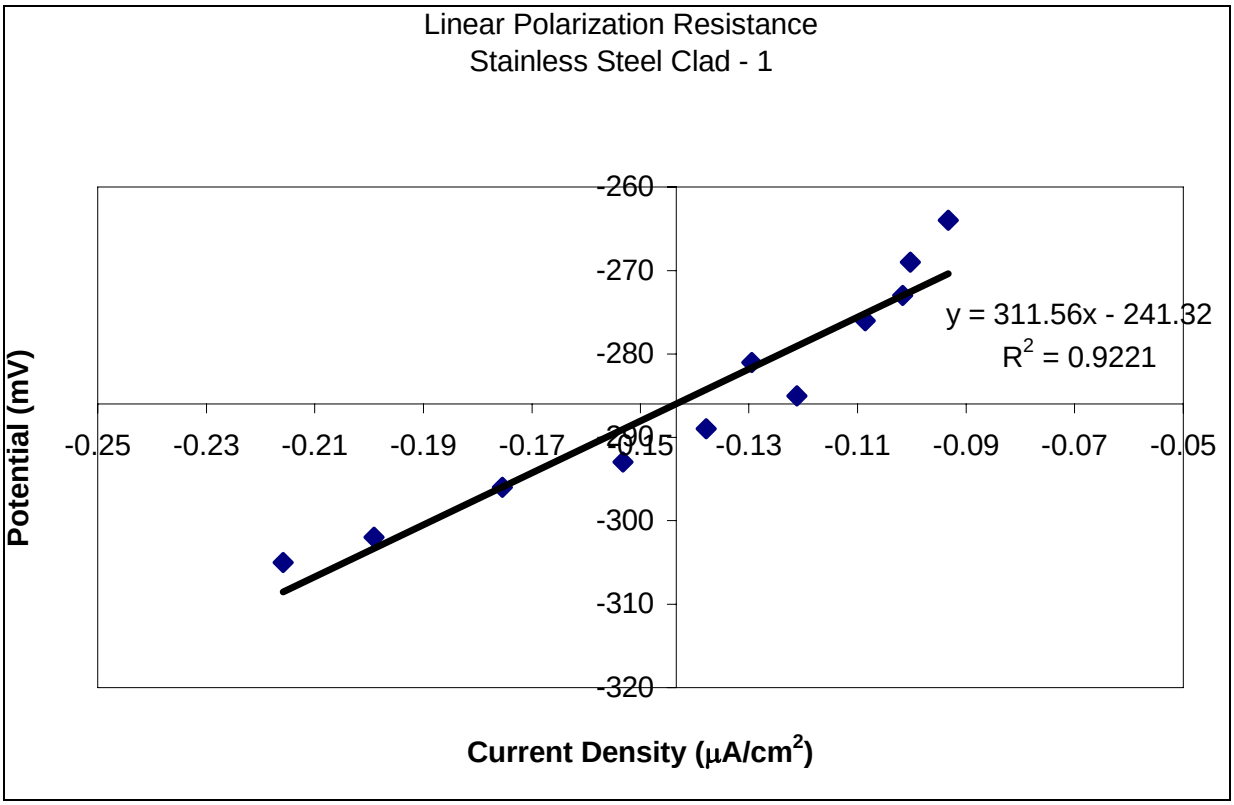
Linear Polarization Resistance
Stainless Steel Clad - 1
y = 311.56x - 241.32
R2 = 0.9221
Potential (mV)
-260
-270
-280
-290
-300
-310
-320
-0.25
-0.23
-0.21
-0.19
-0.17
-0.15
-0.13
-0.11
-0.09
-0.07
-0.05
Current Density (µA/cm2)

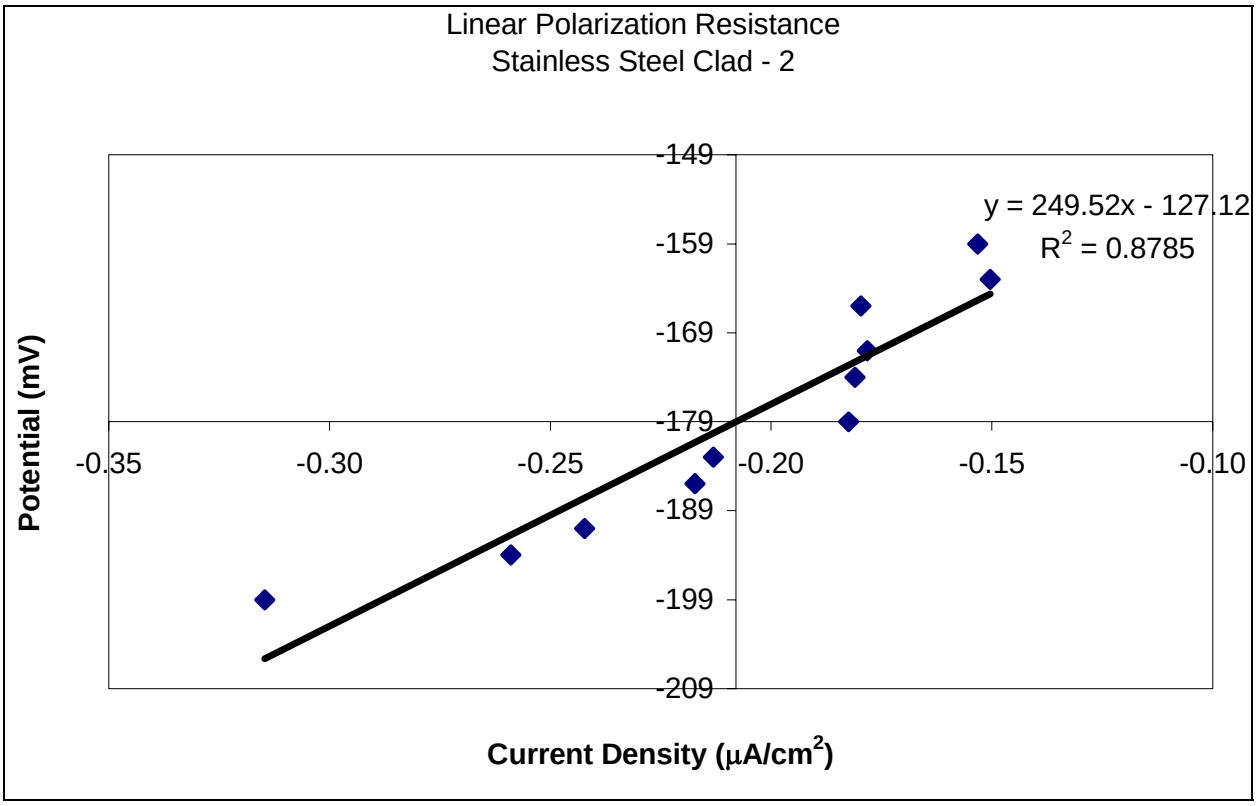
Linear Polarization Resistance
Stainless Steel Clad - 2
y = 249.52x - 127.12
R2 = 0.8785
Potential (mV)
-149
-159
-169
-179
-189
-199
-209
-0.35
-0.30
-0.25
-0.20
-0.15
-0.10
Current Density (µA/cm2)

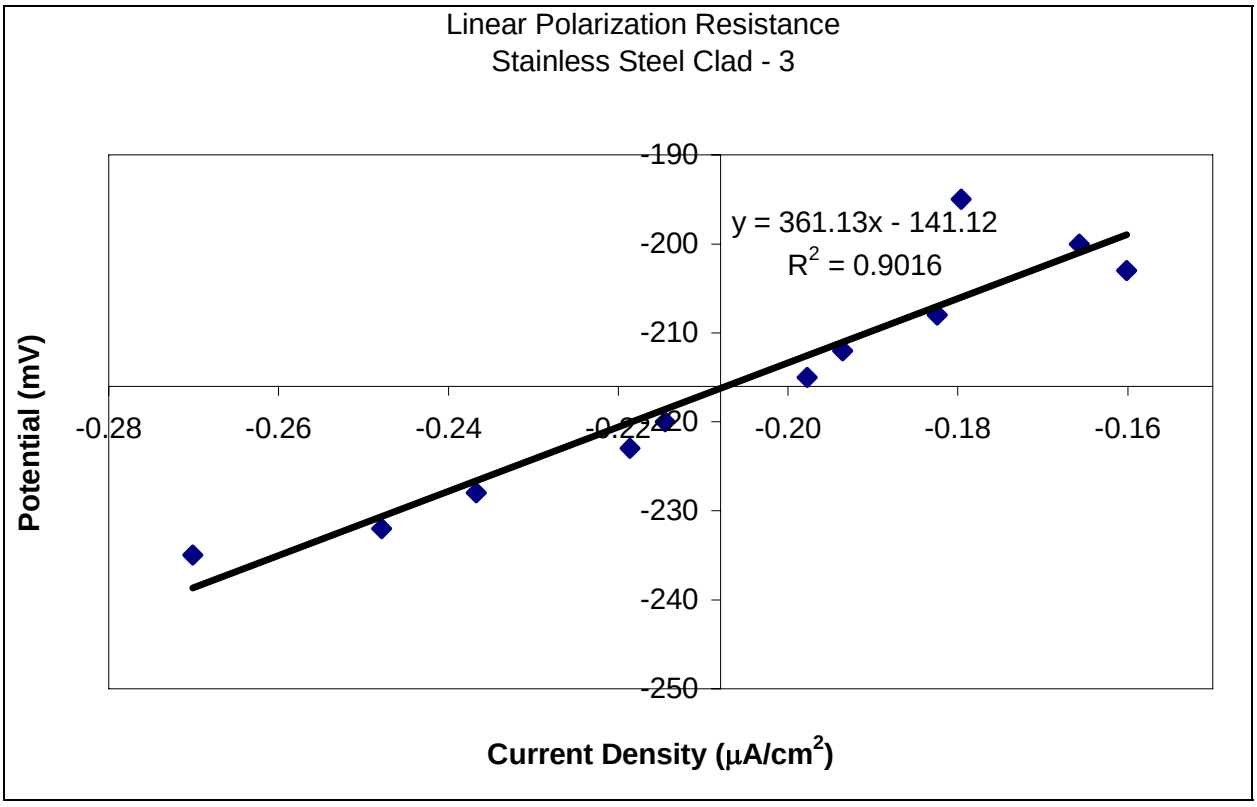
Linear Polarization Resistance
Stainless Steel Clad - 3
y = 361.13x - 141.12
R2 = 0.9016
Potential (mV)
-190
-200
-210
-220
-230
-240
-250
-0.28
-0.26
-0.24
-0.22
-0.20
-0.18
-0.16
Current Density (µA/cm2)

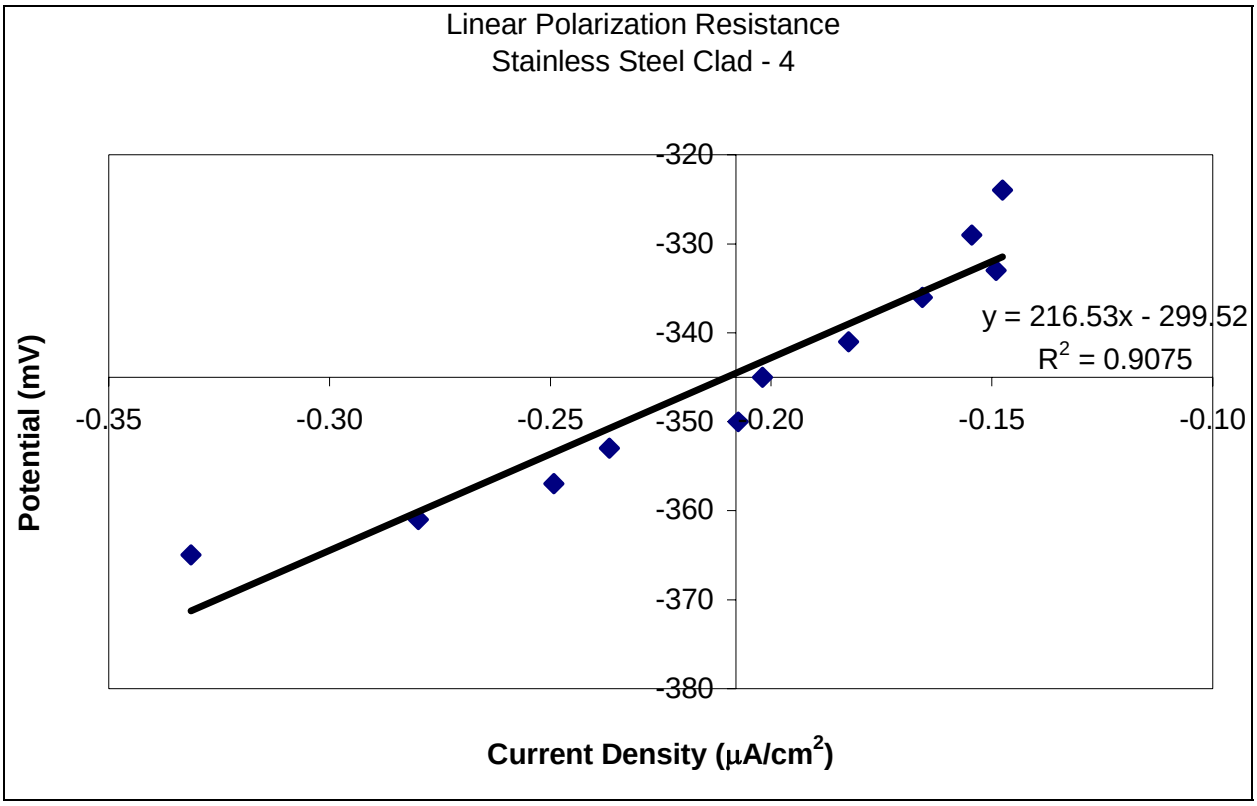
Linear Polarization Resistance
Stainless Steel Clad - 4
-320
-330
-340
-350
-360
-370
-380
-0.35
-0.30
-0.25
-0.20
-0.15
-0.10
y = 216.53x - 299.52
R2 = 0.9075
Potential (mV)
Current Density (µA/cm2)

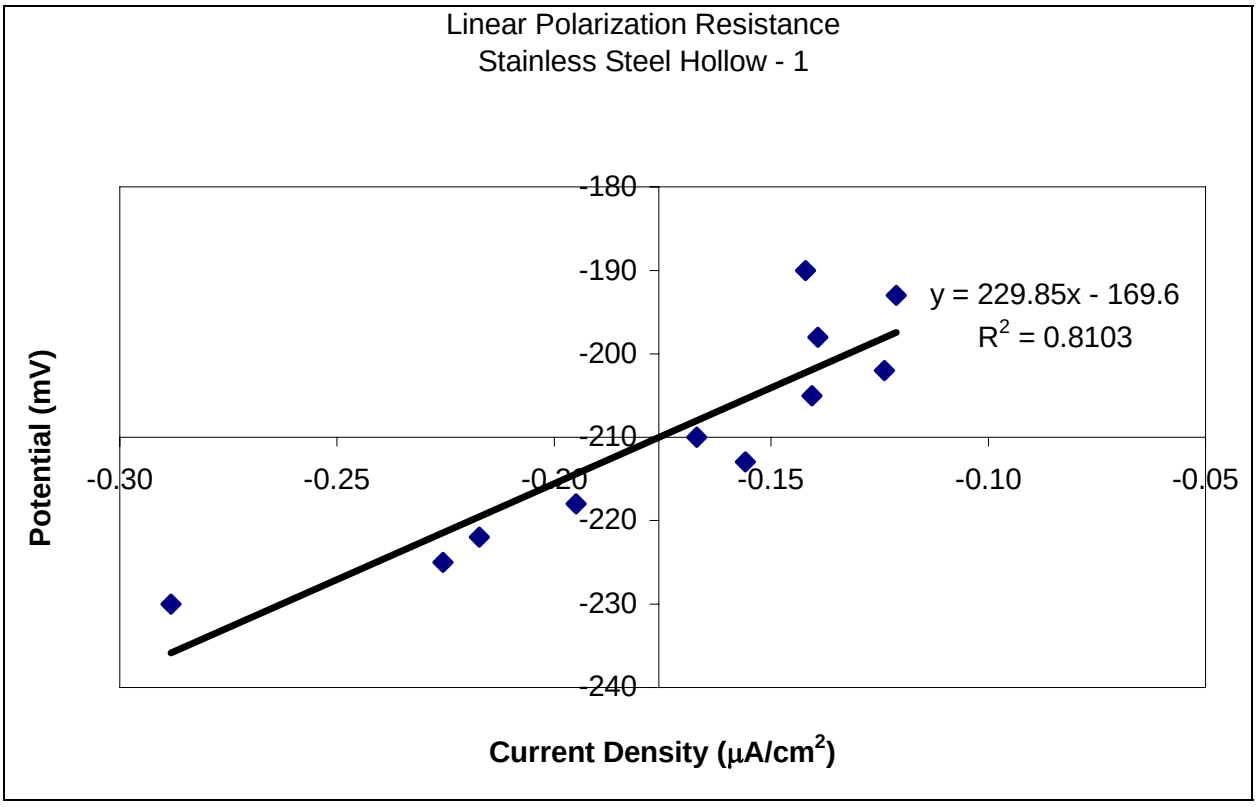
Linear Polarization Resistance
Stainless Steel Hollow - 1
-180
-190
-200
-210
-220
-230
-240
-0.30
-0.25
-0.20
-0.15
-0.10
-0.05
y = 229.85x - 169.6
R2 = 0.8103
Potential (mV)
Current Density (µA/cm2)

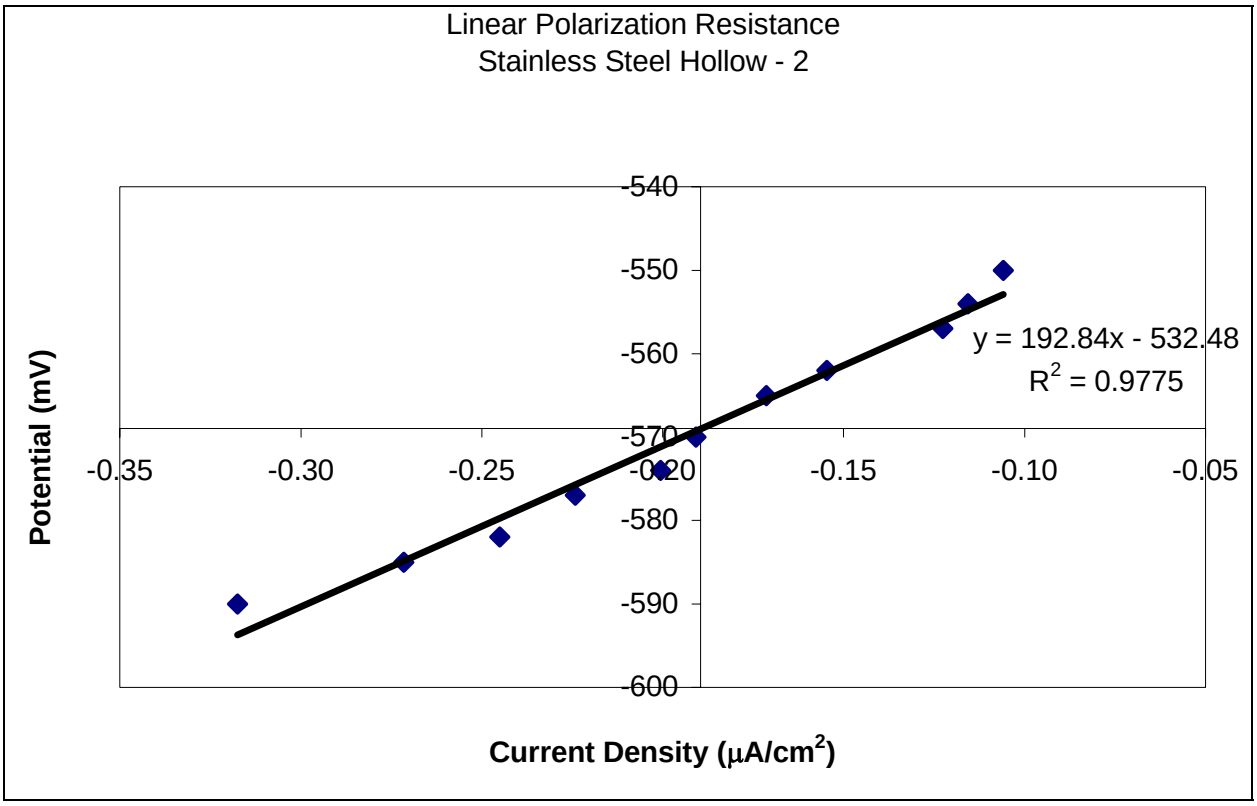
Linear Polarization Resistance
Stainless Steel Hollow - 2
Potential (mV)
-540
-550
-560
-570
-580
-590
-600
-0.35
-0.30
-0.25
-0.20
-0.15
-0.10
-0.05
y = 192.84x - 532.48
R2 = 0.9775
Current Density (µA/cm2)

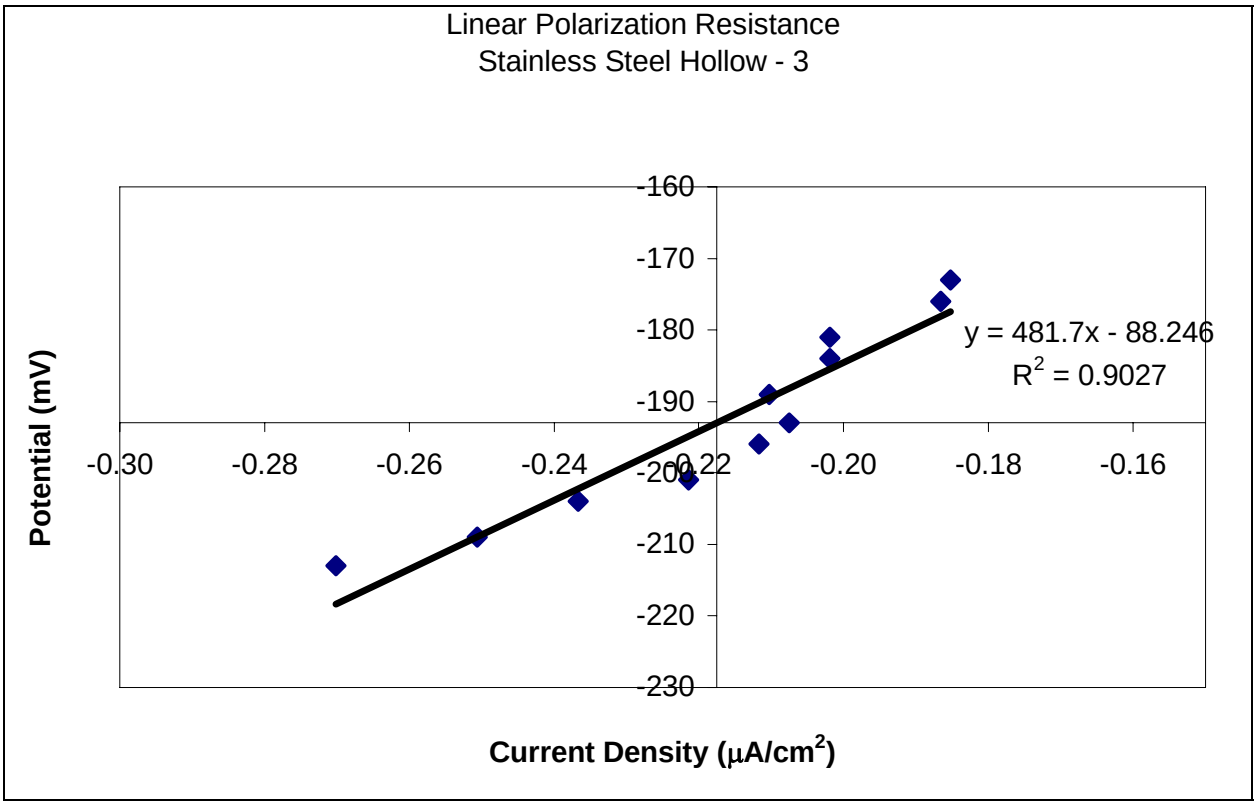
Linear Polarization Resistance
Stainless Steel Hollow - 3
Potential (mV)
-160
-170
-180
-190
-200
-210
-220
-230
-0.30
-0.28
-0.26
-0.24
-0.22
-0.20
-0.18
-0.16
y = 481.7x - 88.246
R2 = 0.9027
Current Density (µA/cm2)

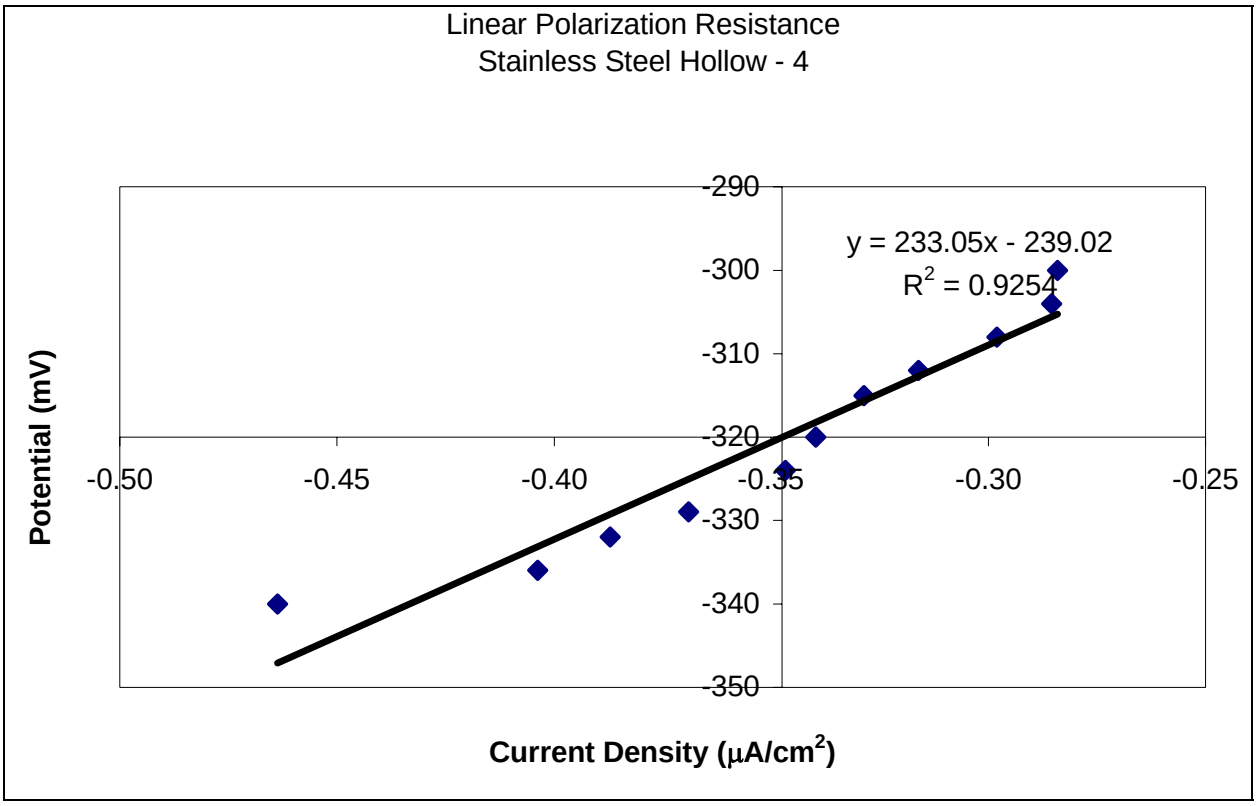
Linear Polarization Resistance
Stainless Steel Hollow - 4
y = 233.05x - 239.02
R2 = 0.9254
Potential (mV)
-290
-300
-310
-320
-330
-340
-350
-0.50
-0.45
-0.40
-0.35
-0.30
-0.25
Current Density (µA/cm2)

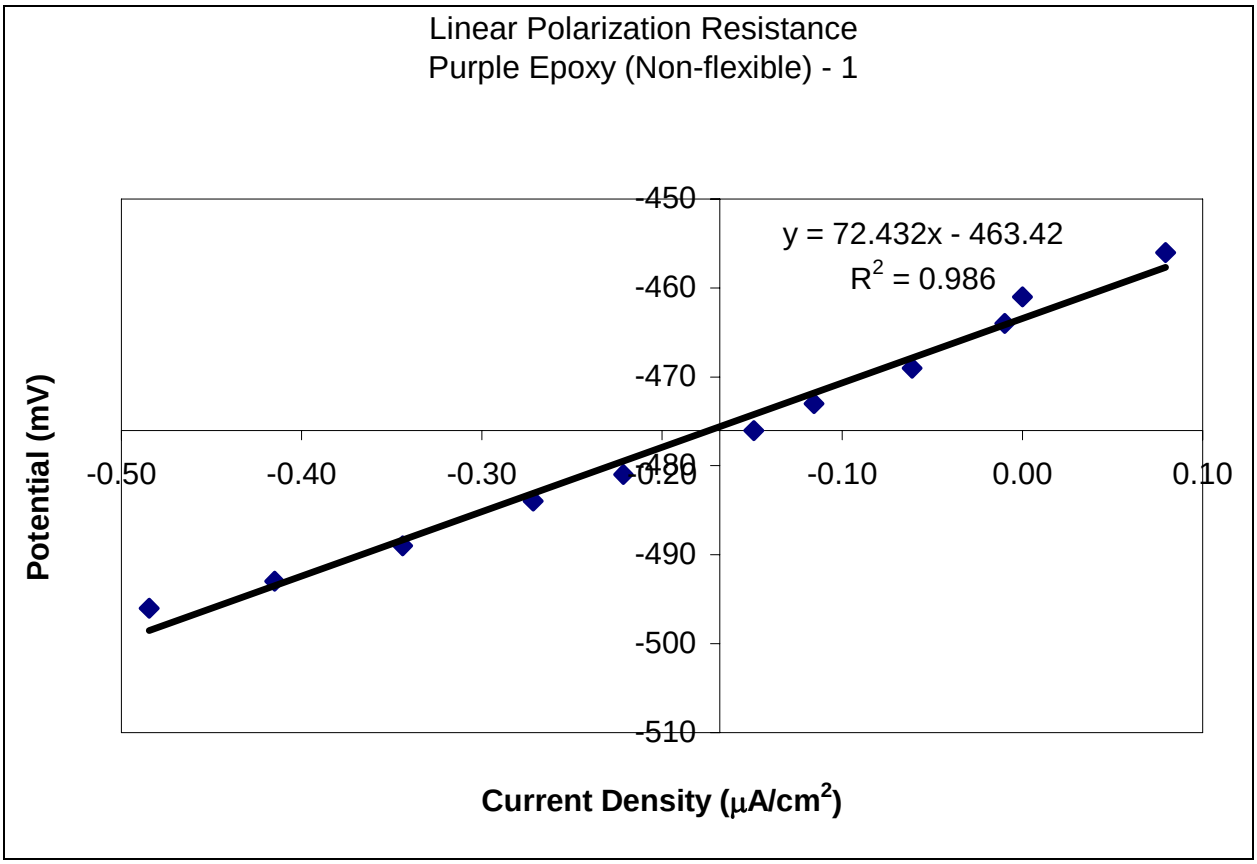
Linear Polarization Resistance
Purple Epoxy (Non-flexible) - 1
y = 72.432x - 463.42
R2 = 0.986
Potential (mV)
-450
-460
-470
-480
-490
-500
-510
-0.50
-0.40
-0.30
-0.20
-0.10
0.00
0.10
Current Density (µA/cm2)

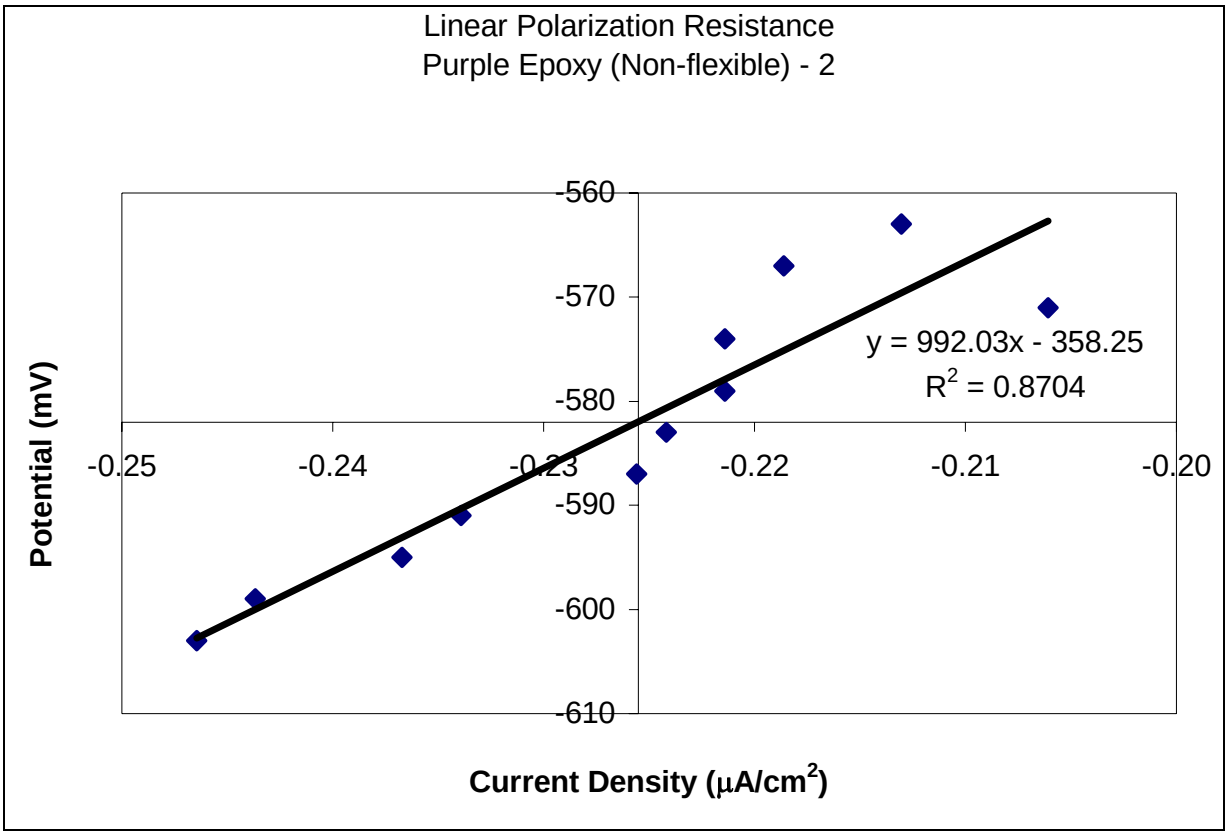
Linear Polarization Resistance
Purple Epoxy (Non-flexible) - 2
Potential (mV)
-560
-570
-580
-590
-600
-610
-0.25
-0.24
-0.23
-0.22
-0.21
-0.20
y = 992.03x - 358.25
R2 = 0.8704
Current Density (µA/cm2)

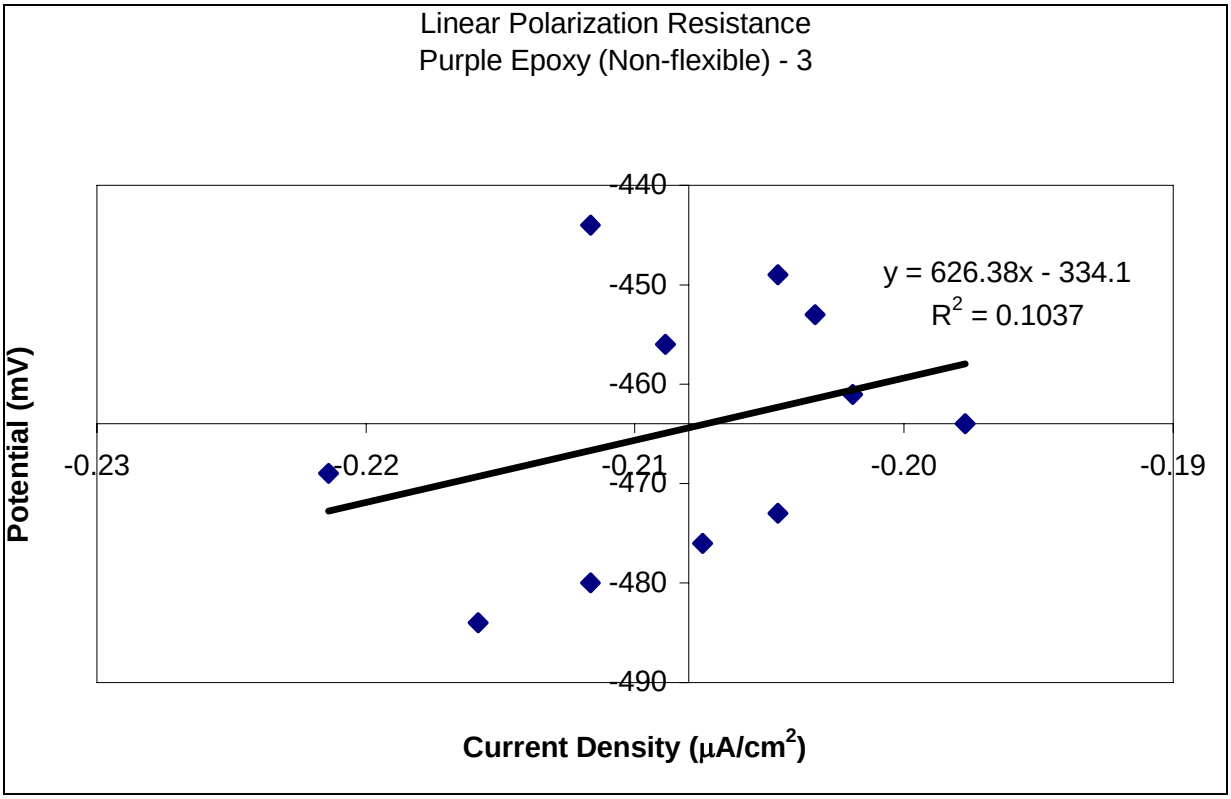
Linear Polarization Resistance
Purple Epoxy (Non-flexible) - 3
Potential (mV)
-440
-450
-460
-470
-480
-490
-0.23
-0.22
-0.21
-0.20
-0.19
y = 626.38x - 334.1
R2 = 0.1037
Current Density (µA/cm2)

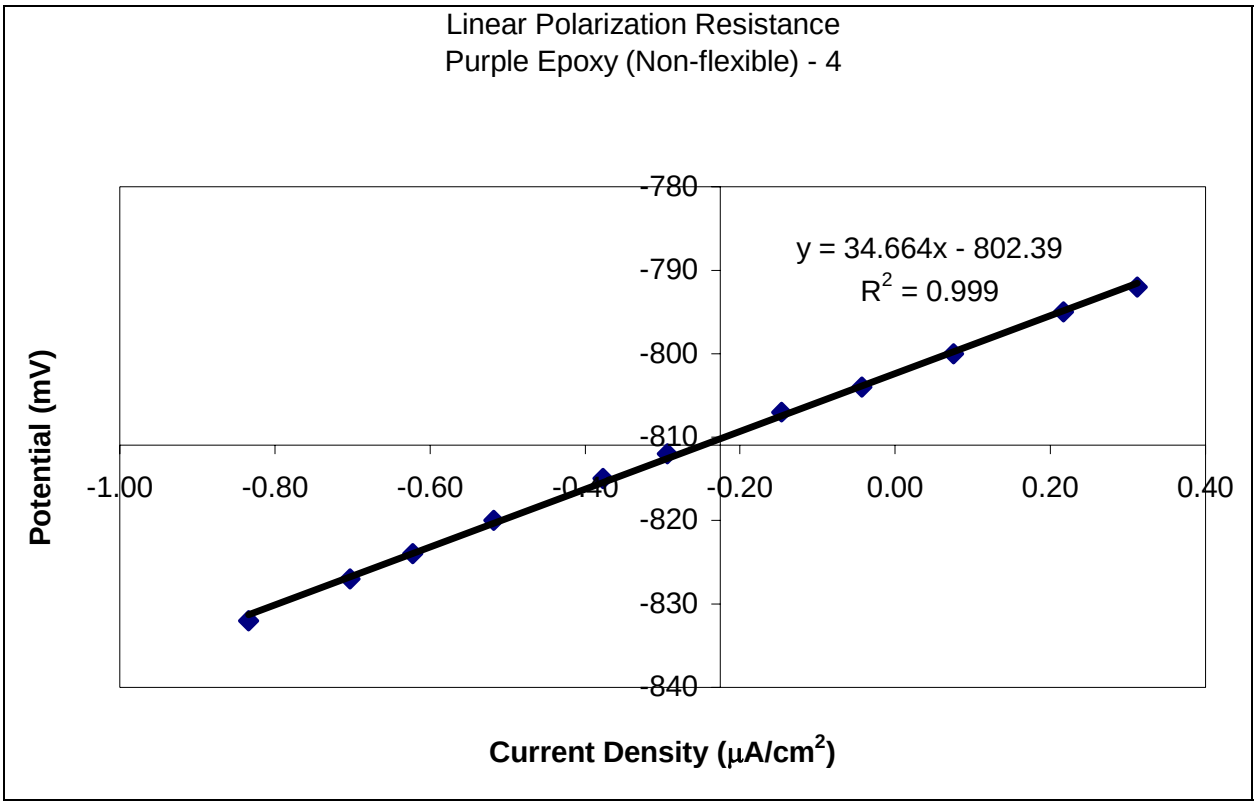
Linear Polarization Resistance
Purple Epoxy (Non-flexible) - 4
y = 34.664x - 802.39
R2 = 0.999
Potential (mV)
-780
-790
-800
-810
-820
-830
-840
-1.00
-0.80
-0.60
-0.40
-0.20
0.00
0.20
0.40
Current Density (µA/cm2)

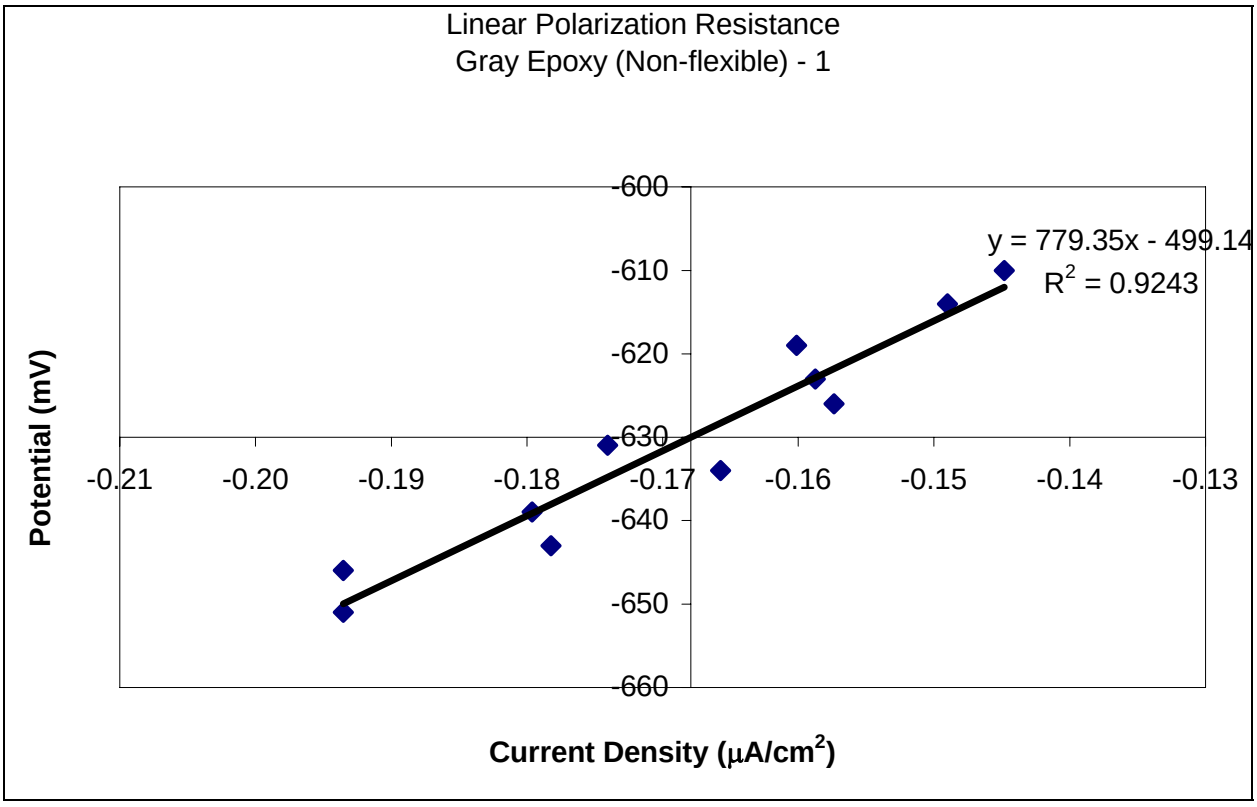
Linear Polarization Resistance
Gray Epoxy (Non-flexible) - 1
y = 779.35x - 499.14
R2 = 0.9243
Potential (mV)
-600
-610
-620
-630
-640
-650
-660
-0.21
-0.20
-0.19
-0.18
-0.17
-0.16
-0.15
-0.14
-0.13
Current Density (µA/cm2)

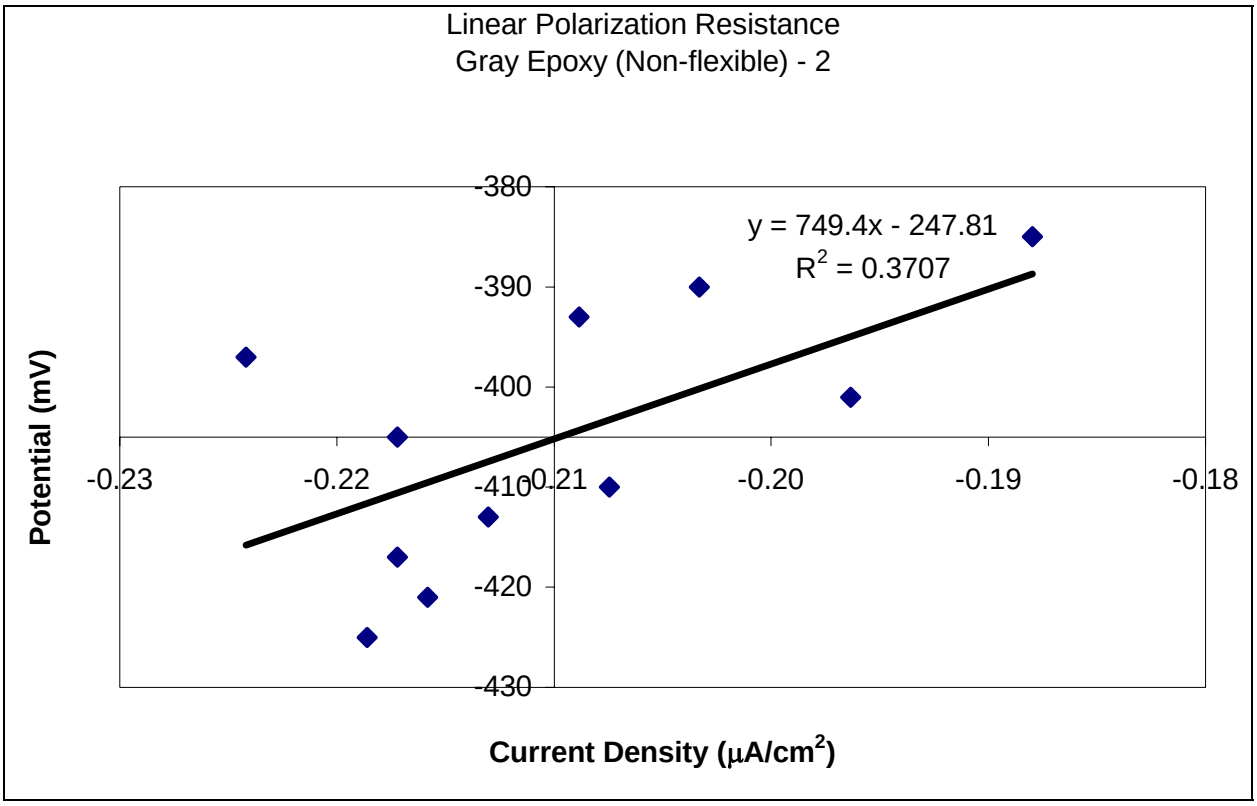
Linear Polarization Resistance
Gray Epoxy (Non-flexible) - 2
y = 749.4x - 247.81
R2 = 0.3707
-380
-390
-400
-410
-420
-430
-0.23
-0.22
-0.21
-0.20
-0.19
-0.18
Potential (mV)
Current Density (µA/cm2)

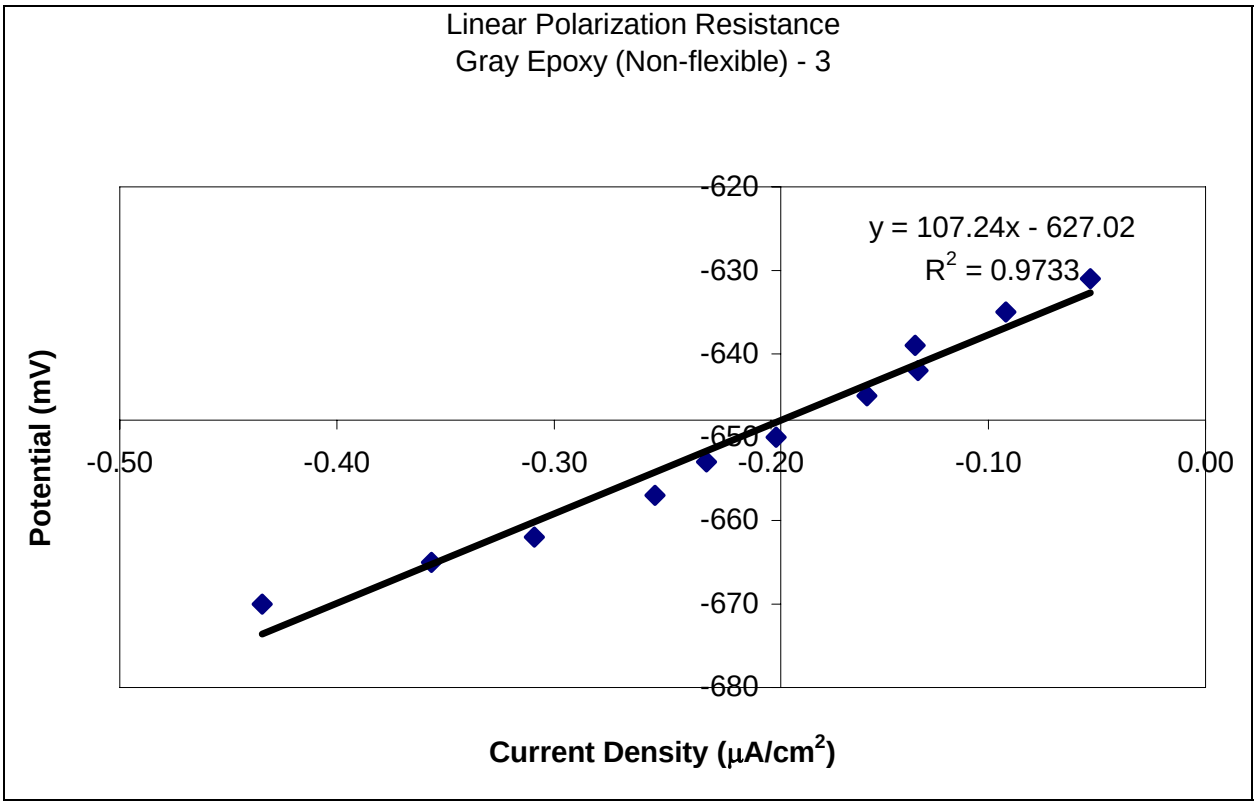
Linear Polarization Resistance
Gray Epoxy (Non-flexible) - 3
y = 107.24x - 627.02
R2 = 0.9733
-620
-630
-640
-650
-660
-670
-680
-0.50
-0.40
-0.30
-0.20
-0.10
0.00
Potential (mV)
Current Density (µA/cm2)

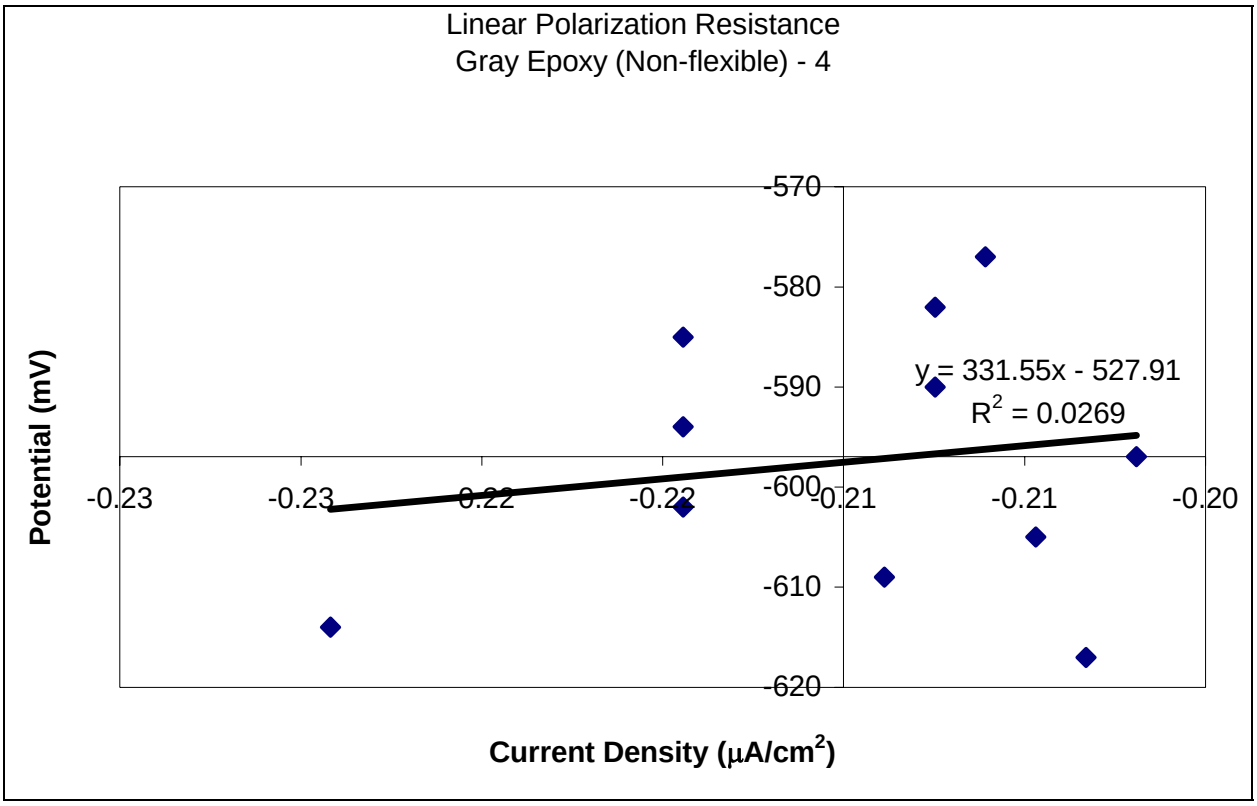
Linear Polarization Resistance
Gray Epoxy (Non-flexible) - 4
Potential (mV)
-570
-580
-590
-600
-610
-620
-0.23
-0.23
-0.22
-0.22
-0.21
-0.21
-0.20
y = 331.55x - 527.91
R2 = 0.0269
Current Density (µA/cm2)

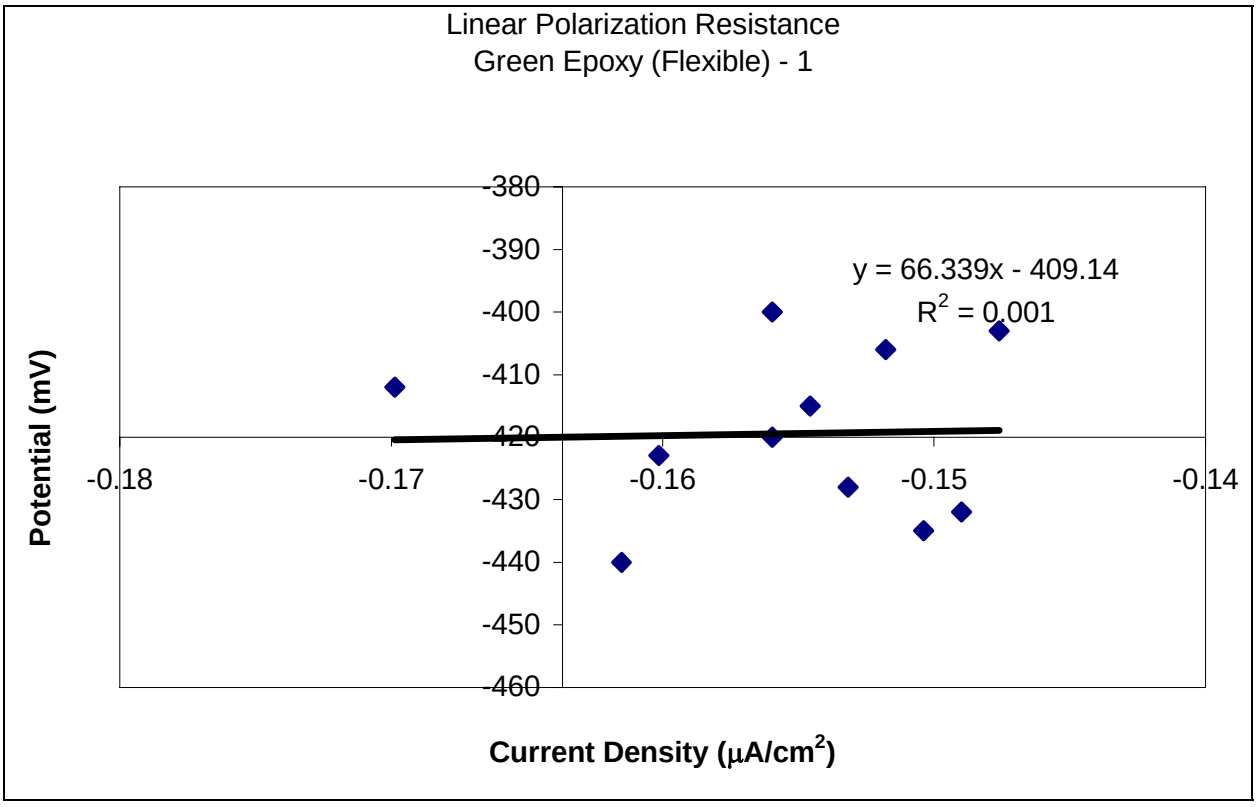
Linear Polarization Resistance
Green Epoxy (Flexible) - 1
Potential (mV)
-380
-390
-400
-410
-420
-430
-440
-450
-460
-0.18
-0.17
-0.16
-0.15
-0.14
y = 66.339x - 409.14
R2 = 0.001
Current Density (µA/cm2)

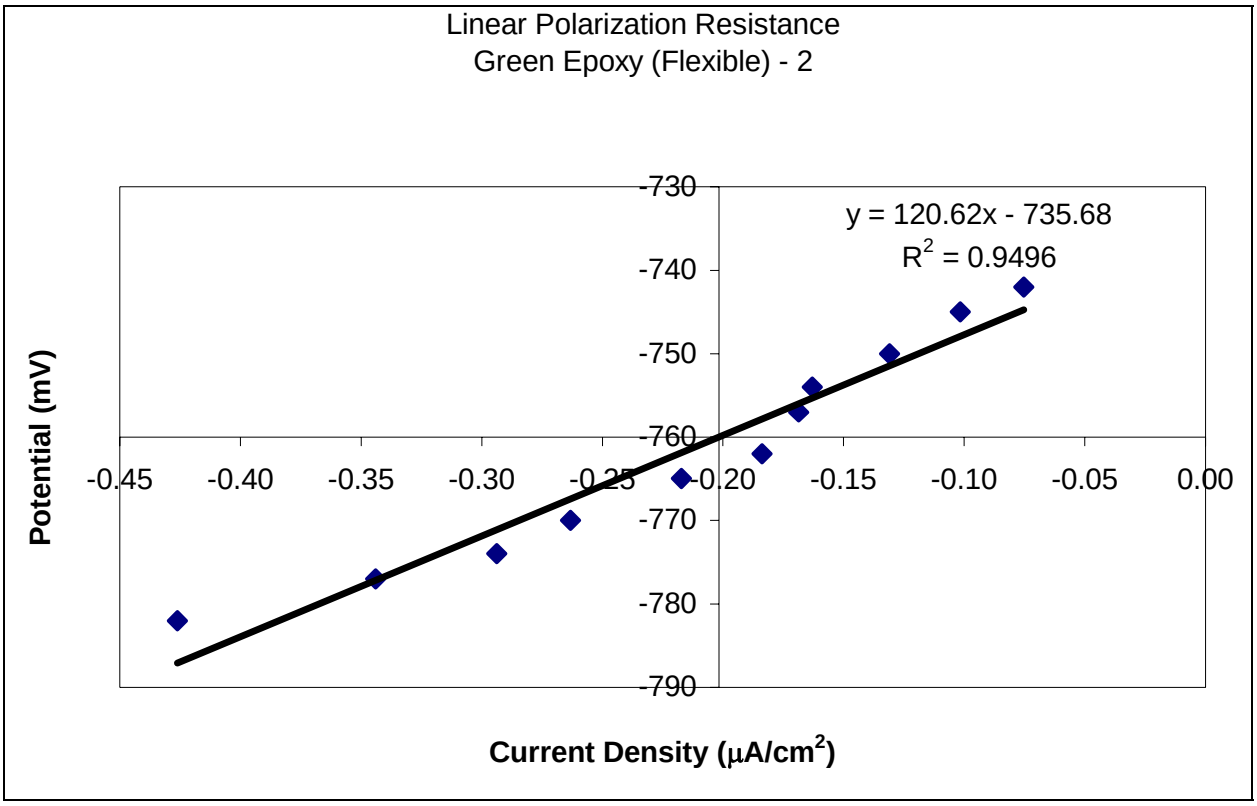
Linear Polarization Resistance
Green Epoxy (Flexible) - 2
y = 120.62x - 735.68
R2 = 0.9496
Potential (mV)
-730
-740
-750
-760
-770
-780
-790
-0.45
-0.40
-0.35
-0.30
-0.25
-0.20
-0.15
-0.10
-0.05
0.00
Current Density (µA/cm2)

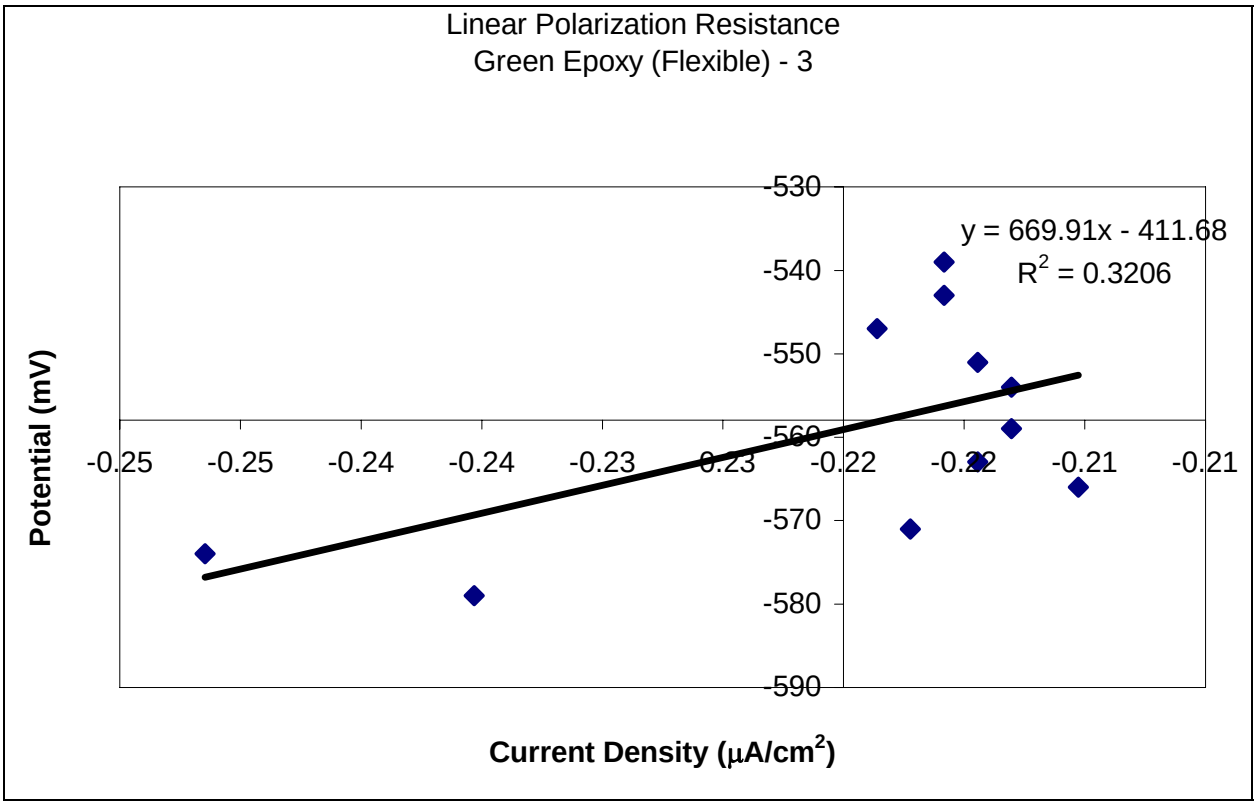
Linear Polarization Resistance
Green Epoxy (Flexible) - 3
y = 669.91x - 411.68
R2 = 0.3206
Potential (mV)
-530
-540
-550
-560
-570
-580
-590
-0.25
-0.25
-0.24
-0.24
-0.23
-0.23
-0.22
-0.22
-0.21
-0.21
Current Density (µA/cm2)

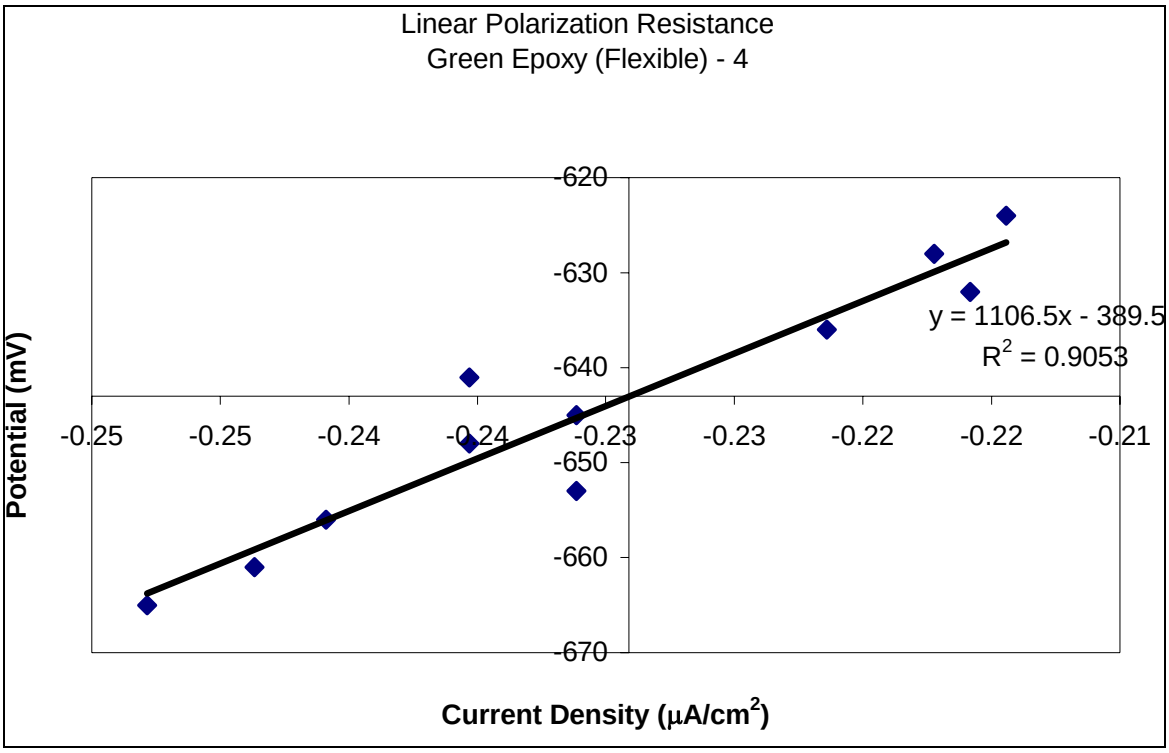
Linear Polarization Resistance
Green Epoxy (Flexible) - 4
Potential (mV)
-620
-630
-640
-650
-660
-670
-0.25
-0.25
-0.24
-0.24
-0.23
-0.23
-0.22
-0.22
-0.21
y = 1106.5x - 389.5
R2 = 0.9053
Current Density (µA/cm2)

APPENDIX C: Concrete Mix Proportions

Phase I Mix Proportions

Material		Content (kg/m^3)		Content (lb./cu. yd.)		Unit Proportions	
Cement		399		672		1.00	
Fine Aggregate	Total Aggregate	734	1834	1237	3092	1.84	4.60
Coarse Aggregate		1100		1855		2.76	
Water		167		282		0.42	

Phase II Mix Proportions

Material		Content (kg/m^3)		Content (lb./cu. yd.)		Unit Proportions	
Cement		313		527		1.00	
Fine Aggregate	Total Aggregate	939	1956	1582	3297	3.00	6.25
Coarse Aggregate		1017		1714		3.25	
Water		131		222		0.65	

APPENDIX D: Chloride Thresholds

Average Chloride Thresholds (from Reference 10)

Material	**Average Chloride Threshold (lbs. of Cl^- per cu. yd.)**
Carbon Steel	0.8
Microcomposite Steel	7.7
Stainless steel (304)	8.5
Stainless steel (316)	18.1

APPENDIX E: Half-Cell Potentials and Linear Polarization Resistance Laboratory Results

Carbon Steel A

Potential (mV)	Potential var. from Half-cell (mV)	ΔE (mV)	Current (μA)	ΔI (μA)	Current Density (μA/cm^2)	Current var. from Half-cell (μA)	Current Density var. from Half-cell (μA/cm^2)
-661	-21	0	22.76	0	3.17	-26.17	-3.64
-657	-17	4	15.28	-7.48	2.13	-18.69	-2.60
-653	-13	4	10.89	-4.39	1.52	-14.3	-1.99
-650	-10	3	6.06	-4.83	0.84	-9.47	-1.32
-645	-5	5	-0.11	-6.17	-0.02	-3.3	-0.46
-641	-1	4	-3.41	-3.3	-0.47	0	0.00
-636	4	5	-9.59	-6.18	-1.34	6.18	0.86
-633	7	3	-12.57	-2.98	-1.75	9.16	1.28
-629	11	4	-17.26	-4.69	-2.40	13.85	1.93
-624	16	5	-22.88	-5.62	-3.19	19.47	2.71
-621	19	3	-25.89	-3.01	-3.61	22.48	3.13

Carbon Steel B

Potential (mV)	Potential var. from Half-cell (mV)	ΔE (mV)	Current (μA)	ΔI (μA)	Current Density (μA/cm^2)	Current var. from Half-cell (μA)	Current Density var. from Half-cell (μA/cm^2)
-651	-22	0	28.24	0	3.93	-25.25	-3.52
-646	-17	5	19.01	-9.23	2.65	-16.02	-2.23
-643	-14	3	13.54	-5.47	1.89	-10.55	-1.47
-637	-8	6	5.85	-7.69	0.81	-2.86	-0.40
-634	-5	3	1.68	-4.17	0.23	1.31	0.18
-630	-1	4	2.99	1.31	0.42	0	0.00
-626	3	4	-9.51	-12.5	-1.32	12.5	1.74
-622	7	4	-12.83	-3.32	-1.79	15.82	2.20
-618	11	4	-18.93	-6.1	-2.64	21.92	3.05
-614	15	4	-22.11	-3.18	-3.08	25.1	3.50
-610	19	4	-26.05	-3.94	-3.63	29.04	4.04

Carbon Steel C

Potential (mV)	Potential var. from Half-cell (mV)	ΔE (mV)	Current (μA)	ΔI (μA)	Current Density (μA/cm^2)	Current var. from Half-cell (μA)	Current Density var. from Half-cell (μA/cm^2)
-623	-21	0	46.81	0	6.52	-113.22	-15.77
-619	-17	4	18.78	-28.03	2.61	-85.19	-11.86
-614	-12	5	-11.41	-30.19	-1.59	-55	-7.66
-611	-9	3	-27.58	-16.17	-3.84	-38.83	-5.41
-607	-5	4	-52.25	-24.67	-7.28	-14.16	-1.97
-603	-1	4	-66.41	-14.16	-9.25	0	0.00
-599	3	4	-79.61	-13.2	-11.09	13.2	1.84
-595	7	4	-102.34	-22.73	-14.25	35.93	5.00
-591	11	4	-113.55	-11.21	-15.81	47.14	6.56
-587	15	4	-126.87	-13.32	-17.67	60.46	8.42
-583	19	4	-139.06	-12.19	-19.36	72.65	10.12

Carbon Steel D

Potential (mV)	Potential var. from Half-cell (mV)	DE (mV)	Current (mA)	ΔI (μA)	Current Density (μA/cm^2)	Current var. from Half-cell (μA)	Current Density var. from Half-cell (μA/cm^2)
-714	-20	0	46.61	0	6.49	-64.06	-8.92
-711	-17	3	32.7	-13.91	4.55	-50.15	-6.98
-706	-12	5	15.12	-17.58	2.11	-32.57	-4.54
-703	-9	3	4.88	-10.24	0.68	-22.33	-3.11
-700	-6	3	3.79	-1.09	0.53	-21.24	-2.96
-695	-1	5	-17.45	-21.24	-2.43	0	0.00
-691	3	4	-25.36	-7.91	-3.53	7.91	1.10
-687	7	4	-38.24	-12.88	-5.32	20.79	2.89
-683	11	4	-44.64	-6.4	-6.22	27.19	3.79
-679	15	4	-53.69	-9.05	-7.48	36.24	5.05
-675	19	4	-65.02	-11.33	-9.05	47.57	6.62

Microcomposite Steel A

Potential (mV)	Potential var. from Half-cell (mV)	ΔE (mV)	Current (μA)	ΔI (μA)	Current Density (μA/cm^2)	Current var. from Half-cell (μA)	Current Density var. from Half-cell (μA/cm^2)
-312	-20	0	1.91	0	0.32	-0.36	-0.06
-308	-16	4	1.79	-0.12	0.30	-0.24	-0.04
-303	-11	5	1.73	-0.06	0.29	-0.18	-0.03
-300	-8	3	1.64	-0.09	0.27	-0.09	-0.02
-296	-4	4	1.61	-0.03	0.27	-0.06	-0.01
-292	0	4	1.55	-0.06	0.26	0	0.00
-289	3	3	1.44	-0.11	0.24	0.11	0.02
-284	8	5	1.37	-0.07	0.23	0.18	0.03
-280	12	4	1.32	-0.05	0.22	0.23	0.04
-276	16	4	1.3	-0.02	0.22	0.25	0.04
-272	20	4	1.34	0.04	0.22	0.21	0.04

Microcomposite Steel B

Potential (mV)	Potential var. from Half-cell (mV)	ΔE (mV)	Current (μA)	ΔI (μA)	Current Density (μA/cm^2)	Current var. from Half-cell (μA)	Current Density var. from Half-cell (μA/cm^2)
-299	-21	0	2.92	0	0.49	-1.51	-0.25
-294	-16	5	2.3	-0.62	0.38	-0.89	-0.15
-290	-12	4	1.94	-0.36	0.32	-0.53	-0.09
-286	-8	4	1.68	-0.26	0.28	-0.27	-0.05
-282	-4	4	1.48	-0.2	0.25	-0.07	-0.01
-279	-1	3	1.41	-0.07	0.24	0	0.00
-274	4	5	1.22	-0.19	0.20	0.19	0.03
-270	8	4	1.17	-0.05	0.20	0.24	0.04
-266	12	4	0.98	-0.19	0.16	0.43	0.07
-262	16	4	1.13	0.15	0.19	0.28	0.05
-254	24	8	0.84	-0.29	0.14	0.57	0.10

Microcomposite Steel C

Potential (mV)	Potential var. from Half-cell (mV)	ΔE (mV)	Current (μA)	ΔI (μA)	Current Density (μA/cm^2)	Current var. from Half-cell (μA)	Current Density var. from Half-cell (μA/cm^2)
-592	-21	0	7.59	0	1.27	-7.14	-1.19
-588	-17	4	5.01	-2.58	0.84	-4.56	-0.76
-584	-13	4	3.73	-1.28	0.62	-3.28	-0.55
-580	-9	4	2.5	-1.23	0.42	-2.05	-0.34
-575	-4	5	1.19	-1.31	0.20	-0.74	-0.12
-572	-1	3	0.45	-0.74	0.08	0	0.00
-567	4	5	-0.5	-0.95	-0.08	0.95	0.16
-564	7	3	-1.14	-0.64	-0.19	1.59	0.27
-560	11	4	-1.77	-0.63	-0.30	2.22	0.37
-555	16	5	-2.71	-0.94	-0.45	3.16	0.53
-552	19	3	-3.18	-0.47	-0.53	3.63	0.61

Microcomposite Steel F

Potential (mV)	Potential var. from Half-cell (mV)	ΔE (mV)	Current (μA)	ΔI (μA)	Current Density (μA/cm^2)	Current var. from Half-cell (μA)	Current Density var. from Half-cell (μA/cm^2)
-587	-20	0	4.88	0	0.82	-7.05	-1.18
-584	-17	3	2.86	-2.02	0.48	-5.03	-0.84
-580	-13	4	1.32	-1.54	0.22	-3.49	-0.58
-575	-8	5	-0.3	-1.62	-0.05	-1.87	-0.31
-572	-5	3	-0.96	-0.66	-0.16	-1.21	-0.20
-567	0	5	-2.17	-1.21	-0.36	0	0.00
-564	3	3	-2.58	-0.41	-0.43	0.41	0.07
-560	7	4	-3.33	-0.75	-0.56	1.16	0.19
-555	12	5	-4.43	-1.1	-0.74	2.26	0.38
-552	15	3	-4.68	-0.25	-0.78	2.51	0.42
-547	20	5	-5.62	-0.94	-0.94	3.45	0.58

Stainless Steel-Clad A

Potential (mV)	Potential var. from Half-cell (mV)	ΔE (mV)	Current (μA)	ΔI (μA)	Current Density (μA/cm^2)	Current var. from Half-cell (μA)	Current Density var. from Half-cell (μA/cm^2)
-235	-19	0	1.94	0	0.27	-0.52	-0.07
-232	-16	3	1.78	-0.16	0.25	-0.36	-0.05
-228	-12	4	1.7	-0.08	0.24	-0.28	-0.04
-223	-7	5	1.57	-0.13	0.22	-0.15	-0.02
-220	-4	3	1.54	-0.03	0.21	-0.12	-0.02
-215	1	5	1.42	-0.12	0.20	0	0.00
-212	4	3	1.39	-0.03	0.19	0.03	0.00
-208	8	4	1.31	-0.08	0.18	0.11	0.02
-203	13	5	1.15	-0.16	0.16	0.27	0.04
-200	16	3	1.19	0.04	0.17	0.23	0.03
-195	21	5	1.29	0.1	0.18	0.13	0.02

Stainless Steel-Clad B

Potential (mV)	Potential var. from Half-cell (mV)	ΔE (mV)	Current (μA)	ΔI (μA)	Current Density (μA/cm^2)	Current var. from Half-cell (μA)	Current Density var. from Half-cell (μA/cm^2)
-299	-20	0	1.72	0	0.24	-0.7	-0.10
-294	-15	5	1.59	-0.13	0.22	-0.57	-0.08
-291	-12	3	1.37	-0.22	0.19	-0.35	-0.05
-287	-8	4	1.19	-0.18	0.17	-0.17	-0.02
-283	-4	4	1.1	-0.09	0.15	-0.08	-0.01
-279	0	4	1.02	-0.08	0.14	0	0.00
-274	5	5	0.5	-0.52	0.07	0.52	0.07
-271	8	3	1.04	0.54	0.14	-0.02	0.00
-266	13	5	0.53	-0.51	0.07	0.49	0.07
-263	16	3	0.93	0.4	0.13	0.09	0.01
-259	20	4	1.03	0.1	0.14	-0.01	0.00

Stainless Steel-Clad B(2)

Potential (mV)	Potential var. from Half-cell (mV)	ΔE (mV)	Current (μA)	ΔI (μA)	Current Density (μA/cm^2)	Current var. from Half-cell (μA)	Current Density var. from Half-cell (μA/cm^2)
-305	-19	0	1.55	0	0.22	-0.68	-0.09
-302	-16	3	1.43	-0.12	0.20	-0.56	-0.08
-296	-10	6	1.26	-0.17	0.18	-0.39	-0.05
-293	-7	3	1.1	-0.16	0.15	-0.23	-0.03
-289	-3	4	0.99	-0.11	0.14	-0.12	-0.02
-285	1	4	0.87	-0.12	0.12	0	0.00
-281	5	4	0.93	0.06	0.13	-0.06	-0.01
-276	10	5	0.78	-0.15	0.11	0.09	0.01
-273	13	3	0.73	-0.05	0.10	0.14	0.02
-269	17	4	0.72	-0.01	0.10	0.15	0.02
-264	22	5	0.67	-0.05	0.09	0.2	0.03

Stainless Steel-Clad D

Potential (mV)	Potential var. from Half-cell (mV)	ΔE (mV)	Current (μA)	ΔI (μA)	Current Density (μA/cm^2)	Current var. from Half-cell (μA)	Current Density var. from Half-cell (μA/cm^2)
-199	-20	0	2.26	0	0.31	-0.95	-0.13
-194	-15	5	1.86	-0.4	0.26	-0.55	-0.08
-191	-12	3	1.74	-0.12	0.24	-0.43	-0.06
-186	-7	5	1.56	-0.18	0.22	-0.25	-0.03
-183	-4	3	1.53	-0.03	0.21	-0.22	-0.03
-179	0	4	1.31	-0.22	0.18	0	0.00
-174	5	5	1.3	-0.01	0.18	0.01	0.00
-171	8	3	1.28	-0.02	0.18	0.03	0.00
-166	13	5	1.29	0.01	0.18	0.02	0.00
-163	16	3	1.08	-0.21	0.15	0.23	0.03
-159	20	4	1.1	0.02	0.15	0.21	0.03

Stainless Steel-Clad E

Potential (mV)	Potential var. from Half-cell (mV)	ΔE (mV)	Current (μA)	ΔI (μA)	Current Density (μA/cm^2)	Current var. from Half-cell (μA)	Current Density var. from Half-cell (μA/cm^2)
-365	-20	0	2.38	0	0.33	-0.93	-0.13
-361	-16	4	2.01	-0.37	0.28	-0.56	-0.08
-357	-12	4	1.79	-0.22	0.25	-0.34	-0.05
-353	-8	4	1.7	-0.09	0.24	-0.25	-0.03
-350	-5	3	1.49	-0.21	0.21	-0.04	-0.01
-345	0	5	1.45	-0.04	0.20	0	0.00
-341	4	4	1.31	-0.14	0.18	0.14	0.02
-336	9	5	1.19	-0.12	0.17	0.26	0.04
-333	12	3	1.07	-0.12	0.15	0.38	0.05
-329	16	4	1.11	0.04	0.15	0.34	0.05
-324	21	5	1.06	-0.05	0.15	0.39	0.05

Stainless Steel Hollow A

Potential (mV)	Potential var. from Half-cell (mV)	ΔE (mV)	Current (μA)	ΔI (μA)	Current Density (μA/cm^2)	Current var. from Half-cell (μA)	Current Density var. from Half-cell (μA/cm^2)
-340	-20	0	3.33	0	0.46	-0.89	-0.12
-336	-16	4	2.9	-0.43	0.40	-0.46	-0.06
-332	-12	4	2.78	-0.12	0.39	-0.34	-0.05
-329	-9	3	2.65	-0.13	0.37	-0.21	-0.03
-324	-4	5	2.49	-0.16	0.35	-0.05	-0.01
-320	0	4	2.44	-0.05	0.34	0	0.00
-315	5	5	2.36	-0.08	0.33	0.08	0.01
-312	8	3	2.27	-0.09	0.32	0.17	0.02
-308	12	4	2.14	-0.13	0.30	0.3	0.04
-304	16	4	2.05	-0.09	0.29	0.39	0.05
-300	20	4	2.04	-0.01	0.28	0.4	0.06

Stainless Steel Hollow B

Potential (mV)	Potential var. from Half-cell (mV)	ΔE (mV)	Current (μA)	ΔI (μA)	Current Density (μA/cm^2)	Current var. from Half-cell (μA)	Current Density var. from Half-cell (μA/cm^2)
-590	-21	0	2.28	0	0.32	-0.91	-0.13
-585	-16	5	1.95	-0.33	0.27	-0.58	-0.08
-582	-13	3	1.76	-0.19	0.25	-0.39	-0.05
-577	-8	5	1.61	-0.15	0.22	-0.24	-0.03
-574	-5	3	1.44	-0.17	0.20	-0.07	-0.01
-570	-1	4	1.37	-0.07	0.19	0	0.00
-565	4	5	1.23	-0.14	0.17	0.14	0.02
-562	7	3	1.11	-0.12	0.15	0.26	0.04
-557	12	5	0.88	-0.23	0.12	0.49	0.07
-554	15	3	0.83	-0.05	0.12	0.54	0.08
-550	19	4	0.76	-0.07	0.11	0.61	0.08

Stainless Steel Hollow D

Potential (mV)	Potential var. from Half-cell (mV)	ΔE (mV)	Current (μA)	ΔI (μA)	Current Density (μA/cm^2)	Current var. from Half-cell (μA)	Current Density var. from Half-cell (μA/cm^2)
-230	-20	0	2.07	0	0.29	-0.87	-0.12
-225	-15	5	1.62	-0.45	0.23	-0.42	-0.06
-222	-12	3	1.56	-0.06	0.22	-0.36	-0.05
-218	-8	4	1.4	-0.16	0.19	-0.2	-0.03
-213	-3	5	1.12	-0.28	0.16	0.08	0.01
-210	0	3	1.2	0.08	0.17	0	0.00
-205	5	5	1.01	-0.19	0.14	0.19	0.03
-202	8	3	0.89	-0.12	0.12	0.31	0.04
-198	12	4	1	0.11	0.14	0.2	0.03
-193	17	5	0.87	-0.13	0.12	0.33	0.05
-190	20	3	1.02	0.15	0.14	0.18	0.03

Stainless Steel Hollow F

Potential (mV)	Potential var. from Half-cell (mV)	ΔE (mV)	Current (μA)	ΔI (μA)	Current Density (μA/cm^2)	Current var. from Half-cell (μA)	Current Density var. from Half-cell (μA/cm^2)
-213	-20	0	1.94	0	0.27	-0.45	-0.06
-209	-16	4	1.8	-0.14	0.25	-0.31	-0.04
-204	-11	5	1.7	-0.1	0.24	-0.21	-0.03
-201	-8	3	1.59	-0.11	0.22	-0.1	-0.01
-196	-3	5	1.52	-0.07	0.21	-0.03	0.00
-193	0	3	1.49	-0.03	0.21	0	0.00
-189	4	4	1.51	0.02	0.21	-0.02	0.00
-184	9	5	1.45	-0.06	0.20	0.04	0.01
-181	12	3	1.45	0	0.20	0.04	0.01
-176	17	5	1.34	-0.11	0.19	0.15	0.02
-173	20	3	1.33	-0.01	0.19	0.16	0.02

Purple Non-flexible Epoxy A

Potential (mV)	Potential var. from Half-cell (mV)	ΔE (mV)	Current (μA)	ΔI (μA)	Current Density (μA/cm^2)	Current var. from Half-cell (μA)	Current Density var. from Half-cell (μA/cm^2)
-484	-20	0	1.55	0	0.22	-0.13	-0.02
-480	-16	4	1.52	-0.03	0.21	-0.1	-0.01
-476	-12	4	1.49	-0.03	0.21	-0.07	-0.01
-473	-9	3	1.47	-0.02	0.20	-0.05	-0.01
-469	-5	4	1.59	0.12	0.22	-0.17	-0.02
-464	0	5	1.42	-0.17	0.20	0	0.00
-461	3	3	1.45	0.03	0.20	-0.03	0.00
-456	8	5	1.5	0.05	0.21	-0.08	-0.01
-453	11	3	1.46	-0.04	0.20	-0.04	-0.01
-449	15	4	1.47	0.01	0.20	-0.05	-0.01
-444	20	5	1.52	0.05	0.21	-0.1	-0.01

Purple Non-flexible Epoxy B

Potential (mV)	Potential var. from Half-cell (mV)	ΔE (mV)	Current (μA)	ΔI (μA)	Current Density (μA/cm^2)	Current var. from Half-cell (μA)	Current Density var. from Half-cell (μA/cm^2)
-496	-20	0	3.48	0	0.48	-2.41	-0.34
-493	-17	3	2.98	-0.5	0.41	-1.91	-0.27
-489	-13	4	2.47	-0.51	0.34	-1.4	-0.19
-484	-8	5	1.95	-0.52	0.27	-0.88	-0.12
-481	-5	3	1.59	-0.36	0.22	-0.52	-0.07
-476	0	5	1.07	-0.52	0.15	0	0.00
-473	3	3	0.83	-0.24	0.12	0.24	0.03
-469	7	4	0.44	-0.39	0.06	0.63	0.09
-464	12	5	0.07	-0.37	0.01	1	0.14
-461	15	3	0	-0.07	0.00	1.07	0.15
-456	20	5	-0.57	-0.57	-0.08	1.64	0.23

Purple Non-flexible Epoxy E

Potential (mV)	Potential var. from Half-cell (mV)	ΔE (mV)	Current (μA)	ΔI (μA)	Current Density (μA/cm^2)	Current var. from Half-cell (μA)	Current Density var. from Half-cell (μA/cm^2)
-832	-21	0	5.99	0	0.83	-3.88	-0.54
-827	-16	5	5.05	-0.94	0.70	-2.94	-0.41
-824	-13	3	4.47	-0.58	0.62	-2.36	-0.33
-820	-9	4	3.72	-0.75	0.52	-1.61	-0.22
-815	-4	5	2.71	-1.01	0.38	-0.6	-0.08
-812	-1	3	2.11	-0.6	0.29	0	0.00
-807	4	5	1.05	-1.06	0.15	1.06	0.15
-804	7	3	0.31	-0.74	0.04	1.8	0.25
-800	11	4	-0.54	-0.85	-0.08	2.65	0.37
-795	16	5	-1.56	-1.02	-0.22	3.67	0.51
-792	19	3	-2.24	-0.68	-0.31	4.35	0.61

Purple Non-flexible Epoxy F

Potential (mV)	Potential var. from Half-cell (mV)	ΔE (mV)	Current (μA)	ΔI (μA)	Current Density (μA/cm^2)	Current var. from Half-cell (μA)	Current Density var. from Half-cell (μA/cm^2)
-603	-21	0	1.77	0	0.25	-0.16	-0.02
-599	-17	4	1.75	-0.02	0.24	-0.14	-0.02
-595	-13	4	1.7	-0.05	0.24	-0.09	-0.01
-591	-9	4	1.68	-0.02	0.23	-0.07	-0.01
-587	-5	4	1.62	-0.06	0.23	-0.01	0.00
-583	-1	4	1.61	-0.01	0.22	0	0.00
-579	3	4	1.59	-0.02	0.22	0.02	0.00
-574	8	5	1.59	0	0.22	0.02	0.00
-571	11	3	1.48	-0.11	0.21	0.13	0.02
-567	15	4	1.57	0.09	0.22	0.04	0.01
-563	19	4	1.53	-0.04	0.21	0.08	0.01

Gray Non-flexible Epoxy A

Potential (mV)	Potential var. from Half-cell (mV)	ΔE (mV)	Current (μA)	ΔI (μA)	Current Density (μA/cm^2)	Current var. from Half-cell (μA)	Current Density var. from Half-cell (μA/cm^2)
-617	-20	0	1.46	0	0.20	-0.01	0.00
-614	-17	3	1.61	0.15	0.22	-0.16	-0.02
-609	-12	5	1.5	-0.11	0.21	-0.05	-0.01
-605	-8	4	1.47	-0.03	0.20	-0.02	0.00
-602	-5	3	1.54	0.07	0.21	-0.09	-0.01
-597	0	5	1.45	-0.09	0.20	0	0.00
-594	3	3	1.54	0.09	0.21	-0.09	-0.01
-590	7	4	1.49	-0.05	0.21	-0.04	-0.01
-585	12	5	1.54	0.05	0.21	-0.09	-0.01
-582	15	3	1.49	-0.05	0.21	-0.04	-0.01
-577	20	5	1.48	-0.01	0.21	-0.03	0.00

Gray Non-flexible Epoxy B

Potential (mV)	Potential var. from Half-cell (mV)	ΔE (mV)	Current (μA)	ΔI (μA)	Current Density (μA/cm^2)	Current var. from Half-cell (μA)	Current Density var. from Half-cell (μA/cm^2)
-425	-20	0	1.57	0	0.22	-0.01	0.00
-421	-16	4	1.55	-0.02	0.22	0.01	0.00
-417	-12	4	1.56	0.01	0.22	0	0.00
-413	-8	4	1.53	-0.03	0.21	0.03	0.00
-410	-5	3	1.49	-0.04	0.21	0.07	0.01
-405	0	5	1.56	0.07	0.22	0	0.00
-401	4	4	1.41	-0.15	0.20	0.15	0.02
-397	8	4	1.61	0.2	0.22	-0.05	-0.01
-393	12	4	1.5	-0.11	0.21	0.06	0.01
-390	15	3	1.46	-0.04	0.20	0.1	0.01
-385	20	5	1.35	-0.11	0.19	0.21	0.03

Gray Non-flexible Epoxy C

Potential (mV)	Potential var. from Half-cell (mV)	ΔE (mV)	Current (μA)	ΔI (μA)	Current Density (μA/cm^2)	Current var. from Half-cell (μA)	Current Density var. from Half-cell (μA/cm^2)
-651	-21	0	1.39	0	0.19	-0.14	-0.02
-646	-16	5	1.39	0	0.19	-0.14	-0.02
-643	-13	3	1.28	-0.11	0.18	-0.03	0.00
-639	-9	4	1.29	0.01	0.18	-0.04	-0.01
-634	-4	5	1.19	-0.1	0.17	0.06	0.01
-631	-1	3	1.25	0.06	0.17	0	0.00
-626	4	5	1.13	-0.12	0.16	0.12	0.02
-623	7	3	1.14	0.01	0.16	0.11	0.02
-619	11	4	1.15	0.01	0.16	0.1	0.01
-614	16	5	1.07	-0.08	0.15	0.18	0.03
-610	20	4	1.04	-0.03	0.14	0.21	0.03

Gray Non-flexible Epoxy D

Potential (mV)	Potential var. from Half-cell (mV)	ΔE (mV)	Current (μA)	ΔI (μA)	Current Density (μA/cm^2)	Current var. from Half-cell (μA)	Current Density var. from Half-cell (μA/cm^2)
-670	-22	0	3.12	0	0.43	-1.7	-0.24
-665	-17	5	2.56	-0.56	0.36	-1.14	-0.16
-662	-14	3	2.22	-0.34	0.31	-0.8	-0.11
-657	-9	5	1.82	-0.4	0.25	-0.4	-0.06
-653	-5	4	1.65	-0.17	0.23	-0.23	-0.03
-650	-2	3	1.42	-0.23	0.20	0	0.00
-645	3	5	1.12	-0.3	0.16	0.3	0.04
-642	6	3	0.95	-0.17	0.13	0.47	0.07
-639	9	3	0.96	0.01	0.13	0.46	0.06
-635	13	4	0.66	-0.3	0.09	0.76	0.11
-631	17	4	0.38	-0.28	0.05	1.04	0.14

Green Flexible Epoxy B

Potential (mV)	Potential var. from Half-cell (mV)	ΔE (mV)	Current (μA)	ΔI (μA)	Current Density (μA/cm^2)	Current var. from Half-cell (μA)	Current Density var. from Half-cell (μA/cm^2)
-782	-22	0	3.06	0	0.43	-1.74	-0.24
-777	-17	5	2.47	-0.59	0.34	-1.15	-0.16
-774	-14	3	2.11	-0.36	0.29	-0.79	-0.11
-770	-10	4	1.89	-0.22	0.26	-0.57	-0.08
-765	-5	5	1.56	-0.33	0.22	-0.24	-0.03
-762	-2	3	1.32	-0.24	0.18	0	0.00
-757	3	5	1.21	-0.11	0.17	0.11	0.02
-754	6	3	1.17	-0.04	0.16	0.15	0.02
-750	10	4	0.94	-0.23	0.13	0.38	0.05
-745	15	5	0.73	-0.21	0.10	0.59	0.08
-742	18	3	0.54	-0.19	0.08	0.78	0.11

Green Flexible Epoxy C

Potential (mV)	Potential var. from Half-cell (mV)	ΔE (mV)	Current (μA)	ΔI (μA)	Current Density (μA/cm^2)	Current var. from Half-cell (μA)	Current Density var. from Half-cell (μA/cm^2)
-665	-22	0	1.78	0	0.25	-0.12	-0.02
-661	-18	4	1.75	-0.03	0.24	-0.09	-0.01
-656	-13	5	1.73	-0.02	0.24	-0.07	-0.01
-653	-10	3	1.66	-0.07	0.23	0	0.00
-648	-5	5	1.69	0.03	0.24	-0.03	0.00
-645	-2	3	1.66	-0.03	0.23	0	0.00
-641	2	4	1.69	0.03	0.24	-0.03	0.00
-636	7	5	1.59	-0.1	0.22	0.07	0.01
-632	11	4	1.55	-0.04	0.22	0.11	0.02
-628	15	4	1.56	0.01	0.22	0.1	0.01
-624	19	4	1.54	-0.02	0.21	0.12	0.02

Green Flexible Epoxy D

Potential (mV)	Potential var. from Half-cell (mV)	ΔE (mV)	Current (μA)	ΔI (μA)	Current Density (μA/cm^2)	Current var. from Half-cell (μA)	Current Density var. from Half-cell (μA/cm^2)
-440	-20	0	1.16	0	0.16	-0.04	-0.01
-435	-15	5	1.08	-0.08	0.15	0.04	0.01
-432	-12	3	1.07	-0.01	0.15	0.05	0.01
-428	-8	4	1.1	0.03	0.15	0.02	0.00
-423	-3	5	1.15	0.05	0.16	-0.03	0.00
-420	0	3	1.12	-0.03	0.16	0	0.00
-415	5	5	1.11	-0.01	0.15	0.01	0.00
-412	8	3	1.22	0.11	0.17	-0.1	-0.01
-406	14	6	1.09	-0.13	0.15	0.03	0.00
-403	17	3	1.06	-0.03	0.15	0.06	0.01
-400	20	3	1.12	0.06	0.16	0	0.00

Green Flexible Epoxy E

Potential (mV)	Potential var. from Half-cell (mV)	ΔE (mV)	Current (μA)	ΔI (μA)	Current Density (μA/cm^2)	Current var. from Half-cell (μA)	Current Density var. from Half-cell (μA/cm^2)
-579	-21	0	1.69	0	0.24	-0.16	-0.02
-574	-16	5	1.77	0.08	0.25	-0.24	-0.03
-571	-13	3	1.56	-0.21	0.22	-0.03	0.00
-566	-8	5	1.51	-0.05	0.21	0.02	0.00
-563	-5	3	1.54	0.03	0.21	-0.01	0.00
-559	-1	4	1.53	-0.01	0.21	0	0.00
-554	4	5	1.53	0	0.21	0	0.00
-551	7	3	1.54	0.01	0.21	-0.01	0.00
-547	11	4	1.57	0.03	0.22	-0.04	-0.01
-543	15	4	1.55	-0.02	0.22	-0.02	0.00
-539	19	4	1.55	0	0.22	-0.02	0.00

APPENDIX F: Chloride Test Results

WSDOT Slab Core 1

Sample	Depth (x)	Depth (in.)	Chloride (mg/kg)	Chloride (mass%)	kg/m^3	lb./cu. yd.
C1-1	4	0.16	1700	0.170	4.3	7.16
C1-2	8	0.31	3500	0.350	8.8	14.75
C1-3	12	0.47	3500	0.350	8.8	14.75
C1-4	16	0.63	3100	0.310	7.8	13.06
C1-5	20	0.79	2100	0.210	5.3	8.85
C1-6	24	0.94	2200	0.220	5.5	9.27
C1-7	28	1.10	1700	0.170	4.3	7.16
C1-8	32	1.26	1500	0.150	3.8	6.32
C1-9	36	1.42	1400	0.140	3.5	5.90
C1-10	40	1.57	1000	0.100	2.5	4.21
C1-11	44	1.73	1100	0.110	2.8	4.64
C1-12	48	1.89	740	0.074	1.9	3.12
C1-13	52	2.05	700	0.070	1.8	2.95
C1-14	56	2.20	630	0.063	1.6	2.65
C1-15	60	2.36	410	0.041	1.0	1.73
C1-BG	70	2.76	170	0.017	0.4	0.72

WSDOT Slab Core 2

Sample	Depth (x)	Depth (in.)	Chloride (mg/kg)	Chloride (mass%)	kg/m^3	lb./cu. yd.
C2-1	4	0.16	1200	0.120	3.0	5.06
C2-2	8	0.31	3500	0.350	8.8	14.75
C2-3	12	0.47	3300	0.330	8.3	13.91
C2-4	16	0.63	2900	0.290	7.3	12.22
C2-5	20	0.79	2800	0.280	7.0	11.80
C2-6	24	0.94	2400	0.240	6.0	10.11
C2-7	28	1.10	2300	0.230	5.8	9.69
C2-8	32	1.26	2100	0.210	5.3	8.85
C2-9	36	1.42	1600	0.160	4.0	6.74
C2-10	40	1.57	1000	0.100	2.5	4.21
C2-11	44	1.73	790	0.079	2.0	3.33
C2-12	48	1.89	850	0.085	2.1	3.58
C2-13	52	2.05	610	0.061	1.5	2.57
C2-14	56	2.20	380	0.038	1.0	1.60
C2-15	60	2.36	410	0.041	1.0	1.73
C2-16	64	2.52	330	0.033	0.8	1.39
C2-17	68	2.68	300	0.030	0.8	1.26
C2-BG	75	2.95	250	0.025	0.6	1.05

WSDOT Slab Core 3

Sample	Depth (x)	Depth (in.)	Chloride (mg/kg)	Chloride (mass%)	kg/m^3	lb./cu. yd.
C3-1	4	0.16	1600	0.160	4.0	6.74
C3-2	8	0.31	1000	0.100	2.5	4.21
C3-3	12	0.47	650	0.065	1.6	2.74
C3-4	16	0.63	440	0.044	1.1	1.85
C3-5	20	0.79	280	0.028	0.7	1.18
C3-6	24	0.94	250	0.025	0.6	1.05
C3-7	28	1.10	160	0.016	0.4	0.67
C3-8	32	1.26	150	0.015	0.4	0.63
C3-9	36	1.42	130	0.013	0.3	0.55
C3-10	40	1.57	85	0.009	0.2	0.36
C3-11	44	1.73	170	0.017	0.4	0.72
C3-12	48	1.89	81	0.008	0.2	0.34
C3-13	52	2.05	59	0.006	0.1	0.25
C3-14	56	2.20	35	0.004	0.1	0.15
C3-BG	70	2.76	10	0.001	0.0	0.04

WSDOT Slab Core 5

Sample	Depth (x)	Depth (in.)	Chloride (mg/kg)	Chloride (mass%)	kg/m^3	lb./cu. yd.
C5-A2	4	0.16	2300	0.23	5.8	9.69
C5-A3	8	0.31	2100	0.21	5.3	8.85
C5-A4	12	0.47	1900	0.19	4.8	8.01
C5-A5	16	0.63	1700	0.17	4.3	7.16
C5-A6	20	0.79	1800	0.18	4.5	7.58
C5-A7	24	0.94	1900	0.19	4.8	8.01
C5-A8	28	1.10	1900	0.19	4.8	8.01
C5-A9	32	1.26	2000	0.2	5.0	8.43
C5-A10	36	1.42	1500	0.15	3.8	6.32
C5-ADB	40	1.57	660	0.066	1.7	2.78
C5-ABG1	44	1.73	260	0.026	0.7	1.10
C5-ABG2	70	2.76	18	0.0018	0.0	

WSDOT Slab Core 6

Sample	Depth (x)	Depth (in.)	Chloride (mg/kg)	Chloride (mass%)	kg/m^3	lb./cu. yd.
C6-A1	4	0.16	2200	0.22	5.5	9.27
C6-A2	8	0.31	2700	0.27	6.8	11.38
C6-A3	12	0.47	2200	0.22	5.5	9.27
C6-A4	16	0.63	1600	0.16	4.0	6.74
C6-A5	20	0.79	1600	0.16	4.0	6.74
C6-A6	24	0.94	1400	0.14	3.5	5.90
C6-A7	28	1.10	1100	0.11	2.8	4.64
C6-A8	32	1.26	780	0.078	2.0	3.29
C6-A9	36	1.42	750	0.075	1.9	3.16
C6-A10	40	1.57	650	0.065	1.6	2.74
C6-A11	44	1.73	690	0.069	1.7	2.91
C6-A12	48	1.89	1000	0.1	2.5	4.21
C6-A13	52	2.05	2000	0.2	5.0	8.43
C6-A14	56	2.20	1500	0.15	3.8	6.32
C6-ABG2	70	2.76	18	0.0018	0.0	0.08

Carbon Steel

Sample	Depth (x)	Depth (in.)	Chloride (mg/kg)	Chloride (mass%)	kg/m^3	lb./cu. yd.
CS-A1	4	0.16	6200	0.620	15.5	26.13
CS-A2	8	0.31	5000	0.500	12.5	21.07
CS-A3	12	0.47	5200	0.520	13.0	21.91
CS-A4	16	0.63	5200	0.520	13.0	21.91
CS-A5	20	0.79	4600	0.460	11.5	19.38
CS-A6	24	0.94	4100	0.410	10.3	17.28
CS-A7	28	1.10	4300	0.430	10.8	18.12
CS-A8	32	1.26	4600	0.460	11.5	19.38
CS-A9	36	1.42	3800	0.380	9.5	16.01
CS-A10	40	1.57	4100	0.410	10.3	17.28
CS-A11	44	1.73	4300	0.430	10.8	18.12
CS-A12	48	1.89	3100	0.310	7.8	13.06
CS-A13	52	2.05	4700	0.470	11.8	19.81
CS-A14	56	2.20	3500	0.350	8.8	14.75
CS-A15	60	2.36	4100	0.410	10.3	17.28

Stainless Steel-Clad

Sample	Depth (x)	Depth (in.)	Chloride (mg/kg)	Chloride (mass%)	kg/m^3	lb./cu. yd.
CL-A1	4	0.16	8900	0.890	22.3	37.50
CL-A2	8	0.31	8100	0.810	20.3	34.13
CL-A3	12	0.47	6700	0.670	16.8	28.23
CL-A4	16	0.63	6300	0.630	15.8	26.55
CL-A5	20	0.79	4800	0.480	12.0	20.23
CL-A6	24	0.94	5200	0.520	13.0	21.91
CL-A7	28	1.10	6100	0.610	15.3	25.70
CL-A8	32	1.26	6400	0.640	16.0	26.97
CL-A9	36	1.42	5400	0.540	13.5	22.75
CL-A10	40	1.57	6900	0.690	17.3	29.08
CL-A11	44	1.73	6100	0.610	15.3	25.70
CL-A12	48	1.89	7800	0.780	19.5	32.87
CL-A13	52	2.05	5600	0.560	14.0	23.60
CL-A14	56	2.20	5300	0.530	13.3	22.33
CL-A15	60	2.36	6600	0.660	16.5	27.81
CL-A16	64	2.52	4800	0.480	12.0	20.23
CL-A17	68	2.68	5600	0.560	14.0	23.60
CL-A18	72	2.83	7000	0.700	17.5	29.50

Stainless Steel Hollow

Sample	Depth (x)	Depth (in.)	Chloride (mg/kg)	Chloride (mass%)	kg/m^3	lb./cu. yd.
H-A1	4	0.16	8541	0.854	21.4	35.99
H-A2	8	0.31	5956	0.596	14.9	25.10
H-A3	12	0.47	5111	0.511	12.8	21.54
H-A4	16	0.63	4596	0.460	11.5	19.37
H-A5	20	0.79	4109	0.411	10.3	17.31
H-A6	24	0.94	3363	0.336	8.4	14.17
H-A7	28	1.10	3345	0.335	8.4	14.10
H-A8	32	1.26	3325	0.333	8.3	14.01
H-A9	36	1.42	4285	0.429	10.7	18.06
H-A10	40	1.57	3571	0.357	8.9	15.05
H-A11	44	1.73	5090	0.509	12.7	21.45
H-A12	48	1.89	3955	0.396	9.9	16.67
H-A13	52	2.05	4256	0.426	10.6	17.93
H-A14	56	2.20	5449	0.545	13.6	22.96

Microcomposite Steel

Sample	Depth (x)	Depth (in.)	Chloride (mg/kg)	Chloride (mass%)	kg/m^3	lb./cu. yd.
DPS-A1	4	0.16	7000	0.700	17.5	29.50
DPS-A2	8	0.31	5800	0.580	14.5	24.44
DPS-A3	12	0.47	6500	0.650	16.3	27.39
DPS-A4	16	0.63	5600	0.560	14.0	23.60
DPS-A5	20	0.79	5400	0.540	13.5	22.75
DPS-A6	24	0.94	5000	0.500	12.5	21.07
DPS-A7	28	1.10	5800	0.580	14.5	24.44
DPS-A8	32	1.26	5300	0.530	13.3	22.33
DPS-A9	36	1.42	4300	0.430	10.8	18.12
DPS-A10	40	1.57	5200	0.520	13.0	21.91
DPS-A11	44	1.73	4600	0.460	11.5	19.38
DPS-A12	48	1.89	5600	0.560	14.0	23.60
DPS-A13	52	2.05	4700	0.470	11.8	19.81
DPS-A14	56	2.20	5000	0.500	12.5	21.07
DPS-A15	60	2.36	4500	0.450	11.3	18.96
DPS-A16	64	2.52	4900	0.490	12.3	20.65

Green Flexible Epoxy

Sample	Depth (x)	Depth (in.)	Chloride (mg/kg)	Chloride (mass%)	kg/m^3	lb./cu. yd.
GE-A1	4	0.16	5686	0.569	14.2	23.96
GE-A2	8	0.31	4841	0.484	12.1	20.40
GE-A3	12	0.47	3939	0.394	9.8	16.60
GE-A4	16	0.63	3865	0.387	9.7	16.29
GE-A5	20	0.79	4472	0.447	11.2	18.84
GE-A6	24	0.94	4064	0.406	10.2	17.13
GE-A7	28	1.10	3849	0.385	9.6	16.22
GE-A8	32	1.26	3611	0.361	9.0	15.22
GE-A9	36	1.42	6844	0.684	17.1	28.84
GE-A10	40	1.57	5461	0.546	13.7	23.01
GE-A11	44	1.73	3317	0.332	8.3	13.98
GE-A12	48	1.89	4135	0.414	10.3	17.42
GE-A13	52	2.05	3711	0.371	9.3	15.64

Purple Non-Flexible Epoxy

Sample	Depth (x)	Depth (in.)	Chloride (mg/kg)	Chloride (mass%)	kg/m3	lb./cu. yd.
E-A1	4	0.16	8600	0.860	21.5	36.24
E-A2	8	0.31	3500	0.350	8.8	14.75
E-A3	12	0.47	6100	0.610	15.3	25.70
E-A4	16	0.63	5800	0.580	14.5	24.44
E-A5	20	0.79	6300	0.630	15.8	26.55
E-A6	24	0.94	5400	0.540	13.5	22.75
E-A7	28	1.10	3500	0.350	8.8	14.75
E-A8	32	1.26	5600	0.560	14.0	23.60
E-A9	36	1.42	3500	0.350	8.8	14.75
E-A10	40	1.57	4900	0.490	12.3	20.65
E-A11	44	1.73	5300	0.530	13.3	22.33
E-A12	48	1.89	4600	0.460	11.5	19.38
E-A13	52	2.05	3500	0.350	8.8	14.75
E-A14	56	2.20	4200	0.420	10.5	17.70
E-A15	60	2.36	5200	0.520	13.0	21.91
E-A16	64	2.52	4800	0.480	12.0	20.23

APPENDIX G: Concrete Technology Laboratories (CTL) Results (Raw Data)

CTL
Construction Technology Laboratories, Inc.
5400 Old Orchard Road
Skokie, Illinois 60077
847.965.7500
Fax 847.965.6541
www.CTLGroup.com

Client:	**University of California**	CTL Project No:	**320487**
Project:	**Chloride Analysis**	CTL Project Mgr.:	**Mohamad A. Nagi**
		Analyst:	**M. Bharucha**
Contact:	**David Kim**	Approved:	
Submitter:	**Mohamad A. Nagi, CTL**	Date Analyzed:	**August 24, 2004**
Date Received:	**August 20, 2004**	Date Reported:	**August 30, 2004**

REPORT of ACID-SOLUBLE CHLORIDE

Sample Identification CTL ID	Client ID	Description	Determined Chloride (Cl) (wt% of sample)
1172301	A1 1	0 - 3/4"	0.058
1172302	A1 2	3/4" - 1 1/2"	0.024
1172303	A1 3	1 1/2" - 2 1/4"	0.018
1172304	A1 4	2 1/4" - 3.0"	0.021
1172305	A1 5	3.0" - 3 3/4"	0.028
1172306	A1 6	3 3/4" - 4 1/2"	0.026
1172307	A2 1	0 - 3/4"	0.070
1172308	A2 2	3/4" - 1 1/2"	0.037
1172309	A2 3	1 1/2" - 2 1/4"	0.023
1172310	A2 4	2 1/4" - 3.0"	0.027
1172311	A2 5	3.0" - 3 3/4"	0.021
1172312	A2 6	3 3/4" - 4 1/2"	0.025
1172313	B1 1	0 - 3/4"	0.477
1172314	B1 2	3/4" - 1 1/2"	0.155
1172315	B1 3	1 1/2" - 2 1/4"	0.105
1172316	B1 4	2 1/4" - 3.0"	0.087
1172317	B1 5	3.0" - 3 3/4"	0.098
1172318	B1 6	3 3/4" - 4 1/2"	0.058
1172319	B2 1	0 - 3/4"	0.339
1172320	B2 2	3/4" - 1 1/2"	0.162
1172321	B2 3	1 1/2" - 2 1/4"	0.121
1172322	B2 4	2 1/4" - 3.0"	0.095
1172323	B2 5	3.0" - 3 3/4"	0.089
1172324	B2 6	3 3/4" - 4 1/2"	0.069

Notes:
1. This analysis represents specifically the samples submitted on a dry (105° C) basis.
2. Analysis by potentiometric titration with silver nitrate. (ASTM C1152)
3. This report may not be reproduced except in its entirety.

CTL
Construction Technology Laboratories, Inc.

5400 Old Orchard Road
Skokie, Illinois 60077
847.965.7500
Fax 847.965.6541
www.CTLGroup.com

Client:	**University of California**	CTL Project No:	**320487**
Project:	**Chloride Analysis**	CTL Project Mgr.:	**Mohamad A. Nagi**
		Analyst:	**M. Bharucha**
Contact:	**David Kim**	Approved:	
Submitter:	**Mohamad A. Nagi, CTL**	Date Analyzed:	**August 24, 2004**
Date Received:	**August 20, 2004**	Date Reported:	**August 30, 2004**

REPORT of ACID-SOLUBLE CHLORIDE

Sample Identification			Determined Chloride (Cl)
CTL ID	Client ID	Description	(wt% of sample)
1172325	C1 1	0 - 3/4"	0.450
1172326	C1 2	3/4" - 1 1/2"	0.347
1172327	C1 3	1 1/2" - 2 1/4"	0.252
1172328	C1 4	2 1/4" - 3.0"	0.238
1172329	C1 5	3.0" - 3 3/4"	0.195
1172330	C1 6	3 3/4" - 4 1/2"	0.191
1172331	C2 1	0 - 3/4"	0.450
1172332	C2 2	3/4" - 1 1/2"	0.333
1172333	C2 3	1 1/2" - 2 1/4"	0.224
1172334	C2 4	2 1/4" - 3.0"	0.192
1172335	C2 5	3.0" - 3 3/4"	0.158
1172336	C2 6	3 3/4" - 4 1/2"	0.169
1172337	D1 1	0 - 3/4"	0.363
1172338	D1 2	3/4" - 1 1/2"	0.141
1172339	D1 3	1 1/2" - 2 1/4"	0.097
1172340	D1 4	2 1/4" - 3.0"	0.060
1172341	D1 5	3.0" - 3 3/4"	0.043
1172342	D1 6	3 3/4" - 4 1/2"	0.054
1172343	D2 1	0 - 3/4"	0.354
1172344	D2 2	3/4" - 1 1/2"	0.212
1172345	D2 3	1 1/2" - 2 1/4"	0.115
1172346	D2 4	2 1/4" - 3.0"	0.079
1172347	D2 5	3.0" - 3 3/4"	0.044
1172348	D2 6	3 3/4" - 4 1/2"	0.038

Notes:
1. This analysis represents specifically the samples submitted on a dry (105° C) basis.
2. Analysis by potentiometric titration with silver nitrate. (ASTM C1152)
3. This report may not be reproduced except in its entirety.

CTL
Construction Technology Laboratories, Inc.

5400 Old Orchard Road
Skokie, Illinois 60077
847.965.7500
Fax 847.965.6541
www.CTLGroup.com

Client:	**University of California**	CTL Project No:	**320487**
Project:	**Chloride Analysis**	CTL Project Mgr.:	**Mohamad A. Nagi**
		Analyst:	**M. Bharucha**
Contact:	**David Kim**	Approved:	
Submitter:	**Mohamad A. Nagi, CTL**	Date Analyzed:	**August 24, 2004**
Date Received:	**August 20, 2004**	Date Reported:	**August 30, 2004**

REPORT of ACID-SOLUBLE CHLORIDE

Sample Identification			Determined Chloride (Cl)
CTL ID	Client ID	Description	(wt% of sample)
1172349	E1 1	0 - 3/4"	0.031
1172350	E1 2	3/4" - 1 1/2"	0.007
1172351	E1 3	1 1/2" - 2 1/4"	0.012
1172352	E1 4	2 1/4" - 3.0"	0.016
1172353	E1 5	3.0" - 3 3/4"	0.013
1172354	E1 6	3 3/4" - 4 1/2"	0.012
1172355	E2 1	0 - 3/4"	0.062
1172356	E2 2	3/4" - 1 1/2"	0.019
1172357	E2 3	1 1/2" - 2 1/4"	0.025
1172358	E2 4	2 1/4" - 3.0"	0.005
1172359	E2 5	3.0" - 3 3/4"	0.018
1172360	E2 6	3 3/4" - 4 1/2"	0.015

Notes:
1. This analysis represents specifically the samples submitted on a dry (105° C) basis.
2. Analysis by potentiometric titration with silver nitrate. (ASTM C1152)
3. This report may not be reproduced except in its entirety.

APPENDIX H: Characteristics of Microcomposite Steel Used in the Research

Information provided by manufacturer.

MMFX Heat Info

Heat history:

MMFX #	*Grade*	*Melting Plant*	*Melt #*	*Melt Date*	*Size*	*Roll Plant*	*Roll#*	*Roll Date*	*Cert Date*
D-55A100	*GR75*	*Nucor, NE*	*710789*	*12/11/2000*	*1 1/4"*	*Nucor, NE*	*710789*	*1/20/2001*	*1/20/2001*

Chemistry info:

C%	*Mn%*	*Si%*	*S%*	*P%*	*Cu%*	*Cr%*	*Ni%*	*Mo%*	*V%*	*Nb%*	*N2 ppm*
0.06	*0.43*	*0.29*	*0.008*	*0.01*	*0.1*	*9.28*	*0.08*	*0.02*	*0.018*	*0.007*	*110*

Machined bars from 1 1/2" 710789 heat

As rolled testing info:

MMFX #	*Testing Location and Date*		*Yield, [PSI]*	*Yield [MPa]*	*0.35% stress Mpa*	*Tensile [PSI]*	*Tensile [MPa]*	*Elongation in 8" [%]*	*Bend Pass /Fail*
D-55A100	*Houston*	*4/2/2004*	*143600*	*990*	*756*	*183000*	*1262*	*16.05*	*P*
D-55A100	*Houston*	*4/2/2004*	*144100*	*994*	*621*	*177700*	*1225*	*13.19*	*P*